

THE UNIVERSITY OF CALGARY

EDGE DETECTION IN THREE-DIMENSIONAL DATA  
WITH APPLICATION TO  
NUCLEAR MEDICAL IMAGES

by

JEFFREY E. BOYD

A THESIS

SUBMITTED TO THE FACULTY OF GRADUATE STUDIES  
IN PARTIAL FULFILLMENT OF THE REQUIREMENTS FOR THE  
DEGREE OF MASTER OF SCIENCE

DEPARTMENT OF ELECTRICAL ENGINEERING  
CALGARY ALBERTA CANADA

MAY 1986

© Jeffrey E. Boyd 1986

Permission has been granted to the National Library of Canada to microfilm this thesis and to lend or sell copies of the film.

The author (copyright owner) has reserved other publication rights, and neither the thesis nor extensive extracts from it may be printed or otherwise reproduced without his/her written permission.

L'autorisation a été accordée à la Bibliothèque nationale du Canada de microfilmer cette thèse et de prêter ou de vendre des exemplaires du film.

L'auteur (titulaire du droit d'auteur) se réserve les autres droits de publication; ni la thèse ni de longs extraits de celle-ci ne doivent être imprimés ou autrement reproduits sans son autorisation écrite.

ISBN 0-315-32681-6

THE UNIVERSITY OF CALGARY  
FACULTY OF GRADUATE STUDIES

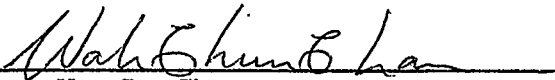
The undersigned certify that they have read, and recommend to the Faculty of Graduate Studies for acceptance, a thesis entitled, "Edge Detection in Three-Dimensional Data With Application to Nuclear Medical Images," submitted by Jeffrey E. Boyd in partial fulfillment of the requirements for the degree of Master of Science.



Supervisor, Dr. R. A. Stein  
Department of Electrical Engineering



Dr. M. R. Smith  
Department of Electrical Engineering



Dr. W. C. Chan  
Department of Electrical Engineering



Dr. G. D. Lodwick  
Department of Surveying Engineering

Date 1986-06-06

## ABSTRACT

While medical images are normally displayed and analysed in two dimensional (2D) form, 3D data are actually available in some situations. In this thesis it is shown that true 3D processing of this data is advantageous. This result is expected in the same way that 2D processing is better than using 1D operations on 2D images. Processing by the mean filter for noise reduction, and the variance filter for edge enhancement are examined. These filters are chosen for their low directional sensitivity and their extensibility to multidimensional forms. Application of these filters to a 3D synthetic image demonstrates the advantage of 3D processing. Tests of the filter methods showed that edge detection was possible with RMS noise levels as high as 3.0 times the height of the edge. These techniques applied to the left ventricle edge detection problem in nuclear cardiac scintigrams confirm that 3D processing produces better edge enhancement than does 2D processing.

## ACKNOWLEDGEMENTS

The author gratefully acknowledges the patience and support of Dr. R. A. Stein in supervising this research. Financial support was received from the Natural Science and Engineering Research Council as a post-graduate scholarship, and also from the Department of Electrical Engineering in the form of graduate teaching assistantships.

A special thanks is given to my parents, whose help, encouragement, and prodding played a significant role in the completion of this research.

Most of all, I thank Solange for standing by my side and always being there.

## TABLE OF CONTENTS

|  |     |
|--|-----|
| Abstract   | iii |
| Acknowledgements   | iv  |
| Table of Contents  | v   |
| List of Tables and Figures   | ix  |
| <br>   |     |
| 1. INTRODUCTION .....  | 1   |
| 1.1 The Problem .....  | 1   |
| 1.2 Purpose .....  | 3   |
| 1.3 Definitions .....  | 5   |
| 1.3.1 Samples .....  | 5   |
| 1.3.2 Windows and the Filtering<br>Operation .....                 | 6   |
| 1.3.3 Multidimensional Signals .....                               | 7   |
| 1.3.4 Signal-to-Noise Ratio .....                                  | 7   |
| 1.3.5 Edge Enhancement, Tracking<br>and Detection .....            | 8   |
| 1.4 Outline .....  | 8   |
| <br>   |     |
| 2. REVIEW OF NOISE REDUCTION AND<br>EDGE ENHANCEMENT METHODS ..... | 13  |
| 2.1 Introduction .....   | 13  |
| 2.2 Noise Reduction Methods .....                                  | 14  |
| 2.2.1 Linear Nonrecursive Filters .....                            | 15  |
| 2.2.2 Median Filters .....   | 18  |

|       |  |    |
|-------|--|----|
| 2.2.3 | Linear Recursive Filters .....                                   | 23 |
| 2.2.4 | Summary of Noise Reduction<br>Methods .....                      | 25 |
| 2.3   | Edge Enhancement Methods .....                                   | 26 |
| 2.3.1 | Thresholding .....   | 26 |
| 2.3.2 | Derivative Methods .....   | 27 |
| 2.3.3 | Nonlinear Masks .....  | 29 |
| 2.3.4 | Sliding Statistical Tests .....                                  | 30 |
| 2.3.5 | Summary of Edge Enhancement<br>Methods .....                     | 32 |
| 2.4   | Summary of Noise Reduction and<br>Edge Enhancement Methods ..... | 33 |
| 3.    | A VARIANCE FILTER FOR EDGE ENHANCEMENT .....                     | 40 |
| 3.1   | Introduction .....   | 40 |
| 3.2   | Variance Filter Limitations<br>Imposed by Noise .....            | 41 |
| 3.2.1 | Effect of Blurring on<br>Window Variance .....                   | 42 |
| 3.2.2 | Effect of Noise on Variance .....                                | 44 |
| 3.2.3 | Confidence of Variance Estimate .....                            | 45 |
| 3.2.4 | Maximum Noise for Accurate<br>Edge Detection .....               | 47 |
| 3.2.5 | Advantages of 3D Processing .....                                | 50 |
| 3.2.6 | Summary of Noise Limitations .....                               | 51 |
| 3.3   | Comparison of Edge Enhancers .....                               | 52 |

|       |   |     |
|-------|---|-----|
| 3.3.1 | Directional Sensitivity .....                                   | 53  |
| 3.3.2 | Filter Decay .....  | 54  |
| 3.3.3 | Probability of Detection of<br>Edges .....                      | 55  |
| 3.3.4 | Comparison of Edge Enhancers .....                              | 57  |
| 3.3.5 | Summary of Edge Enhancer<br>Comparison .....                    | 59  |
| 3.4   | Summary of Variance Analysis .....                              | 59  |
| 4.    | FILTER TESTING .....  | 77  |
| 4.1   | Introduction .....  | 77  |
| 4.2   | The Test Image .....  | 79  |
| 4.3   | The Processing Sequence .....                                   | 80  |
| 4.4   | Theoretical Versus Test Results .....                           | 82  |
| 4.5   | Filtering in 2D Versus 3D .....                                 | 85  |
| 5.    | APPLICATION TO NUCLEAR CARDIAC<br>SCINTIGRAMS .....             | 99  |
| 5.1   | Introduction .....  | 99  |
| 5.2   | Description of the Human Heart<br>and Cardiac Scintigrams ..... | 100 |
| 5.2.1 | The Heart .....   | 100 |
| 5.2.2 | Phases of the Heart Beat<br>and Ejection Fraction .....         | 101 |
| 5.2.3 | Nuclear Scintillation Camera .....                              | 102 |
| 5.3   | Modification to the Edge Tracking                               |     |

|  |     |
|--|-----|
| Algorithm .....  | 105 |
| 5.4 Filter Sequence .....  | 106 |
| 5.5 Results of Application to<br>Cardiac Scintigrams .....       | 107 |
| 5.6 Summary of Cardiac Scintigram<br>Application .....           | 109 |
| 6. DISCUSSION .....  | 126 |
| 6.1 Introduction .....   | 126 |
| 6.2 Summary of Conclusions .....                                 | 126 |
| 6.2.1 Summary of Noise Reduction<br>Methods .....                | 126 |
| 6.2.2 Summary of Edge Enhancement<br>Methods .....               | 127 |
| 6.2.3 Advantages to Three-Dimensional<br>Processing .....        | 128 |
| 6.2.4 Summary of the Filter Testing .....                        | 129 |
| 6.2.5 Summary of the Application to<br>Cardiac Scintigrams ..... | 129 |
| 6.2.6 Main Conclusions .....                                     | 130 |
| 6.3 Recommendations for Further Study .....                      | 130 |
| References .....   | 133 |

## LIST OF TABLES AND FIGURES

| Table  |   | Page |
|--------|---|------|
| 4.1    | Solutions to Equation (3.10) (no prefiltering)  | 86   |
| 4.2    | Solutions to Equations (3.10) and (3.11) (with prefiltering)                                    | 86   |
|        |   |      |
| Figure |   | Page |
| 1.1    | Examples of filtering windows   | 11   |
| 1.2    | The filtering operation   | 12   |
| 2.1    | Demonstration of mean filter blurring   | 34   |
| 2.2    | Bimodal probability density function  | 35   |
| 2.3    | Bimodal probability density function for varying standard deviation                             | 36   |
| 2.4    | Comparison of mean and median filtering   | 37   |
| 2.5    | Gradient filter mask  | 39   |
| 2.6    | Sobel filter masks  | 39   |
| 3.1    | Histogram for samples in a window at an edge with no blurring                                   | 60   |
| 3.2    | Histogram for samples in windows at an edge with blurring parameter, $\alpha=5$ and $\alpha=10$ | 61   |
| 3.3    | Variance versus blurring parameter, $\alpha$  | 62   |
| 3.4    | Probability density function for $\chi^2/df$ for varying $df$                                   | 63   |
| 3.5    | Profile of the output of the variance filter  | 64   |
| 3.6    | Derivation of pixel intensities for directional sensitivity                                     | 65   |
| 3.7    | Directional sensitivity characteristic for the variance filter (normalized)                     | 66   |
| 3.8    | Calculation of distances for filter decay filter (normalized)                                   | 67   |

|      |  |    |
|------|--|----|
| 3.9  | Filter decay characteristic for the variance   | 68 |
| 3.10 | Probablilty density functions for the variance filter output in edge and no edge regions                     | 69 |
| 3.11 | Test windows for calculation of probability characteristics  | 70 |
| 3.12 | Probability of detection versus probability of false detection characteristic for variance filter (SNR = 10) | 71 |
| 3.13 | Comparison of directional sensitivity characteristic for varaince, gradient, and Sobel edge enhancers        | 72 |
| 3.14 | Comparison of filter decay characteristics for variance, gradient, and Sobel edge enhancers                  | 73 |
| 3.15 | Comparison of the probablilty characteristics for variance, gradient, and Sobel edge enhancers               | 75 |
| 4.1  | Generation of the 3D test image  | 87 |
| 4.2  | Example of data in the filtering sequence (standard deviation of noise = 0.5)                                | 88 |
| 4.3  | Pictorial description of the radial search algorithm   | 89 |
| 4.4  | Output of the filter sequence (no prefiltering) with 2D width 3 filters                                      | 90 |
| 4.5  | Output of the filter sequence (no prefiltering) with 2D width 5 filters                                      | 91 |
| 4.6  | Output of the filter sequence (no prefiltering) with 3D width 3 filters                                      | 92 |
| 4.7  | Output of the filter sequence (no prefiltering) with 3D width 5 filters                                      | 93 |
| 4.8  | Output of the filter sequence (with prefiltering) with 2D width 3 filters                                    | 94 |
| 4.9  | Output of the filter sequence (with prefiltering) with 2D width 5 filters                                    | 95 |
| 4.10 | Output of the filter sequence (with prefiltering) with 3D width 3 filters                                    | 96 |

|      |   |     |
|------|---|-----|
| 4.11 | Output of the filter sequence (with prefiltering) with 3D width 5 filters   | 97  |
| 4.12 | 1D analogy of errors caused by blurring   | 98  |
| 5.1  | Cut-away view of the human heart showing blood circulation  | 110 |
| 5.2  | Apparatus for producing nuclear cardiac scintigrams   | 111 |
| 5.3  | Pictorial description of the modified radial search algorithm   | 112 |
| 5.4  | Generation of 3D image from a set of nuclear cardiac scintigrams  | 113 |
| 5.5  | Example of the 3D filter sequence applied to cardiac scintigram data showing the end systole and end diastole images at each step | 114 |
| 5.6  | Results of application to cardiac scintigrams (case 1)  | 116 |
| 5.7  | Results of application to cardiac scintigrams (case 2)  | 117 |
| 5.8  | Results of application to cardiac scintigrams (case 3)  | 118 |
| 5.9  | Results of application to cardiac scintigrams (case 4)  | 119 |
| 5.10 | Results of application to cardiac scintigrams (case 5)  | 120 |
| 5.11 | Integral of the left ventricle region versus time in the heart beat (case 1)  | 121 |
| 5.12 | Integral of the left ventricle region versus time in the heart beat (case 2)  | 122 |
| 5.13 | Integral of the left ventricle region versus time in the heart beat (case 3)  | 123 |
| 5.14 | Integral of the left ventricle region versus time in the heart beat (case 4)  | 124 |
| 5.15 | Integral of the left ventricle region versus time in the heart beat (case 5)  | 125 |

## Chapter 1

### INTRODUCTION

#### 1.1 The Problem

The location of discontinuities in a signal is often desired in signal processing. In multidimensional signals, or images, these discontinuities are edges or boundaries between different regions of the image. The edges can mark boundaries between regions of different intensity, texture, variance or some other characteristic. The accurate location of these edges is frequently central in the interpretation of images. For these reasons the detection of region-defining edges in multidimensional signals is an important area of study.

The importance of this edge location problem has led to the development of many edge enhancement techniques[1-7]. All edge enhancement techniques are limited by image resolution, sharpness of the edge, and particularly, signal-to-noise ratio (a definition is given in Section 1.3.4). As the noise level on a signal

increases, the edges in the signal become more difficult to detect. Consequently, a high signal-to-noise ratio is desirable. Because of limitations in some practical applications, a high noise level must be tolerated. In such cases, methods of noise reduction can be employed. The drawback with these methods is that while, they reduce the level of noise in a signal, they also tend to distort and blur edges in an image. As a result, accurate edge detection and image interpretation may be difficult to achieve.

A specific example of this problem occurs in radiological medical imaging. In medical images, edges between regions of different intensity represent boundaries between anatomical structures and/or anomalies. Presently, high levels of noise must be tolerated because the only way to reduce the noise in the imaging process is to increase the radiation dose, thereby increasing the risk to the patient. Since the side effects of radiation can be life threatening, a signal processing solution to the low signal-to-noise ratio must be sought.

## 1.2 Purpose

The work done for this thesis was motivated by needs in nuclear medical imaging. In medical imaging, image data are sometimes available in three dimensions. An example of such data is computed tomography (CT) scans. A single CT scan is a two dimensional image representing a slice of the patient's internal anatomy. Each sample in the scan is derived from the body's ability to absorb radiation at that location. A series of scans of adjacent slices combine to form a three-dimensional data set with three spatial axes.

Another example of three-dimensional image data is nuclear cardiac scintigrams. The process of producing a cardiac scintigram involves injecting a gamma radiation source into the patient's blood. Radiation emitted by each region of the body is then counted. The scintigram, a two dimensional image, is formed from the counts by letting each image sample equal the gamma radiation count emitted by the corresponding part of the body. Regions of the body containing a large amount of blood, such as the heart, have high counts and can be seen in the scintigram. Because of the movement of the heart during the counting process, the scintigrams must be gated to the heart's beat. A series of 16 scintigrams is produced with each scintigram corresponding to a temporal fraction of the heart's beat.

The scintigrams combine to form a data set with two spatial axes and one temporal axis. A more complete description of the acquisition, properties, and utilization of nuclear cardiac scintigrams is given in Chapter 5.

The purpose of this thesis is to show how three-dimensional signal processing can be applied to these three-dimensional signals. This application is intended to improve noise reduction and edge enhancement in three-dimensional data with a low signal-to-noise ratio. The expected improvement is analogous to that obtained for two-dimensional data by processing in two dimensions rather than in one dimension at a time. Three categories of noise reduction techniques are examined to find a method suitable for edge detection applications. Of these techniques, the mean filter, a type of linear nonrecursive filter, is shown to be most suitable. The novelty of three-dimensional processing raises the need for an edge enhancer that is applicable to any multidimensional situation. A variance filter is proposed to fill this need. The mean filter for noise reduction and the variance filter for edge enhancement demonstrate the effectiveness of three-dimensional image processing.

### 1.3 Definitions

In order to avoid confusion among terms which are common to both statistics and signal processing, but have different meanings in each field, the terminology used throughout this thesis is defined in this section.

#### 1.3.1 Samples

The term "sample" in statistics can refer to a set of data which is taken from a larger population. For example, one could have a sample of 100 height measurements of people in Calgary. In this case the sample contains 100 data and is taken from the population defined by the people who live in Calgary. In signal processing the term "sample" has a different meaning. A sample in signal processing refers to a single datum which represents the value of a signal at one specific position (spatial or temporal). In the previous example of height measurements of people in Calgary, a sample in signal processing would refer to the value of the height of one particular person. For the work presented here the term sample refers to samples in the signal processing sense, that is, an individual datum. The term "pixel" refers to a sample in a two dimensional signal and the term "voxel" refers to a sample in a three dimensional signal.

### 1.3.2 Windows and the Filtering Operation

The term "window" is used frequently here. A window always corresponds to a single sample and is the set of all samples within a region of specified size. Windows are usually centred on the sample to which the window corresponds. To help clarify what is meant by a window, two examples are illustrated in Figure 1.1. The first of these examples shows a one-dimensional window five samples long. The second shows a two-dimensional window which measures three pixels on a side. In this thesis the size of a window refers to the number of samples in a window, and the width of a window refers to the length of the window on a side. For example a three-by-three, two-dimensional window has a size of nine and a width of three. In image processing it is not required that windows be square, and in fact, they may be any shape. It must be noted that in the present context windows are square.

The concept of a window is central to the filtering operation referred to throughout this thesis. In the filtering operation each output sample,  $y_{i,j}$ , is a function of the corresponding input sample,  $x_{i,j}$ , and the samples in the window at that position. The subscripts used here refer to a two dimensional example, but may be extended to any number of dimensions. Figure 1.2 illustrates the

filtering operation pictorially.

### 1.3.3 Multidimensional Signals

Signals in one, two and three dimensions are discussed in this thesis. The terms "one-dimensional", "two-dimensional" and "three-dimensional" are abbreviated as "1D", "2D" and "3D".

### 1.3.4 Signal-to-Noise Ratio

The concept of signal-to-noise ratio(SNR) is important in signal processing. In the strictest sense SNR is the ratio of signal energy to noise energy. In edge enhancement applications, SNR is defined by[8]

$$\text{SNR} = (h/\sigma)^2, \quad (1.1)$$

where  $h$  = edge height

and  $\sigma$  = standard deviation of noise.

Thus, in this definition, the square of the edge height is used instead of the signal energy.

### 1.3.5 Edge Enhancement, Tracking and Detection

Edge enhancement refers to the process by which edges in an input signal are transformed into peaks in an output signal. The process of edge tracking is the process of following the peaks in an edge enhanced image to determine the perimeter of the object defined by the edge. Edge detection involves, first, enhancing edges in an image and then, tracking them, that is, the combination of edge enhancement and edge tracking.

### 1.4 Outline

Noise reduction methods can improve SNR which in turn may lead to better edge detection. In low SNR cases, to which this work is targeted, noise reduction methods are used in combination with edge enhancement in order to improve results. A review of commonly-used noise reduction and edge enhancement methods is presented in Chapter 2. The limitations of these methods are highlighted.

Limitations of the common edge enhancers reviewed in Chapter 2 lead to the proposal of the variance filter as an edge enhancer. The proposed variance filter is analyzed in Chapter 3 where it is shown that the variance filter

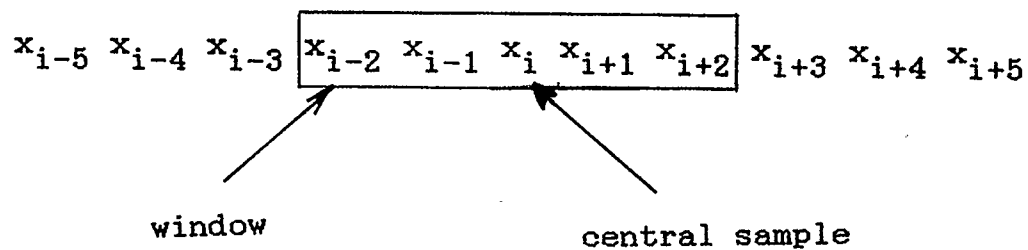
exhibits all the desirable properties of an edge enhancer and that it can be easily extended to work in any multidimensional situation. The analysis also demonstrates the advantage of processing data in 3D as opposed to 2D or 1D. Also in Chapter 3, the variance filter is compared to other commonly used edge enhancers.

A test demonstrating the behavior of the mean filter for noise reduction and the variance filter for edge enhancement is presented in Chapter 4. The test results support the theoretical work done in Chapter 3. The edge enhancement property of the variance filter is demonstrated and the argument for 3D processing versus 2D processing is supported.

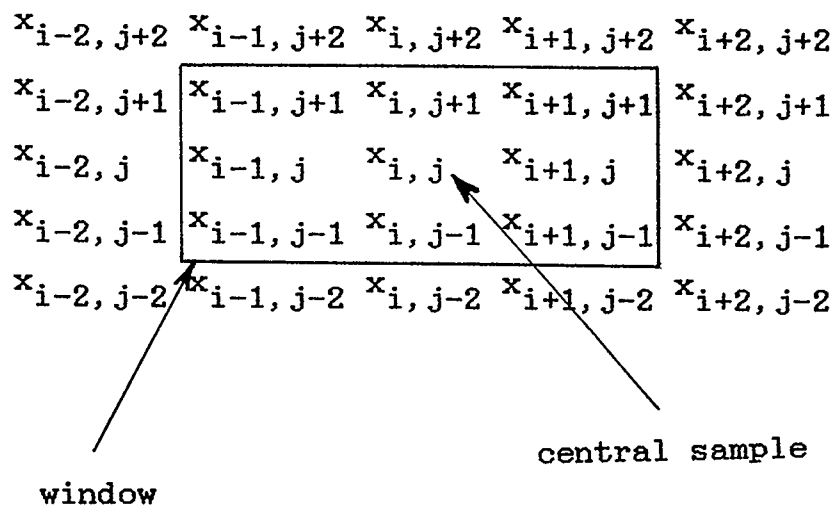
The processing techniques tested in Chapter 4 are applied to cardiac scintigrams in Chapter 5. Cardiac scintigrams are used in medicine to diagnose the condition of the left ventricle of the heart. The left ventricle is the "work horse" of the human heart and is important to any patient's health. Although some automated method for outlining the left ventricle is normally supplied with nuclear cardiac scintigram equipment, none is entirely successful and manual methods are often necessary in order to achieve accurate results. In this chapter it is shown that, even with a rudimentary edge following algorithm,

improved results in enhancement and outlining of the left ventricle may be obtained. It is concluded that with more sophisticated edge tracking algorithms the variance filter combined with some form of noise reduction in 3D can produce excellent results in edge detection.

Finally, in Chapter 6 the theoretical, test and application studies are summarized. Suggestions are made for the direction of future research in the problem of accurate edge detection.



(a)



(b)

Figure 1.1 Examples of filtering windows  
 (a) 1D window of width 5  
 (b) 2D window of width 3

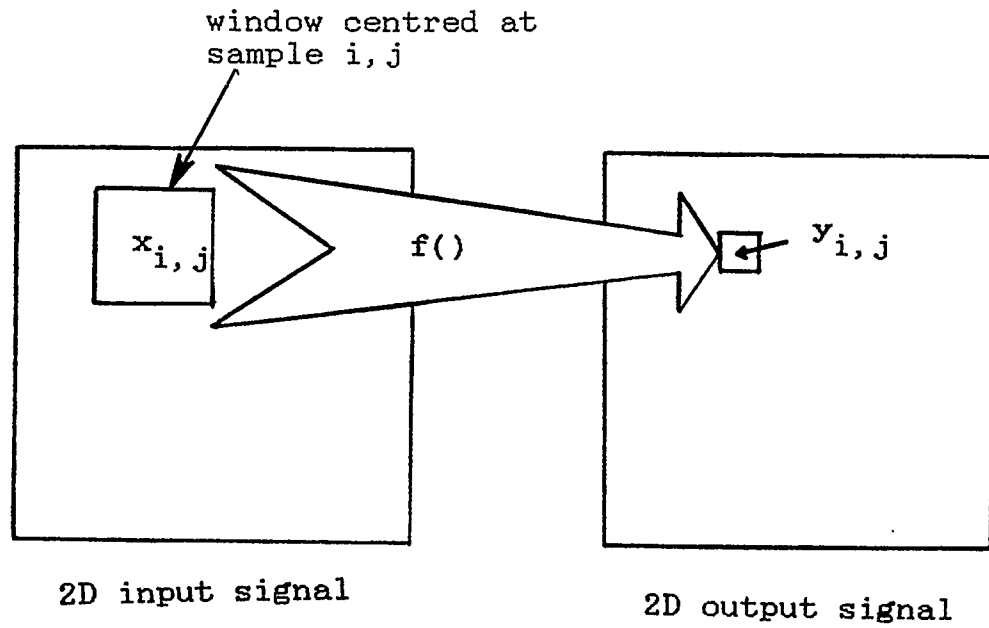


Figure 1.2 The filtering operation

## Chapter 2

REVIEW OF NOISE REDUCTION  
AND EDGE ENHANCEMENT METHODS

### 2.1 Introduction

The detection of edges in images has been a major area of research in image processing for many years. Consequently, many techniques for edge enhancement have been presented in the literature. Since all edge enhancement methods are limited by SNR it is important also to understand noise reduction methods in image processing and their effect on edge enhancement.

The first section of this chapter deals with noise reduction. Three categories of noise reduction techniques are reviewed. This review demonstrates the trade-off between effective noise reduction and blurring of edges in the image. It is also shown that filter methods which rely on bimodal probability distributions in a window at an edge, such as the median filter, behave differently in low SNR situations where the probability distributions are no longer bimodal.

The second section of this chapter is a review of some common methods for edge enhancement. Their advantages and limitations are outlined. The idea of using the variance function for edge enhancement is also introduced in this section.

## 2.2 Noise Reduction Methods

For the purposes of this thesis, noise reduction methods are classified into the following categories:

1. Linear nonrecursive filters
2. Median filters
3. Linear recursive filters

Each category of filter is dealt with separately. Linear nonrecursive filters are described in general and a specific example, the mean filter, is examined. Next, the median filter is presented. It is argued that the median filter relies on a bimodal probability distribution in the image in order to preserve edges. Further, it is shown that when the SNR is low enough, the probability distributions may not be bimodal. Finally, the advantages and disadvantages of linear recursive filters are discussed.

### 2.2.1 Linear Nonrecursive Filters

In a linear nonrecursive filter, the filter output,  $y_{i,j}$ , is a linear function of the samples in the window at the corresponding input sample,  $x_{i,j}$ . Filter output is derived only from input signal samples, hence, these filters are nonrecursive. In contrast, the output of a linear recursive filter, as described in Section 2.2.3, is derived from a linear function of input signal samples and previous output signal samples.

Linear nonrecursive filters have the property of finite impulse response (FIR)[9]. The FIR property means that the output of the filter due to an impulse input will be finite in duration. One can understand this intuitively by realizing that only if the impulse input falls inside the window can it affect the output. Since the window is finite in size, the output due to the impulse must also be finite in size.

A FIR filter can also be thought of as a matched spatial filter (MSF). A MSF is a FIR filter which is matched to a specific input signal. It is the optimum FIR filter for detecting that particular signal. The impulse response of the MSF is equal to the input signal which the filter is to detect[10].

Linear nonrecursive filters can be used for many purposes. To reduce noise, the filter must detect a signal of constant level obscured by noise. The optimum FIR filter for this task is a MSF matched to the constant level. A mean filter is the result. In a mean filter, the output sample,  $y_{i,j}$  is equal to the mean of all the samples in the window centred at  $x_{i,j}$ , for each sample in the input signal. Mathematically the mean filter is given by

$$y_{i,j} = \frac{1}{N} \sum (x_{l,m} \mid x_{l,m} \text{ is in } w_{i,j}) , \quad (2.1)$$

where  $N$  = size of the window, and

$$w_{i,j} = \text{window centred at sample } i,j$$

The improvement in SNR realized by the mean filter is given by[11]

$$\text{SNR}_Y = N(\text{SNR}_X) . \quad (2.2)$$

Although the mean filter is the ideal MSF for constant levels, it is rare that one encounters an image containing only one constant level. At points where one level ends and another begins, i.e., at edges, the mean filter tends to blur or smear the two levels together. This effect is illustrated for a 1D case in Figure 2.1, where the edge is blurred across 11 samples. The number of samples across which the edge is blurred is equal to the window width. In

multidimensional cases the blurring is restricted to the width of the window in each dimension.

Linear nonrecursive filters may also operate in the frequency domain. Standard texts such as Pratt[12], or Gonzalez and Wintz[13] describe how to use fast Fourier transform (FFT) windowing to reduce noise in an image. This method is effective but has drawbacks. FFTs are computationally intensive. 2D FFTs take a relatively long time to compute and in 3D the process would be far too cumbersome to be useful.

In one variation of the mean filter proposed by Lee[14], a local estimate of the mean (as in the mean filter) is combined with a local estimate of the variance to obtain the best estimate of a pixel value. The method is effective in images where there is low noise. However, in situations where the SNR is less than 1, noise reduction is not as good, although edges are not blurred as much as with the mean filter.

A signal which has been subject to distortion and has additive noise can be recovered by a Wiener filter, a variation of the MSF[15]. The Wiener filter selects the optimum weighting of two filters, the inverse of the distortion and a MSF. The process of Wiener filtering was

demonstrated in 2D by Ekstrom[16]. Abramatic and Silverman[17] used nonlinear modifications to Weiner filtering to take into account edge information and improve filtering results. In applications studied for this thesis, there is no applicable model for a distortion process and the Weiner filter reduces to a MSF.

The mean filter is a linear nonrecursive filter and therefore exhibits the property of finite impulse response. It has been shown that as a matched spatial filter the mean filter is the optimum FIR filter for detecting a constant level obscured by noise. The FIR response property leads to finite blurring of edges in images. These properties make the mean filter an acceptable approach to noise reduction in images.

### 2.2.2 Median Filters

The median filter follows the same basic filtering operation as linear nonrecursive filters, but a nonlinear rather than linear function is used. Calculation of the median of a set of numbers is done by first rank ordering that set. The median is then the value at the centre of the ordered numbers. The use of the median as a filtering function is given mathematically by

$$y_{i,j} = \text{Median}\{x_{l,m} | x_{l,m} \text{ is in } w_{i,j}\} . \quad (2.3)$$

For a normally distributed variable the mean, median and mode (the mode of a variable is the value which occurs most frequently) are equal. Therefore, the median shares the desirable feature of the mean filter in that it is the optimum FIR filter for the detection of a constant level.

This research presents an original analysis of the median filter. This analysis is extrapolated to show the limitations of the median filter. The important difference between the mean and the median occurs when the filter encounters an edge. At an edge, the extent to which the median filter behaves like a mean filter depends on the likelihood that the median will equal the mean. At an edge, the probability distribution of samples in the window is bimodal and symmetrical as shown in Figure 2.2. Figure 2.2 shows the distribution as being continuous. For the continuous distribution the median will equal the mean. The histogram of samples in a window represents an approximation to the continuous probability distribution. The accuracy of the approximation depends on the number of samples used to calculate that approximation. An increased window size will serve to increase the accuracy of the histogram in the window. Therefore, as the number of samples in a window is increased the likelihood that the

median will equal the mean also increases. If the number of samples is sufficiently low, the median will be different from the mean, and be drawn towards one of the two modes. Ideally, there will be no sample values near the mean and each pixel will be clearly associated with one mode.

The distribution shown in Figure 2.2 represents a case with low noise making two modes clearly visible. If the standard deviation of the noise is increased the two modes join together. There will no longer be two modes in the distribution at the point where the standard deviation of the noise is equal to one half of the step size at the edge. Figure 2.3 shows a series of bimodal distributions based on the sum of two normal distributions with an equal probability for each mode and equal standard deviations. The single mode which exists when the standard deviation is half the step size corresponds to the median and the mean of the distribution. When noise is high, the output of the median filter is not apt to fall near one of the two sides of the edge. It is most likely that the median will equal the mean.

Figure 2.4 shows the median and mean filtering of two identical 1D signals with different noise levels. In the situation where there is no noise the output of the median

filter is identical to the input, but the mean filter has blurred the edge. In contrast, the case where the noise is one half the step size shows that the median filter blurs the edge as much as the mean filter. The presence of noise has modified the behaviour of the median filter such that it behaves similarly to the mean filter.

Several variations on the median filter have been used. A separable median filter for noise reduction in 2D was demonstrated by Narendra[18]. An adaptive median presented by Stein and Fowlow[19] used a priori knowledge of edge height to decide whether or not to use the actual median of a particular window or to use a different percentile. Lee and Kassam have used several variations of the median filter including what they term a modified trim mean (MTM) filter[20].

Narayanan and Rosenfeld used global statistics to select which pixels in a window to use as input to a mean filter[21]. Their method takes advantage of the optimum MSF characteristic of the mean while attempting to avoid edge blurring. Global statistics are used to find the modes in an image. Each mode corresponds to one area of constant intensity. The mean of the entire window is used to determine to which mode the central pixel in the image belongs. Only those pixels which fall within a specified

range about the chosen mode are used to calculate a second average. This selection process should therefore take only those samples which correspond to a single mode, that is, one constant level, and avoid blurring between levels.

The global statistics method is mentioned here along with the median filter, and its variations, because they all exhibit the same fault. It is assumed that the noise on the image is low enough that modes corresponding to different image regions exist. As demonstrated above, not all the modes exist in a high noise situation, and therefore, any method which relies on distinct modes fails in high noise.

The median filter has some of the desirable properties of the mean filter. Under conditions where noise is low and the number of samples in a window is not large, the median filter can reduce the amount of blurring in noise reduction. In general, in high noise situations, the median filter and other filters which rely on distinct modes will not preserve edges as they may do with low noise.

### 2.2.3 Linear Recursive Filters

In relation to the basic filtering operation, the output of a recursive filter may be thought of as a function of the samples in two windows, one window being on the input signal and the other on the output. Only outputs which have been previously calculated can be used in the window over the output. For a linear recursive filter, each output sample is a linear function of input samples in the corresponding window and previously calculated outputs. The filter is recursive because previous outputs are fed back into the filter, and it is linear because the filter uses a linear function of window samples.

Linear recursive filters are designed in two steps. First, a stable analogue transfer function is produced based on a stable analogue design. Second, a stable z-domain transfer function is derived from the analogue transfer function by means of the bilinear transform. A detailed explanation of the 1D technique is found in Antoniou[22]. Bruton and Bartley[23] extended this method to multidimensional filters.

Linear recursive filters have advantages over linear nonrecursive filters. In general, a linear recursive filter requires a smaller window to attain the same noise

reduction. A smaller window reduces the number of computations required for each filter output. In addition, steeper transitions between pass bands and rejection bands in the frequency response of the filter are realizable with recursive filters[24].

There are two drawbacks to the use of recursive linear filters. First, recursive filters have nonzero phase response. This is a problem, particularly in cases where edge detection is important. Edges are blurred asymmetrically and the edge position will be shifted. This problem can be easily compensated for by passing the filter over the data twice, in opposite directions. The result of passing the filter twice in opposite directions is a zero phase response and no shifting of edges[25].

Second, recursive filters have infinite impulse response (IIR)[26]. Theoretically, the output of an IIR filter passing over an edge will never reach equilibrium at that edge. In practice, however, the output can be assumed to have reached equilibrium if the output is within some arbitrary fraction of the step size. The net result is that, as the bandwidth of the recursive filter is decreased, the SNR is improved, but the filter takes longer to reach equilibrium at an edge and blurring will be severe.

Linear recursive filters are advantageous because excellent noise reduction may be obtained with a smaller window, as opposed to a linear nonrecursive filter. Also, much steeper transitions from the pass band to the rejection band are realizable with linear recursive filters. A nonzero phase response is exhibited by linear recursive filters, but this may be easily compensated for. The greatest disadvantage to linear recursive filters arises out of their IIR property. With IIR, the blurring at edges may be infinite and depends entirely on the filter bandwidth.

#### 2.2.4 Summary of Noise Reduction Methods

Of the noise reduction methods reviewed, only the median filter and its variations are effective in reducing noise while maintaining the edges in an image. In situations where the SNR is low, all the filters, including the median, fail to remove noise without blurring edges. In each case a trade-off is made between noise reduction and edge preservation. Because of its simplicity, effective noise reduction, and known, finite blurring (due to FIR) the mean filter is used in the present study.

### 2.3 Edge Enhancement Methods

The need for accurate detection of edges in digital images has led to the development of many edge enhancement methods. Because of the volume of literature on edge enhancement only a brief outline of some better known methods is given in this section. These methods are:

1. Thresholding
2. Derivative methods
3. Non-linear masks
4. Sliding statistical tests

Advantages and disadvantages of each of the edge enhancement methods are presented.

#### 2.3.1 Thresholding

Thresholding is the simplest method of edge detection. A threshold value is selected based on some a priori knowledge of the two levels which constitute the edge. Then the threshold is used to determine whether or not any individual sample is part of an object or background. Suppose an object is higher in intensity than the background. If a sample value is greater than the threshold value it is assumed that the sample lies inside

the object. Similarly, if a sample value is lower than the threshold it is assumed that the sample is in the background. As such, thresholding is not strictly edge detection or enhancement but detection of object versus nonobject data. However, since an edge is the face between object and nonobject data, thresholding can provide rudimentary edge detection.

### 2.3.2 Derivative Methods

An extensive description of derivative methods is given by Pratt[27]. Derivative methods use either the first derivative, as in the compass gradient method, or the second derivative, as with Laplacian masks, to detect edges. The derivative methods have several major handicaps. Because the derivative operators are linear, derivative methods are linear nonrecursive filters. The transfer function of a derivative filter is that of a high pass filter. For this reason derivative filters amplify high frequency noise. In particular, Laplacian filters are virtually unusable in low SNR situations.

When a noise reduction filter has been previously applied to an image, image edges are blurred. The magnitude of the derivative at a blurred edge is less than

that at a sharp edge. Therefore, gradient filters exhibit diminished performance due to blurred edges after noise reduction.

Because the compass gradient filter is used later in this thesis for comparison purposes, it is described here in some detail. The mathematical formulation of the compass gradient filter is given by

$$y_{i,j} = (x_{i,j+1} + x_{i+1,j+1} + x_{i+1,j} + x_{i+1,j-1} + x_{i,j-1}) - (x_{i-1,j+1} + x_{i-1,j} + x_{i-1,j-1} + 2x_{i,j}) \quad (2.4)$$

Equation (2.4) is for a 2D window of width 3. Figure 2.5 shows the mask of filter coefficients which are applied to a window to implement the filter. Each coefficient in the mask is used as a multiplier for the corresponding sample in the window. The direction in which edges are enhanced is indicated in Figure 2.5.

As indicated in Figure 2.5, the compass gradient filters exhibit the undesirable property of being directionally sensitive, that is, each compass gradient filter enhances edges in one particular direction only. In practice, edges may have any orientation. Normally two or more compass gradient filters sensitive to different directions must be combined to eliminate directional

sensitivity.

### 2.3.3 Nonlinear Masks

In response to the inadequacies of gradient methods, several ad hoc methods have been developed to improve the performance of edge detectors. These include the Sobel, Roberts, and Kirsch detectors which are all described by Pratt[28]. Analysis of these filters is difficult because they are all nonlinear. They eliminate some of the problems with the derivative filters. Lower noise and directional sensitivity have been achieved with these filters. The performance of these filters was analysed by Abdou and Pratt[29]. Nonlinear mask edge detectors are usually developed by some intuitive process and, therefore, may be difficult to extend to any multidimensional situation.

As with the compass gradient filter, the Sobel edge detector is used later in this thesis for comparison purposes. It is, therefore, presented here in some detail. The Sobel edge detector is defined by

$$y_{i,j} = (X^2 + Y^2)^{1/2} \quad (2.5)$$

where

$$X = (2x_{i+1,j} + x_{i+1,j+1} + x_{i+1,j-1}) - (2x_{i-1,j} + x_{i-1,j+1} + x_{i-1,j-1})$$

and

$$Y = (2x_{i,j+1} + x_{i+1,j+1} + x_{i-1,j+1}) - (2x_{i,j-1} + x_{i+1,j-1} + x_{i-1,j-1}) .$$

Equation (2.5) is for a 2D window of width 3. Figure 2.6 shows the two coefficient masks (the X mask and the Y mask) for the Sobel filter. Although one may devise schemes to extend the Sobel filter to 3D applications, this extension is arbitrary. The arbitrary nature of this extension raises the question; is the extended filter a 3D version of the 2D filter, or is it an entirely different filter. Also, it is not clear how to use different window widths with the Sobel filter. These problems make the Sobel filter inadequate for universal application.

#### 2.3.4 Sliding Statistical Tests

Sliding statistical tests use tests of statistical probability to determine edge locations. This is done by first considering each sample to be a potential edge and two windows, one on each side of the potential edge, are

examined. Some statistic from each of the two windows is compared to determine if there is some significant difference between the regions. If the difference is significant, it is concluded that an edge has been found. For each sample, a window is examined on either side of a potential edge. For example, an edge may be found by comparing the means of the two windows on either side of the edge. The comparison of means is done using the student t test[30]. Variations on this approach are numerous. Edges separating different regions of texture can found by comparing variance or some other indicator of texture and testing for the significance of the difference. Similar work has been presented by Bovik, Huang and Munson[31].

The major disadvantage to this method is that the filters are sensitive to edge orientation. DeSouza[32] only demonstrates his work in 1D profiles of an image. In multidimensional images the two windows for the statistical tests must be reoriented to find edges of different orientation. In 3D, with the number of possible edge orientations, this becomes impractical.

### 2.3.5 Summary of Edge Enhancement Methods

For high SNR cases, thresholding is the simplest and most effective method of edge detection. When the SNR is low, edge enhancement filters must be used. Derivative filters suffer from either too much directional sensitivity, as with the compass gradient, or too much susceptibility to noise, as with the Laplacian operator. Nonlinear operators exhibit good characteristics for edge enhancement, but are not easily extended or modified as applications change. Sliding statistical tests are effective edge enhancers but, as with the compass gradient, they are too sensitive to edge orientation.

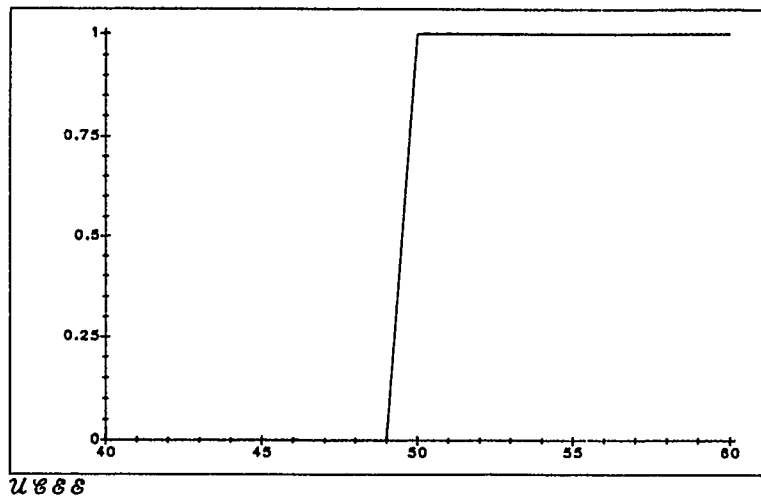
What is needed is an edge enhancer that is not sensitive to edge orientation, not overly susceptible to noise, and is easily extended to any multidimensional application. Such a filter is the variance filter. The variance filter, presented later in this thesis, meets all these needs.

## 2.4 Summary of Noise Reduction and Edge

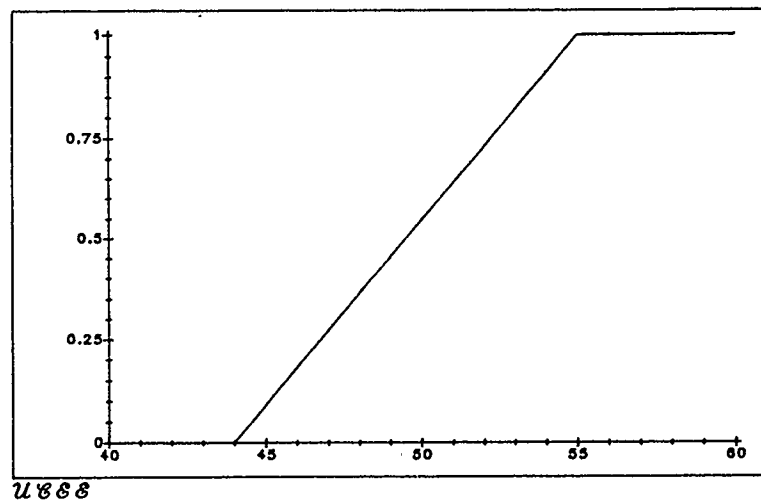
### Enhancement Methods

While the median filter is able to reduce noise without blurring edges in high SNR cases, in low SNR cases it cannot avoid blurring edges. It must be concluded then that of all the noise reduction methods presented, each is equal in low SNR applications. Because of its simplicity and finite edge blurring, the mean filter is the noise reduction method applied through the remainder of this thesis.

Of the edge enhancers presented here, all exhibited some property which made them good edge detectors, but all were limited in some respect. This conclusion led to the author's development of the variance filter as an edge enhancer. The variance filter exhibits an excellent blend of all the desirable edge detector properties. Chapter 3 goes on to analyse the variance filter and show why it should be used in edge enhancement.



(a)



(b)

Figure 2.1 Demonstration of mean filter blurring  
(a) original 1D signal with a sharp edge  
(b) mean filtered (width = 11) signal with blurring

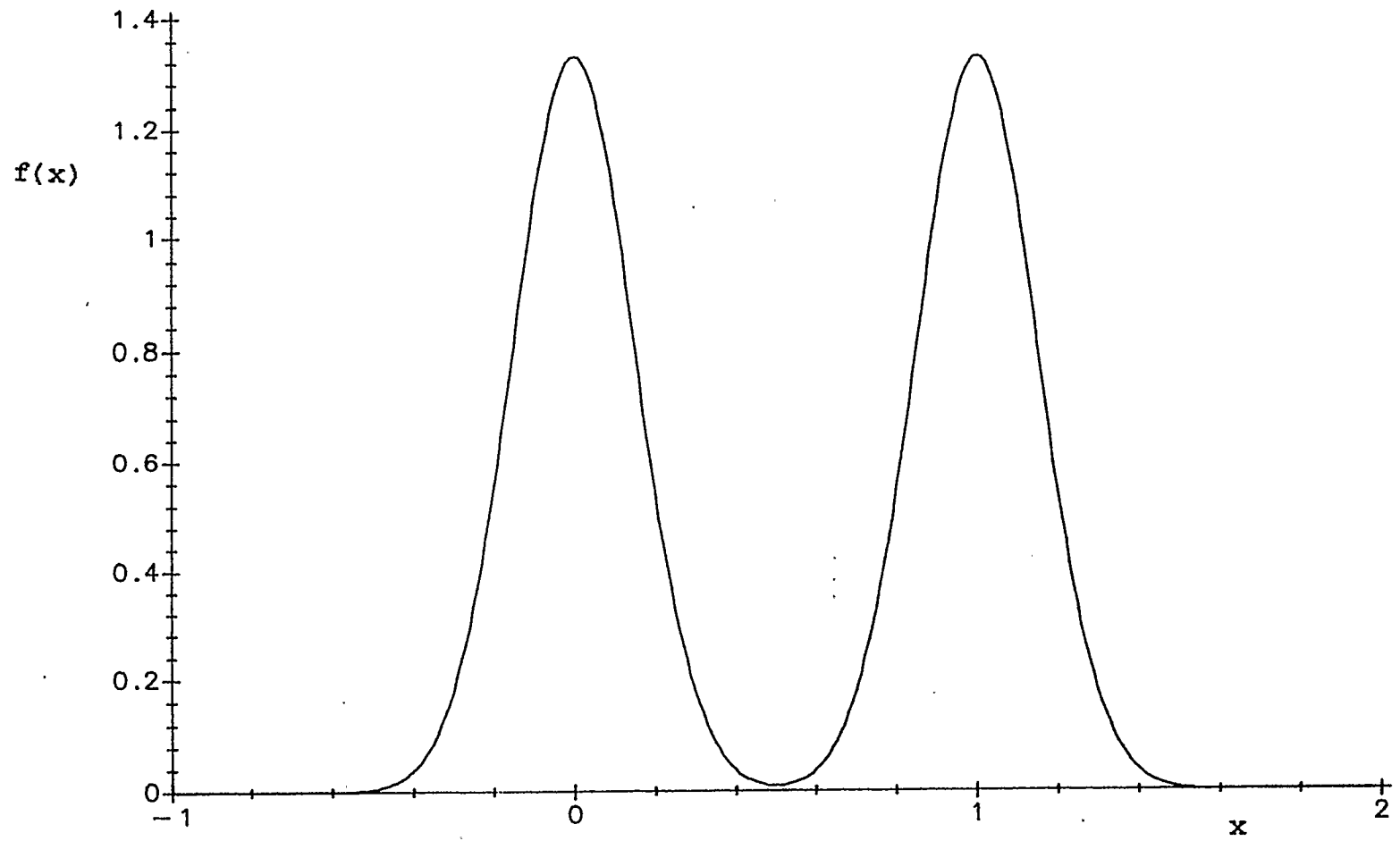


Figure 2.2 Bimodal probability density function  
( $\sigma = 0.15$ )

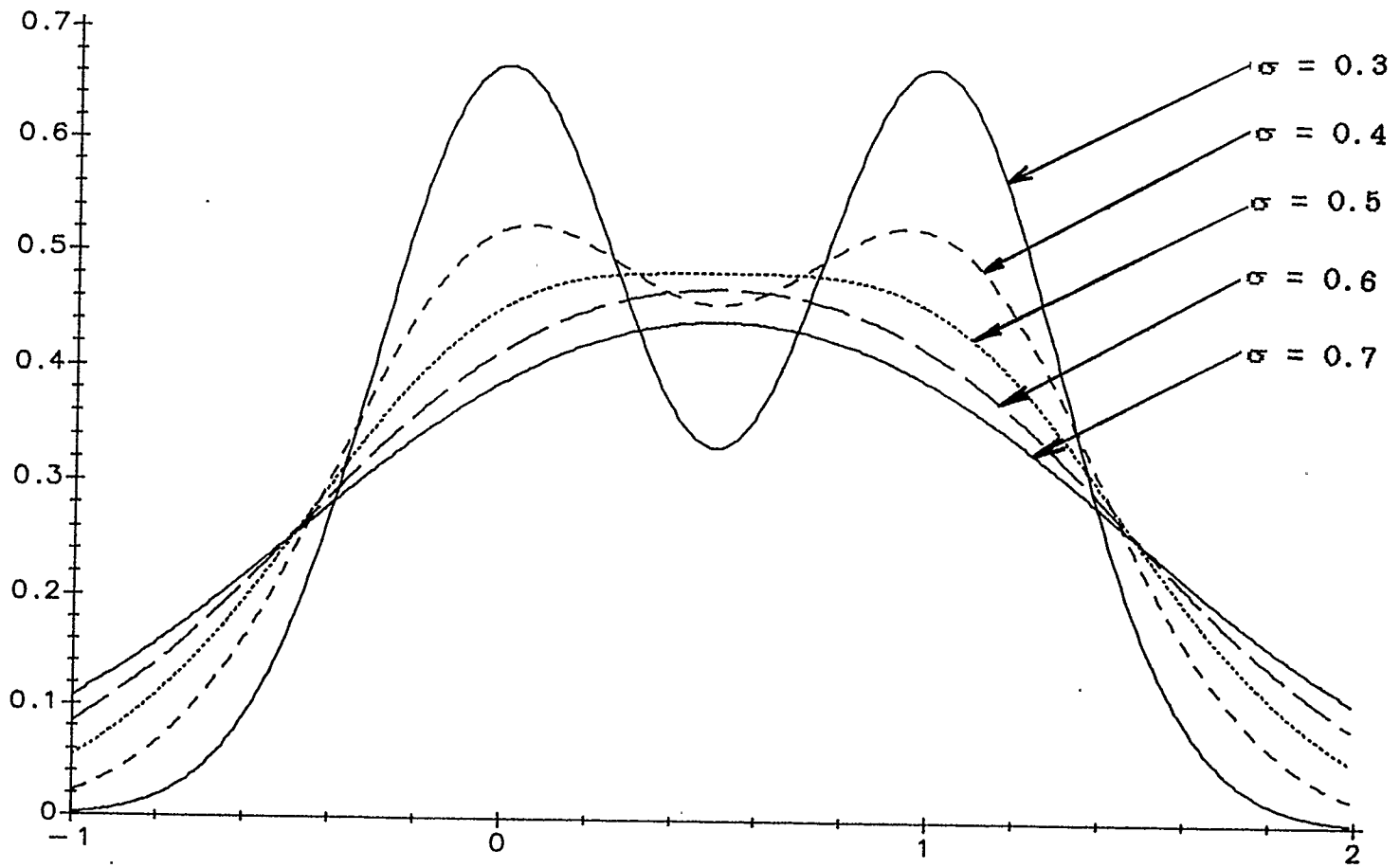
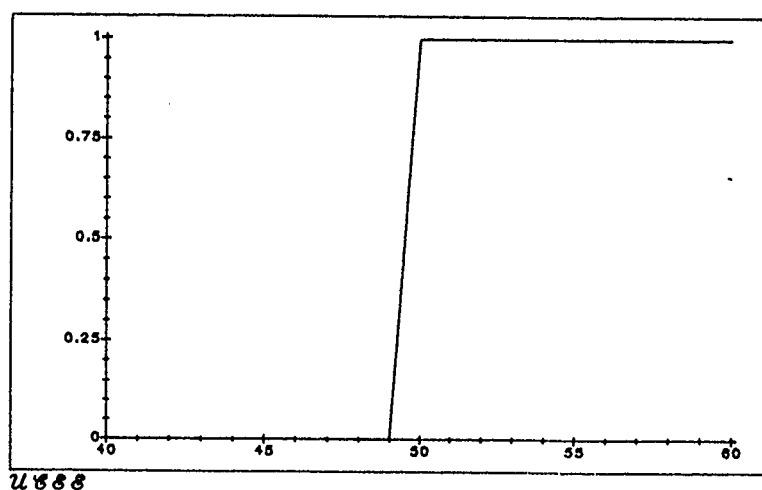
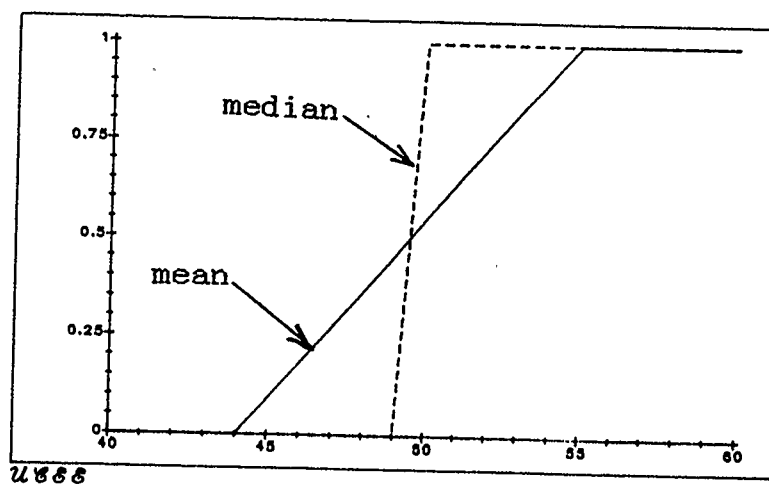


Figure 2.3 Bimodal probability density function for varying standard deviation

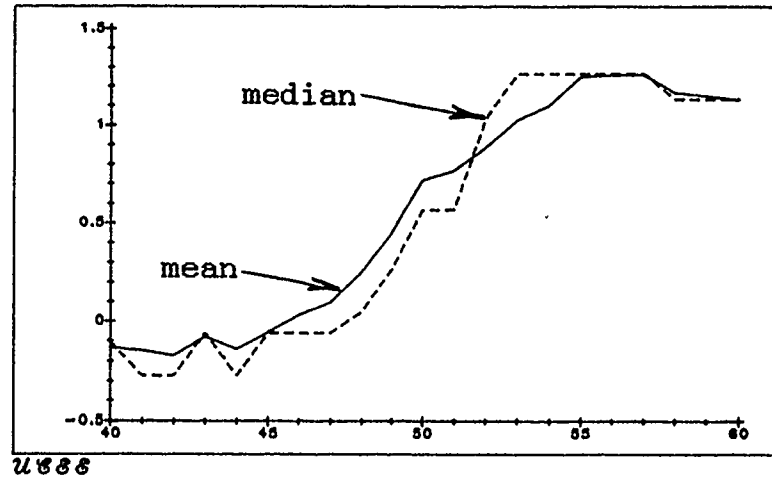


(a)



(b)

Figure 2.4 Comparison of mean and median filtering  
 (a) original 1D signal with a sharp edge  
 (b) signal after mean and median filtering  
 (c) signal after addition of noise ( $\sigma = 0.5$ )  
 and mean and median filtering



(c)

Figure 2.4 (continued)

|    |    |   |                     |
|----|----|---|---------------------|
| -1 | 1  | 1 | enhances positive   |
| -1 | -2 | 1 | edge transitions in |
| -1 | 1  | 1 | this direction      |

—————→

Figure 2.5 Gradient filter mask

| X mask |   |   | Y mask |    |    |
|--------|---|---|--------|----|----|
| -1     | 0 | 1 | -1     | -2 | -1 |
| -2     | 0 | 2 | 0      | 0  | 0  |
| -1     | 0 | 1 | 1      | 2  | 1  |

Sobel operator =  $(X^2 + Y^2)^{1/2}$

Figure 2.6 Sobel filter masks

## Chapter 3

A VARIANCE FILTER FOR EDGE ENHANCEMENT3.1 Introduction

From Chapter 2 it can be seen that each of the presently used edge enhancers has some shortcoming. Although each edge enhancer exhibits some desirable property, some method which combines all these properties into one filter is beneficial. At this point the variance filter is introduced as an edge enhancement filter because it accomplishes this blend of desirable edge enhancement properties.

The variance filter follows the same basic filtering operation as other filters presented so far. In this case the filtering function is nonlinear and it is used nonrecursively. The variance filter is given mathematically by

$$y_{i,j} = \text{variance}(x_{l,m} \mid x_{l,m} \text{ is in } w_{i,j}) \quad (3.1)$$

Each sample in the output image is an estimate of the variance of the corresponding input sample. In image regions where there are no edges, this estimate would

correspond to an estimate of the noise in the image. At an edge, however, the estimate is distorted. It is this distortion or inaccuracy which allows the variance to enhance edges. Since the variance can be calculated for any set of samples, arranged in any order, the variance filter is applicable to windows of any shape, size, or dimension. The indifference of the variance towards the order of samples leads to the filter being isotropic. It is the variance filter's universal applicability which makes it well suited to 3D applications and the comparison of 2D and 3D filtering.

The variance filter as an edge enhancer is analysed in two ways. First, in Section 3.2, it is analysed independently of other filters to determine SNR limitations for accurate edge detection. Second, in Section 3.3, the filter is compared to two common edge detectors.

### 3.2 Variance Filter Limitations Imposed by Noise

In order to know the limitations of the variance filter with respect to SNR, the effects of edge blurring and additive noise on window variance must be understood. This section illustrates these effects on variance. It is shown how the chi-square,  $\chi^2$ , distribution can be used in

conjunction with an understanding of blurring and noise effects to determine the filter's limitations.

### 3.2.1 Effect of Blurring on Window Variance

In order to improve edge enhancement, an image may be prefiltered to reduce noise. Since noise reduction filters have the property of blurring edges, it is important to understand what effect the blurring has on the variance at an edge.

Because blurring takes place only at edges, a window placed symmetrically across an edge is examined. The edge is of unit height and the symmetrical placement ensures that half of the window's samples are on the high side of the edge and the other half on the low side. Initially, it is assumed that there is no noise on the signal. With no prefiltering, the histogram of the samples in the window is shown in Figure 3.1. The equation for the variance,  $\sigma^2$ , of a variable,  $x$ , is given by

$$\sigma^2 = \frac{1}{N}\sum x^2 - \left(\frac{1}{N}\sum x\right)^2 \quad (3.2)$$

Applying equation(3.2) to the data of Figure 3.1 yields

$$\sigma^2 = 0.25 . \quad (3.3)$$

Therefore, the maximum possible variance for an edge of unit size is 0.25.

If the edge is blurred, the variance for the window decreases. Let  $\alpha$  be the number of discrete levels in the histogram for a window at an edge. It is assumed that the samples are distributed evenly among the discrete levels. For example, in the ideal case (Figure 3.1) there are two discrete levels with the samples evenly distributed between them. In this case  $\alpha=2$ . Figure 3.2 shows examples of histograms with  $\alpha=5$ , and  $\alpha=10$ . Such histograms result from prefiltering and  $\alpha$  is a blurring parameter. The worst case for the variance filter occurs when the samples are evenly distributed among the possible values. Data from a window with a specified value for  $\alpha$  are used to calculate  $\sigma^2$  using Equation(3.2). Therefore, it is possible to plot variance versus the blurring parameter,  $\alpha$ . This is shown in Figure 3.3. Note that the variance depends only on the shape of the distribution, not  $N$ , the number of samples in it.

Figure 3.3 is useful because it predicts the value of the peak variance after blurring. The shape of the curve indicates that after the blurring parameter is increased to approximately  $\alpha=10$ , there is little change in the variance with increased blurring. In fact, the variance is limited to about  $\sigma^2=0.08$  for any blurring above  $\alpha=20$ . Thus, with

either a 2D filter of width 5 (i.e.  $\alpha=25$ ), or a 3D filter of width 5 (i.e.  $\alpha=125$ ), the expected variance at an edge is approximately 0.08.

### 3.2.2 Effect of Noise on Variance

So far only the case of no noise has been examined. The variance for a signal with noise can be expressed by modifying equation(3.2). In the following equations the subscript 's' refers to the signal, the subscript 'n' refers to the noise. The modification of equation(3.2) yields

$$\sigma^2 = \frac{1}{N} \sum (x_s + x_n)^2 - \left[ \frac{1}{N} \sum (x_s + x_n) \right]^2 \quad (3.4)$$

Equation (3.4) expands to

$$\sigma^2 = \frac{1}{N} \sum x_s^2 - \left( \frac{1}{N} \sum x_s \right)^2 + \frac{1}{N} \sum x_n^2 - \left( \frac{1}{N} \sum x_n \right)^2 + \frac{2}{N} \sum x_s x_n - 2 \frac{1}{N} \sum x_s \sum x_n \quad (3.5)$$

The first and second terms of Equation(3.5) form the variance of the signal and the third and fourth terms form the variance of the noise. The fifth term is the correlation of the signal to the noise. Since the signal and noise are normally statistically independent this correlation may be assumed to be zero. The mean of the noise, and hence the summation of the noise, is expected to

be zero so the sixth term may also be assumed to be zero.

Thus Equation(3.5) reduces to

$$\sigma^2 = \sigma_s^2 + \sigma_n^2 . \quad (3.6)$$

Equation(3.6) states that if the noise is not correlated to the signal, the variance of a signal obscured by noise is equal to the sum of the variance of the signal and the variance of the noise. Thus, peaks in the variance due to edges in the signal are still peaks when noise is added. However, there is some degree of uncertainty in the peak and noise variances. This uncertainty leads to the obscuring of variance peaks when the noise level is high, as is shown in the following sections.

### 3.2.3 Confidence of Variance Estimate

As with the mean, the variance calculated for a window is only an estimate of variance in that region. The degree of confidence in the variance estimate, is defined by the chi-square ( $\chi^2$ ) distribution. The  $\chi^2$  distribution is a probability function and defines a confidence interval for an estimated variance based on that estimate and the degrees of freedom used to calculate it[33]. For example, a 90 percent confidence interval for  $\sigma^2$  is defined by

$$\frac{S^2}{\chi_{5\%}^2/df} < \sigma^2 < \frac{S^2}{\chi_{95\%}^2/df}, \quad (3.7)$$

where  $df$  is the number of degrees of freedom, and  $S^2$  is the estimate of the variance. The number of degrees of freedom is equal to the number of samples in the estimate minus one. The  $\chi^2/df$  distribution is shown in Figure 3.4 for three values of  $df$ . In Figure 3.4, the function  $f(\chi^2)$  refers to the probability distribution, or the probability density function, of the  $\chi^2$  variable. For convenience, tables are normally used when working with the  $\chi^2$  distribution. An example of such tables is shown in Dixon and Massey[34]. As an example, if one were to estimate the variance at a particular pixel with a 2D window of width 5, there would be 25 samples in the estimate, and 24 degrees of freedom. From a  $\chi^2/df$  distribution table the calculated 95 percent confidence interval is

$$\frac{s^2}{1.64} < \sigma^2 < \frac{s^2}{0.517} \quad (3.8)$$

This means that one is 95 percent confident that the actual variance,  $\sigma^2$ , for this window lies between these two limits.

#### 3.2.4 Maximum Noise for Accurate Edge Detection

At this point all the information has been presented to allow the calculation of the maximum noise with accurate edge detection. The output of the variance can be divided into two regions: 1) background, regions where no edge is present, and 2) peaks, regions where an edge is present. So long as the values of the variance peaks are greater than the background values, edge detection is possible. When background values are as great as peak values, errors in edge detection occur. Figure 3.5 shows a typical profile of the variance filter output. The confidence intervals for the peak variance and the background variance are also shown in Figure 3.5. When the two confidence intervals do not overlap, the background is not likely to vary higher than the peak; edge detection is possible. If the intervals do overlap, background samples may be

mistaken for peak samples and errors in edge detection will occur. The limiting case occurs when the gap between the two confidence intervals equals zero.

The background variance is the variance of the noise after prefiltering and the peak variance is the variance at the edge plus the background variance. Therefore, the difference between the peak variance and the background variance is the variance of the step. As indicated in Equation(3.7), a multiplier based on the  $\chi^2/df$  distribution is applied to the variance estimate to establish a confidence interval. Let U and L be these multipliers for the upper and lower limits of the confidence interval. The limiting case for noise, when the gap between the background and peak confidence intervals is zero, is then expressed by

$$L(\sigma_n^2 + \sigma_{\text{step}}^2) = U(\sigma_n^2) . \quad (3.9)$$

Rearranging Equation(3.9) yields

$$\sigma_n^2 = \frac{\sigma_{\text{step}}^2}{(U/L - 1)} . \quad (3.10)$$

Note that in Equation (3.10)  $\sigma_n^2$  represents the noise energy in the image after prefiltering. If a mean filter is used

for prefiltering, noise energy before mean filtering is given by

$$\sigma_{in}^2 = N \sigma_n^2, \quad (3.11)$$

which is simply another way of stating Equation(2.2). Equation(3.10) is used to calculate the maximum allowable noise after prefiltering. The maximum noise before prefiltering is then calculated from Equation(3.11).

An example using an edge of unit height is presented here. If a 2D filter of width 5 is used the number of pixels in the window,  $N$ , is 25 and the number of degrees of freedom,  $df$ , is 24. From a  $\chi^2/df$  table,  $U$  and  $L$  can be found for a confidence interval of 90 percent. The size of the confidence interval chosen here is arbitrary. Figure 3.3 indicates that the expected variance at the step is 0.08. Application of equation(3.10) shows that the maximum allowed noise variance before prefiltering is 0.049. If the image is prefiltered with a mean filter, the allowed noise before prefiltering is calculated with Equation(3.11). The maximum allowable noise increases by a factor of  $N=25$ , yielding a value of 1.225 for the noise variance.

The selection of the confidence interval affects the

result of the above calculation. In the above example the confidence interval was 90 percent. This means that the probability of classifying a peak as background was 0.05 and the probability of classifying a background sample as a peak was 0.05. The probability of making an error is the combined probability of making each type of error. For the above example we get

$$p(\text{error}) = 0.05 + 0.05 - (0.05)(0.05) = 0.0975, \quad (3.12)$$

that is, the probability of making an error at an edge with the input noise at the defined limit is 9.75 percent.

The selection of the confidence interval is arbitrary. It was found during the testing presented in Chapter 4 that a confidence interval of 90 percent yields results which corresponded well to the observed practical limits.

### 3.2.5 Advantages of 3D Processing

At this point it should be apparent that it is better to process image data in 3D wherever possible. Two effects lead to this conclusion. Firstly, increased window size yields better filtering results. Secondly, a greater

filter width causes more blurring and distortion of edges. 3D processing takes advantage of an extra dimension in the data to increase window size and reduce window width.

To illustrate briefly, suppose that one were to filter a signal to reduce the noise variance by a factor of approximately 120. If the signal is processed in 1D, a window exactly 120 samples long is required and edges are blurred by this amount. However, in 2D a window of width 11 contains 121 pixels and edges are blurred by approximately 11 pixels. Continuing to 3D, a window of width 5 contains 125 voxels and blurs edges by approximately 5 voxels. Thus, as the number of dimensions increases, window width and blurring decrease while maintaining the same level of noise reduction.

In general, it may be concluded that as many dimensions as possible should be used in processing images.

### 3.2.6 Summary of Noise Limitations

The effects of blurring and noise on the variance filter have been shown analytically. In conjunction with the  $\chi^2$  distribution, these effects can be used to calculate

the noise limitations of the variance filter. The analysis presented demonstrates the advantages to processing data in 3D rather than 2D.

### 3.3 Comparison of Edge Enhancers

Abdou and Pratt[35] used the following criteria in comparing the performance of edge enhancers:

1. Directional sensitivity
2. Decay of filter output as a function of distance from edge
3. Probability of true detection versus a false detection

Each criterion is described in this section, along with its application to the variance filter. The criteria are used to compare the variance filter to the compass gradient and Sobel edge enhancers. Since current literature deals primarily with 2D filters of width 3, it is this configuration that is used throughout this section. This restriction is also necessary because the Sobel edge enhancer is a 2D width 3 filter and is not easily modified.

### 3.3.1 Directional Sensitivity

The evaluation of directional sensitivity of edge detectors is done using a plot of the filter output versus the orientation of the edge. The window is assumed to be centred over a sharp edge. The intensity of each pixel in the window is the fraction of that pixel which is on the high intensity side of the edge. The derivation of pixel intensities is shown in Figure 3.6[36].

Ideally the variance filter would exhibit zero directional sensitivity, that is, the variance filter is isotropic. However, because of the nature of sampled multidimensional data there is some directional sensitivity. This is entirely due to edges not lining up with the orientation of the axes used for sampling. A graph showing the output of the variance filter versus the orientation of the edge is in Figure 3.7. The values of the filter output are normalized to the output at zero degrees orientation for comparison purposes.

### 3.3.2 Filter Decay

Filter decay is evaluated with a plot of filter output versus the distance of the edge from the centre of the window. As with the orientation test, pixel intensities are equal to the fraction of the pixel which lies on the high intensity side of the edge. Because of the nature of sampled data the output of the variance filter decays differently depending upon the direction of the decay. Therefore, two plots are used, one using the distance from a vertical edge, and one using the distance from a diagonal edge. Figure 3.8 shows how these distances are calculated[37].

Two curves depicting the decay of the variance filter output are shown in Figure 3.9. In Figure 3.9, the vertical edge decay is shown as having a peak when the variance is offset half a pixel from the edge. This is because, in this case, the edge falls directly between pixels. In the case of the diagonal edge, it is not possible for the edge to lie exactly between pixels. If the edge does not fall directly between pixels then the edge is blurred during sampling and the variance output is reduced. For this reason, the peak seen for the vertical edge is not observed for the diagonal edge.

### 3.3.3 Probability of Detection of Edges

The performance indicators discussed so far do not include the accuracy of detection given specific noise conditions. In order to evaluate the accuracy of detection, a plot of probability of correct detection versus probability of false detection is used. This plot is generated from probability distributions of the variance (or other edge enhancer) on the background and the variance at an edge. Figure 3.10 shows a sketch of the probability density functions for the variance in edge and no-edge regions. Also illustrated in Figure 3.10 is an arbitrary threshold. Probabilities of detection and false detection are calculated based on this threshold. The probability of detection is given by

$$P_d = p(\sigma^2 > \text{threshold} \mid \text{edge}) , \quad (3.13)$$

and the probability of false detection is given by

$$P_f = p(\sigma^2 > \text{threshold} \mid \text{no edge}) . \quad (3.14)$$

By varying the threshold throughout the range of the two distributions, and calculating the probabilities for each threshold, a set of points on a probability of detection versus probability of false detection curve is generated.

Since the probability distribution of the variance is

well known and given by the  $\chi^2$  distribution this probability curve can be generated analytically. This is not true of all edge enhancers, but the probability curve may be generated numerically. The numerical method can be used for any edge enhancement method and is therefore used for comparison purposes.

The numerical evaluation works as follows.

1. Generate a histogram for the edge detector applied to sample background windows.
2. Generate a histogram for the edge detector applied to sample edge windows.
3. The histograms are numerical approximations to the probability distribution of the edge detector.
4. Pass a threshold through the histograms and at each threshold calculate the probability of detection and the probability of false detection as given by equations(3.13) and (3.14).
5. Plot the probability of detection versus the probability of false detection.

The background sample windows were generated by adding normally distributed noise of a known standard deviation to a constant level of zero. The two different sample windows used for edges are:

1. Smooth vertical edge
2. Smooth diagonal edge

The sample windows are shown in Figure 3.11. Noise of a known standard deviation was added to each of the above windows.

Figure 3.12 shows the probability plots for the variance filter with a SNR of 10, applied to each of the two edge windows. It should be noted that the two curves lie virtually on top of each other, indicative of the isotropic nature of the variance filter. The selection of a SNR of 10 is arbitrary and may be any value, so long as it remains consistent for comparison purposes.

#### 3.3.4 Comparison of Edge Enhancers

Figures 3.13 and 3.14 compare the variance filter with the compass gradient and Sobel edge enhancers using the sensitivity to orientation and decay performance indicators. As presented, the Sobel enhancer exhibits the

lowest sensitivity to orientation. However, the square of the Sobel enhancer has the same sensitivity as the variance filter. This is perhaps a fairer comparison, since the variance does not apply a square root operator. The small amount of sensitivity that is exhibited by the variance arises from the sampled nature of the data.

The decay of most of the edge detectors is nearly the same. Decay depends upon the window width for all the filters and consequently, there is little information of value here, other than that the variance filter behaves as the others do in this respect.

The comparison of probability of detection plots is the most revealing of the comparisons. Two separate plots are used to compare the probability of detection. These plots are in Figure 3.15 and compare the variance, Sobel, and compass gradient enhancers for each of the two edge windows described in Section 3.3.3.

From Figure 3.15 it can be seen that the variance filter exhibits good edge enhancement properties, is only marginally poorer than the Sobel filter, and is better than the compass gradient filter. Thus the primary advantages to the variance filter are its isotropic nature and its versatility.

### 3.3.5 Summary of Edge Enhancer Comparison

It has been shown that the primary reasons for using a variance filter are 1) its low sensitivity to edge orientation, and 2) its versatility. If one were to filter only in 2D there are better alternatives to the variance filter, but, having demonstrated the advantages to filtering in 3D, the property of versatility becomes important. It is this property which makes the variance filter an excellent choice for examining 3D processing.

### 3.4 Summary of Variance Analysis

A method for calculating the noise limits for variance filter edge detection has been established. The variance filter has been compared to two common edge enhancers using the criteria of sensitivity to edge orientation, filter decay, and probability of detection. This comparison has shown the validity of the variance filter as an edge enhancer in 3D applications. In Chapter 4 the variance filter used in combination with the mean filter is tested with artificially generated images. The analysis presented here is supported by the test results and the advantages of 3D processing are further demonstrated.

frequency of  
occurrences of  $x$

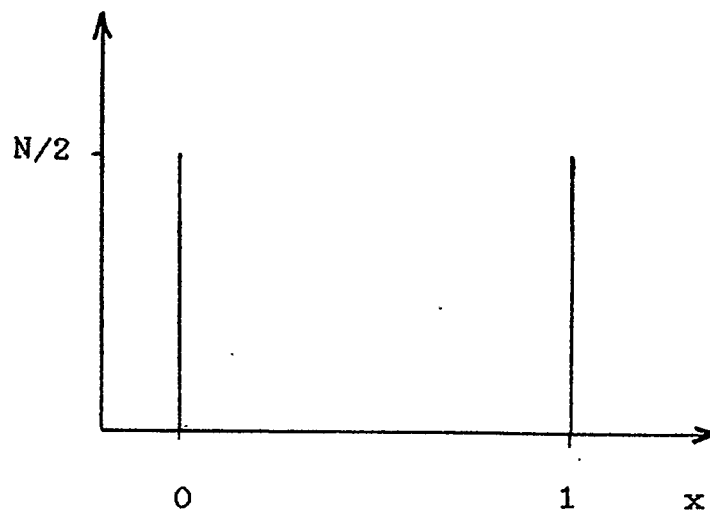
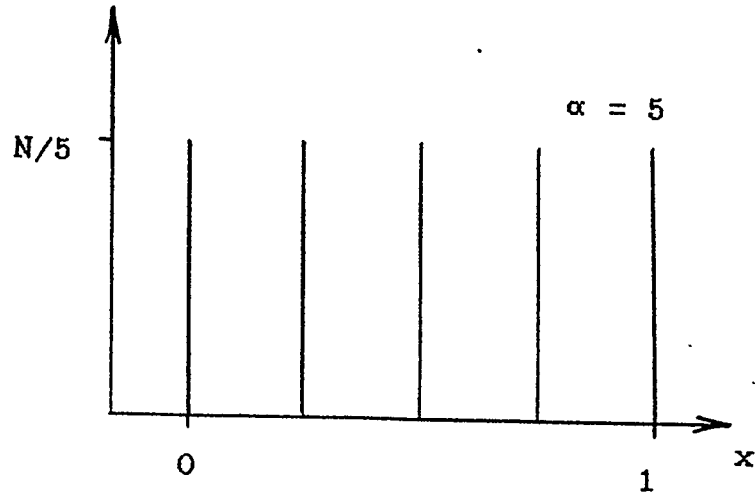


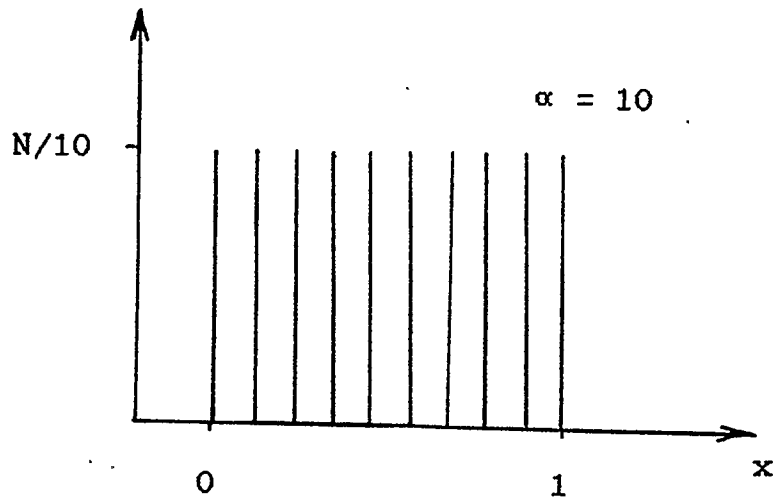
Figure 3.1 Histogram for samples in a window with no blurring

frequency of  
occurrences of  $x$



(a)

frequency of  
occurrences of  $x$



(b)

Figure 3.2 Histogram for samples in windows at an edge with blurring parameter (a)  $\alpha = 5$ , and (b)  $\alpha = 10$ .

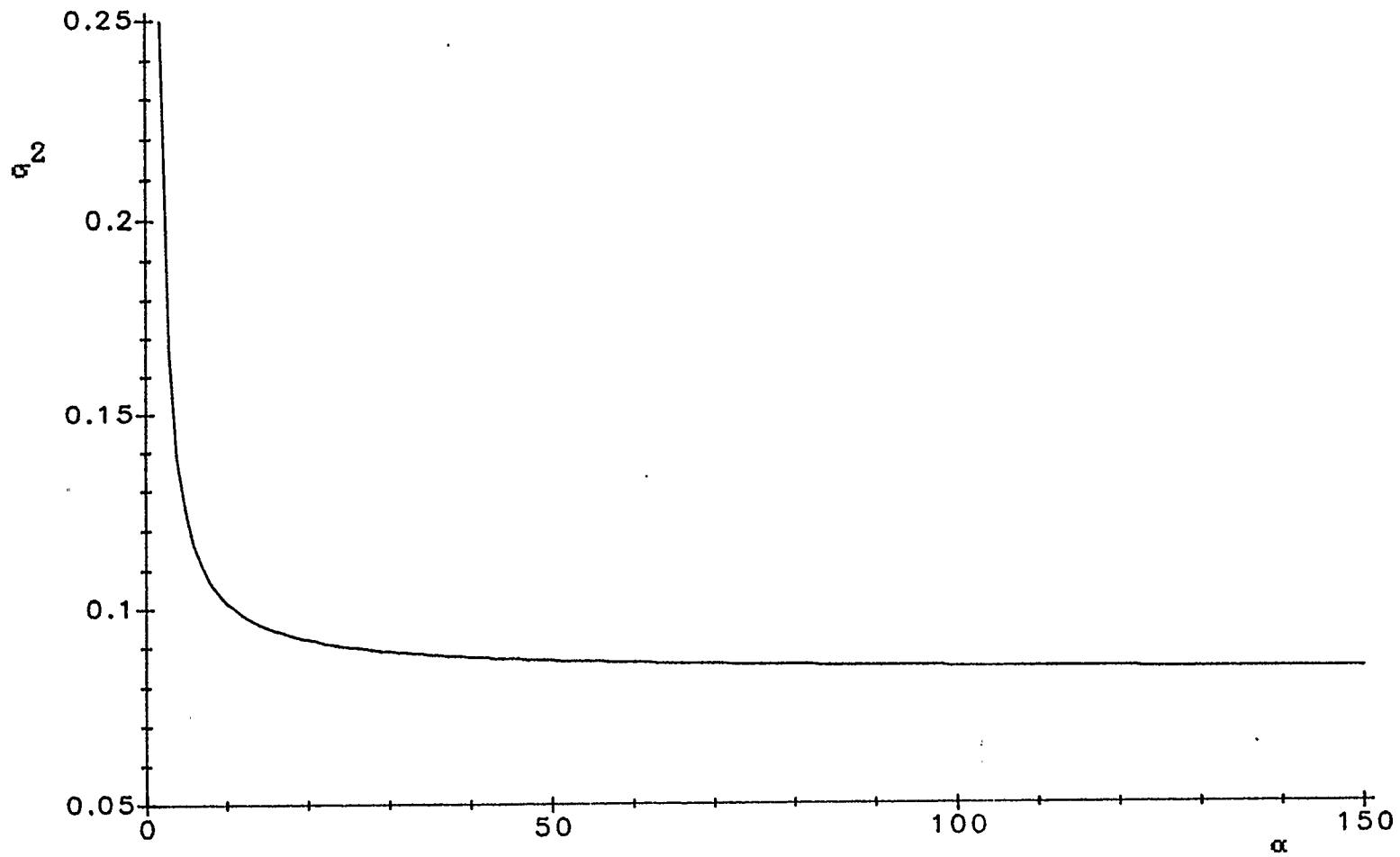


Figure 3.3 Variance versus blurring parameter,  $\alpha$

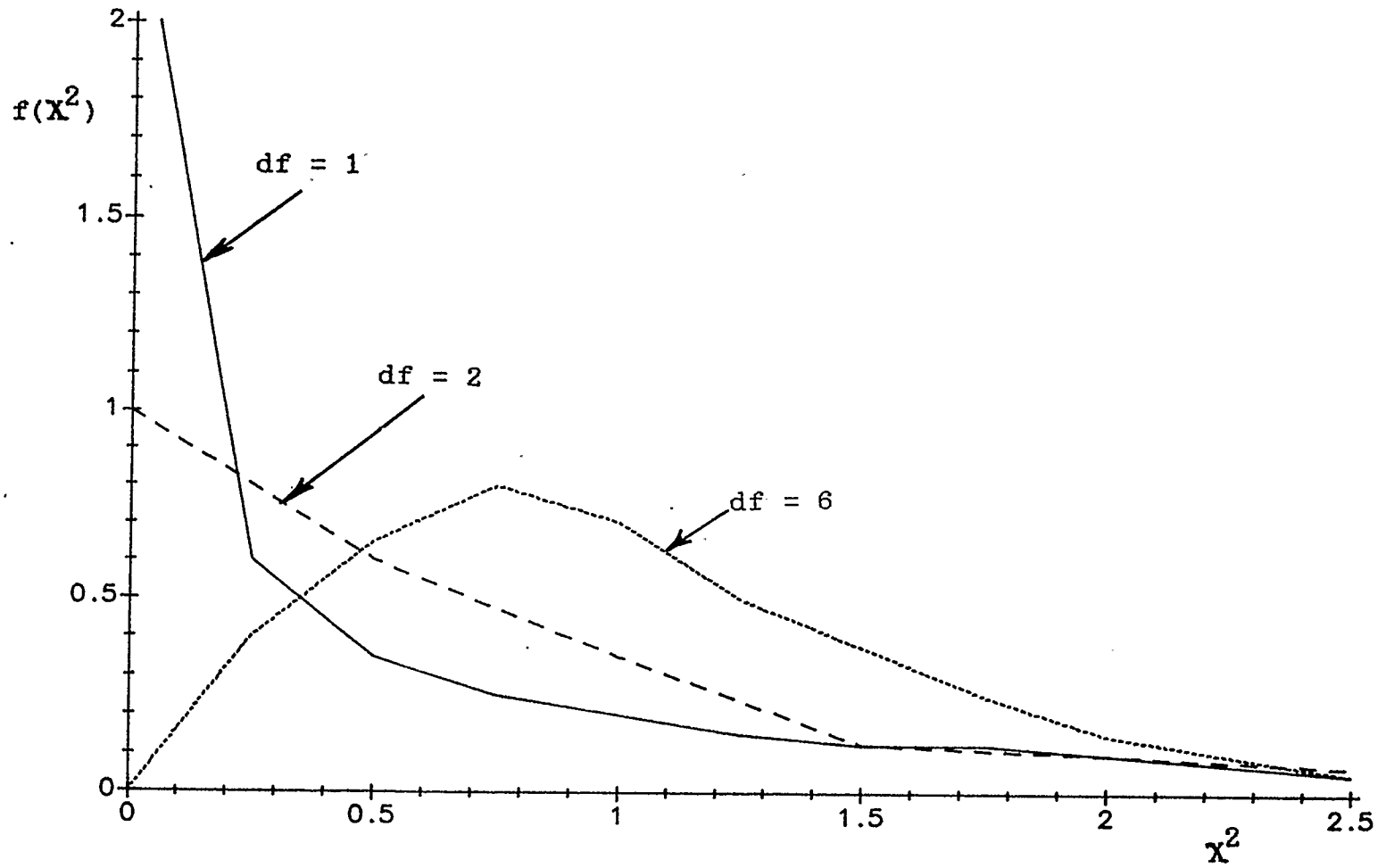


Figure 3.4 Probability density function for  $\chi^2/df$  for varying  $df$ .

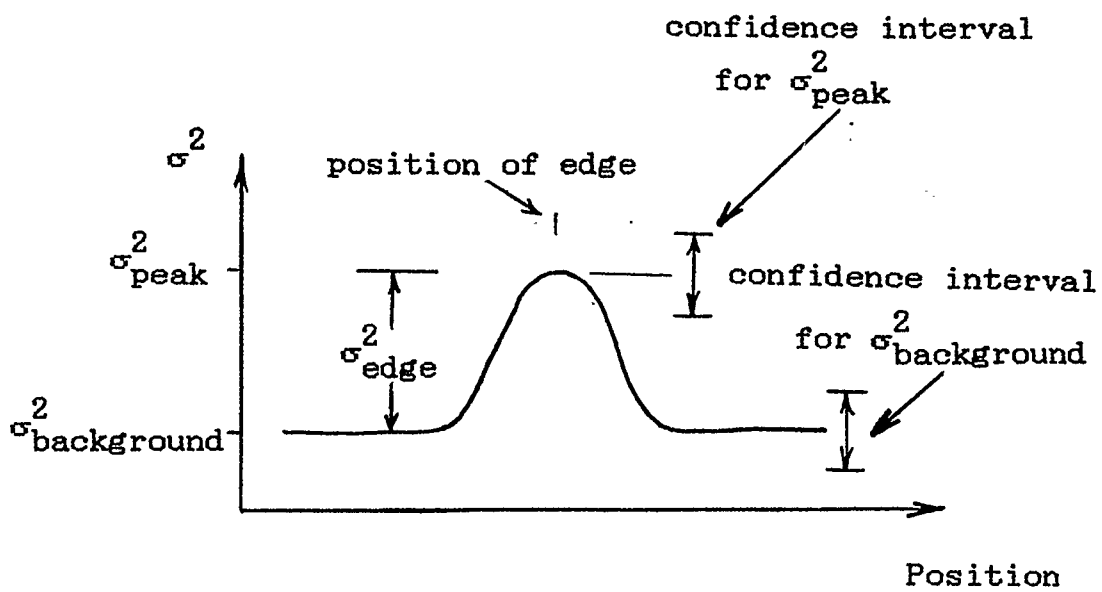
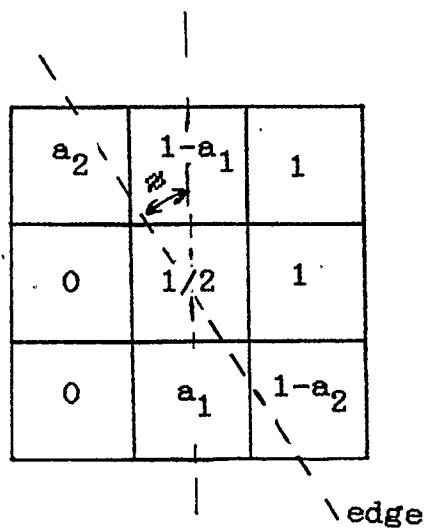


Figure 3.5 Profile of the output of the variance filter



when  
 $0 < \phi < \tan^{-1}(1/3),$

$$\begin{aligned} a_1 &= 1/2 - \tan(\phi) \\ a_2 &= 0 \end{aligned}$$

when  
 $\tan^{-1}(1/3) < \phi < \pi/4,$

$$\begin{aligned} a_1 &= (1 - \tan \phi)^2 / (8 \tan \phi) \\ a_2 &= (3 \tan \phi - 1)^2 / (8 \tan \phi) \end{aligned}$$

Figure 3.6 Derivation of pixel intensities for directional sensitivity.

normalized variance :  
output.

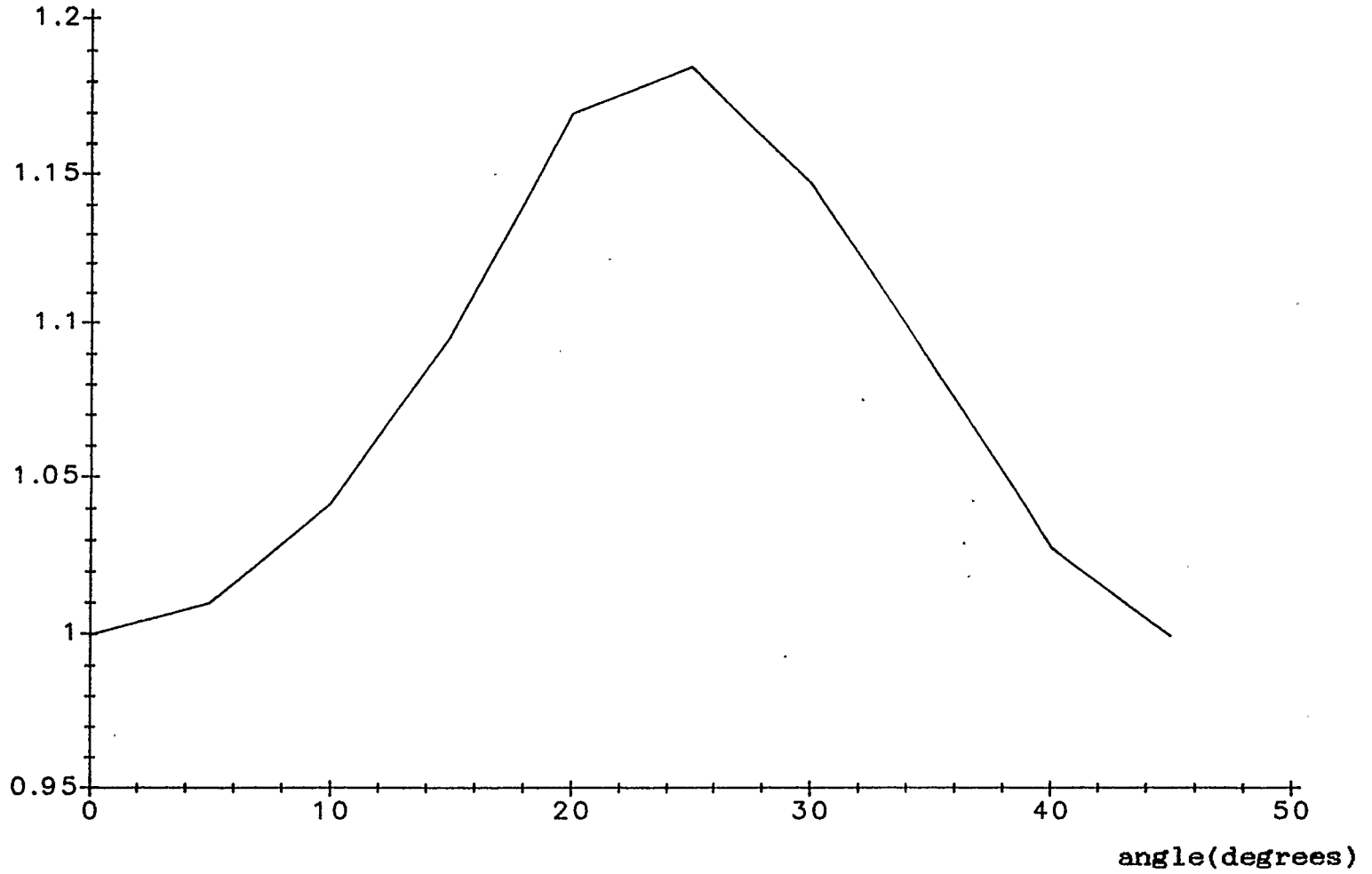


Figure 3.7 Directional sensitivity characteristic for the variance filter (normalized)

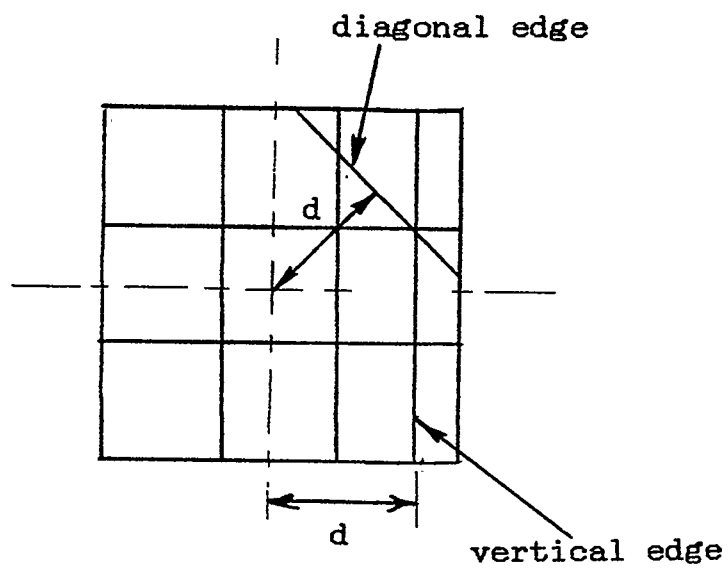


Figure 3.8 Calculation of distances for filter decay

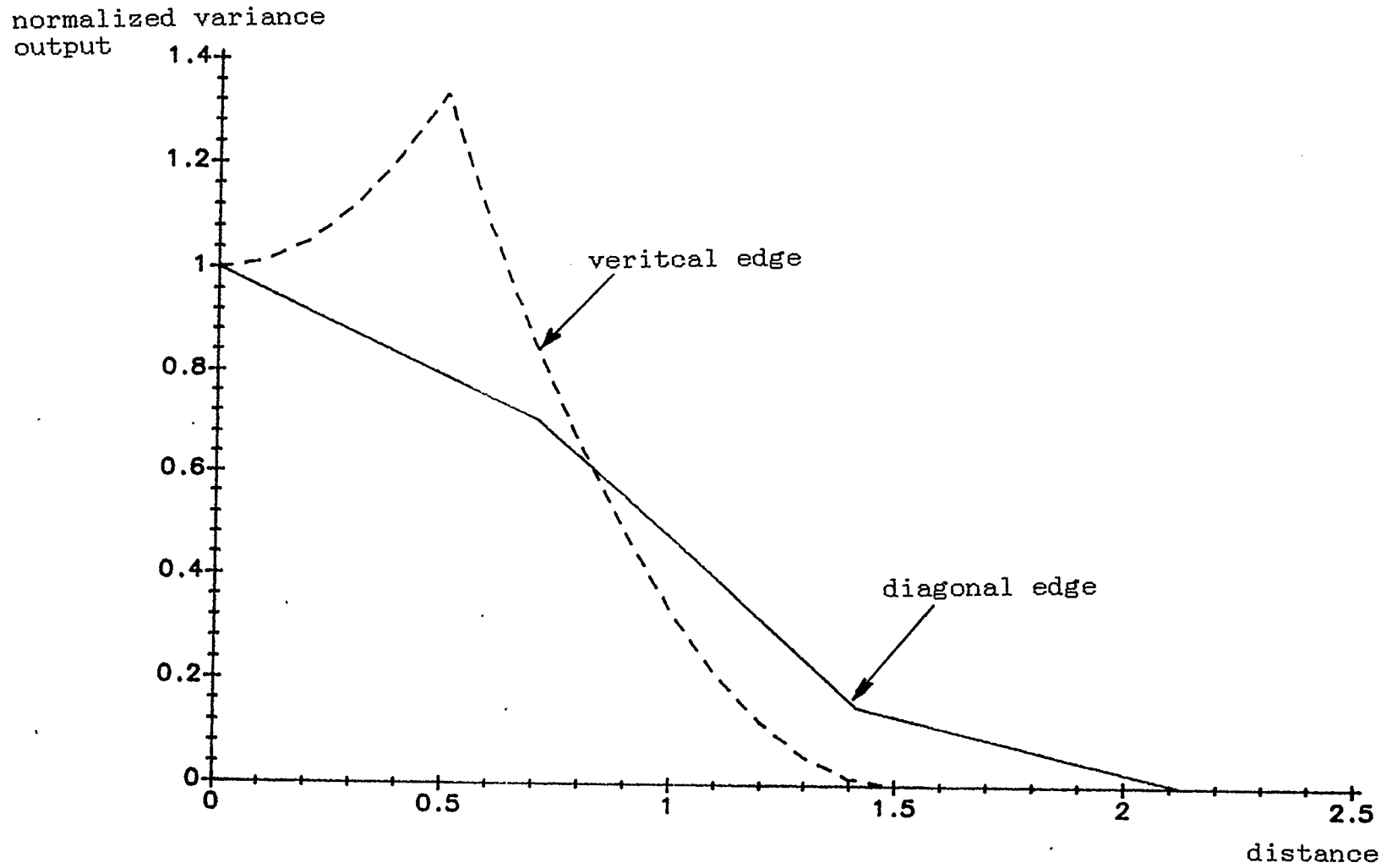


Figure 3.9 Filter decay characteristic for the variance filter (normalized)

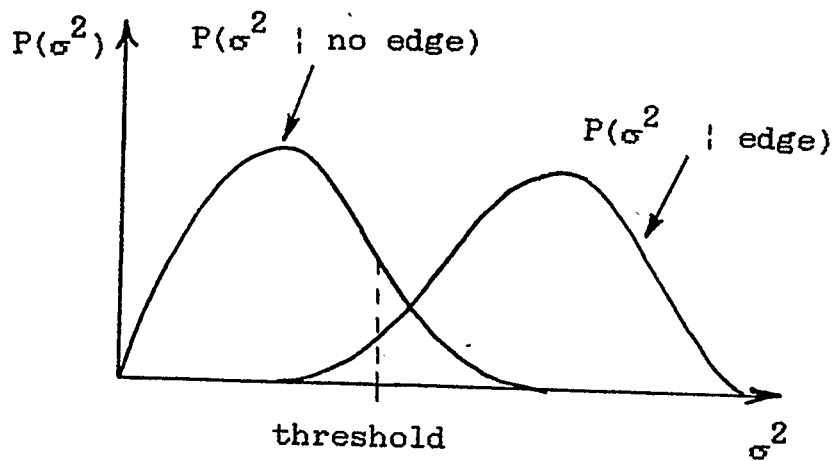


Figure 3.10 Probability density functions for the variance filter output in edge and no edge regions.

|   |     |   |
|---|-----|---|
| 0 | 0.5 | 1 |
| 0 | 0.5 | 1 |
| 0 | 0.5 | 1 |

(a)

|     |     |     |
|-----|-----|-----|
| 0.5 | 1   | 1   |
| 0   | 0.5 | 1   |
| 0   | 0   | 0.5 |

(b)

Figure 3.11 Test windows for calculation of probability characteristics  
(a) vertical edge  
(b) diagonal edge

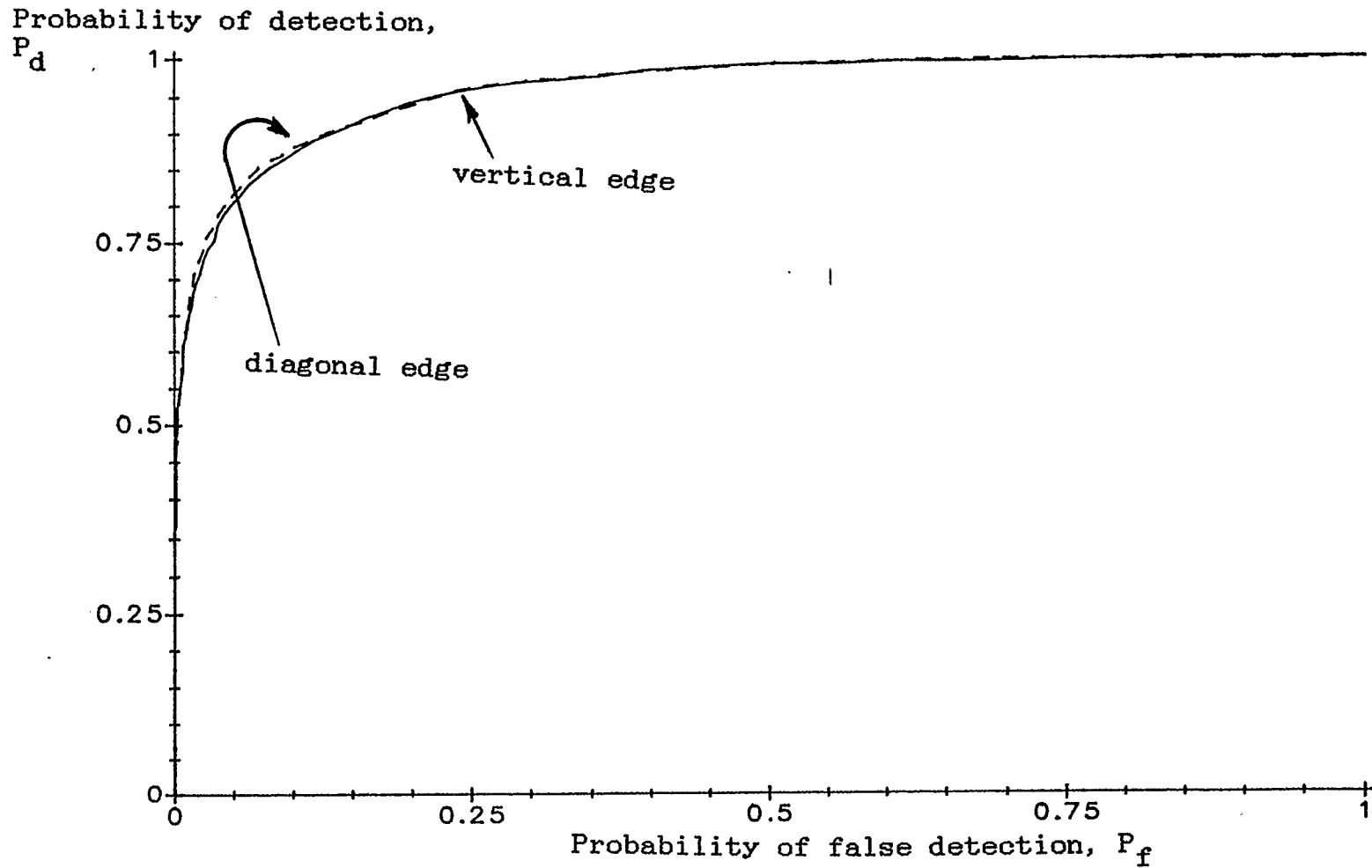


Figure 3.12 Probability of detection versus probability of false detection characteristic for the variance filter (SNR = 10)

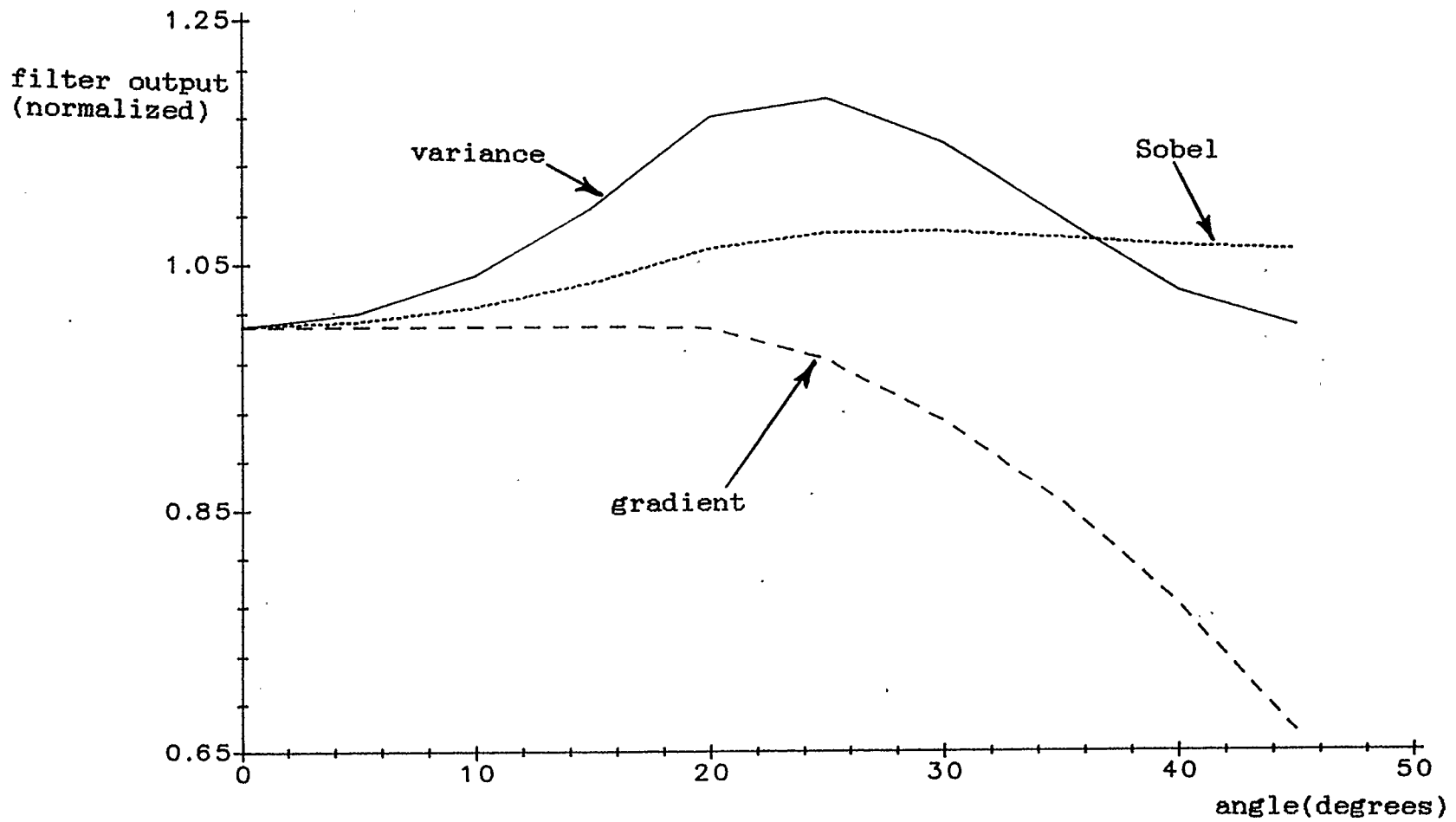


Figure 3.13 Comparison of directional sensitivity characteristic for variance, gradient, and Sobel edge enhancers.

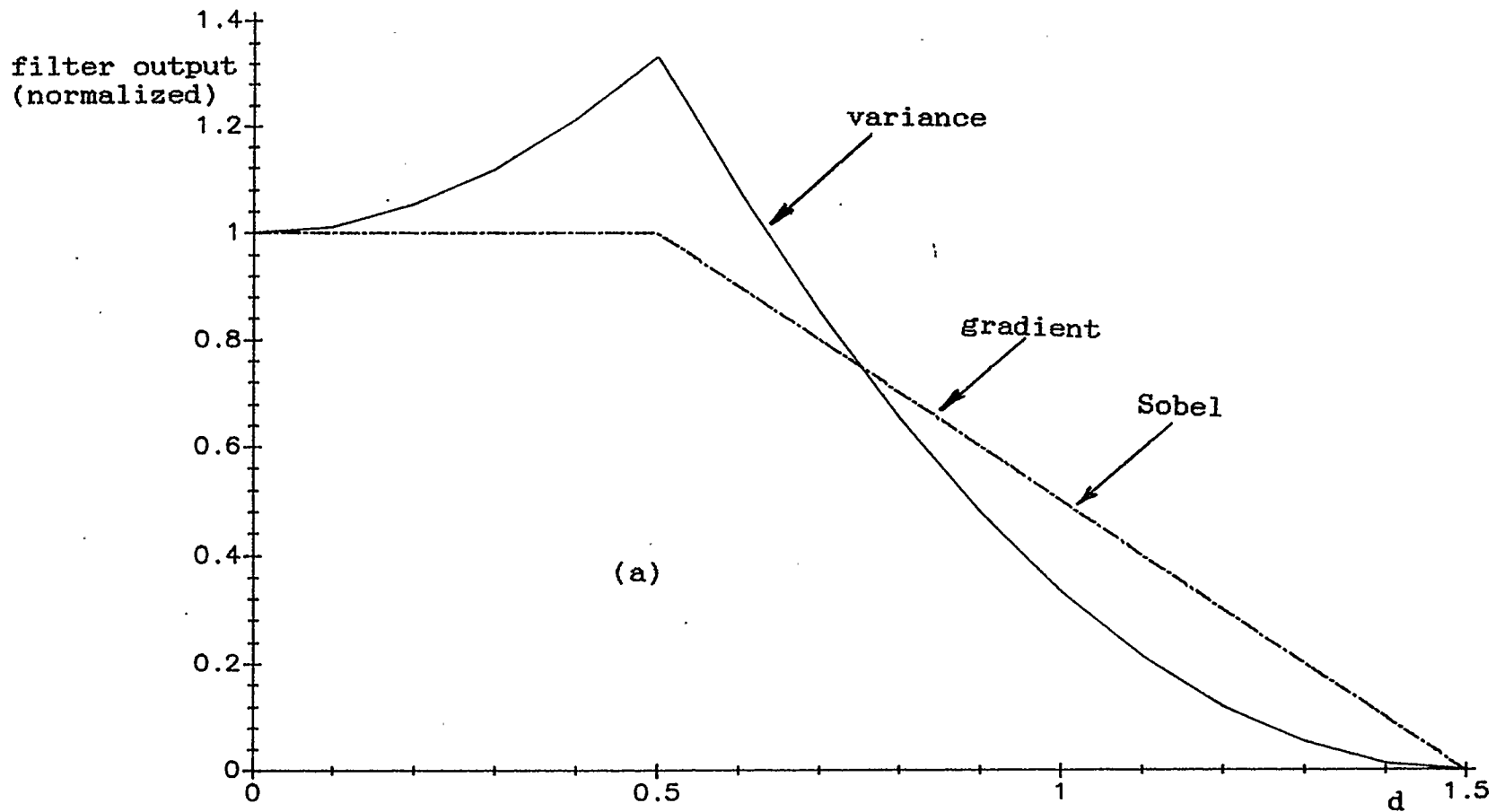


Figure 3.14 Comparison of filter decay characteristics for variance, gradient, and Sobel edge enhancers.  
 (a) vertical edge  
 (b) diagonal edge

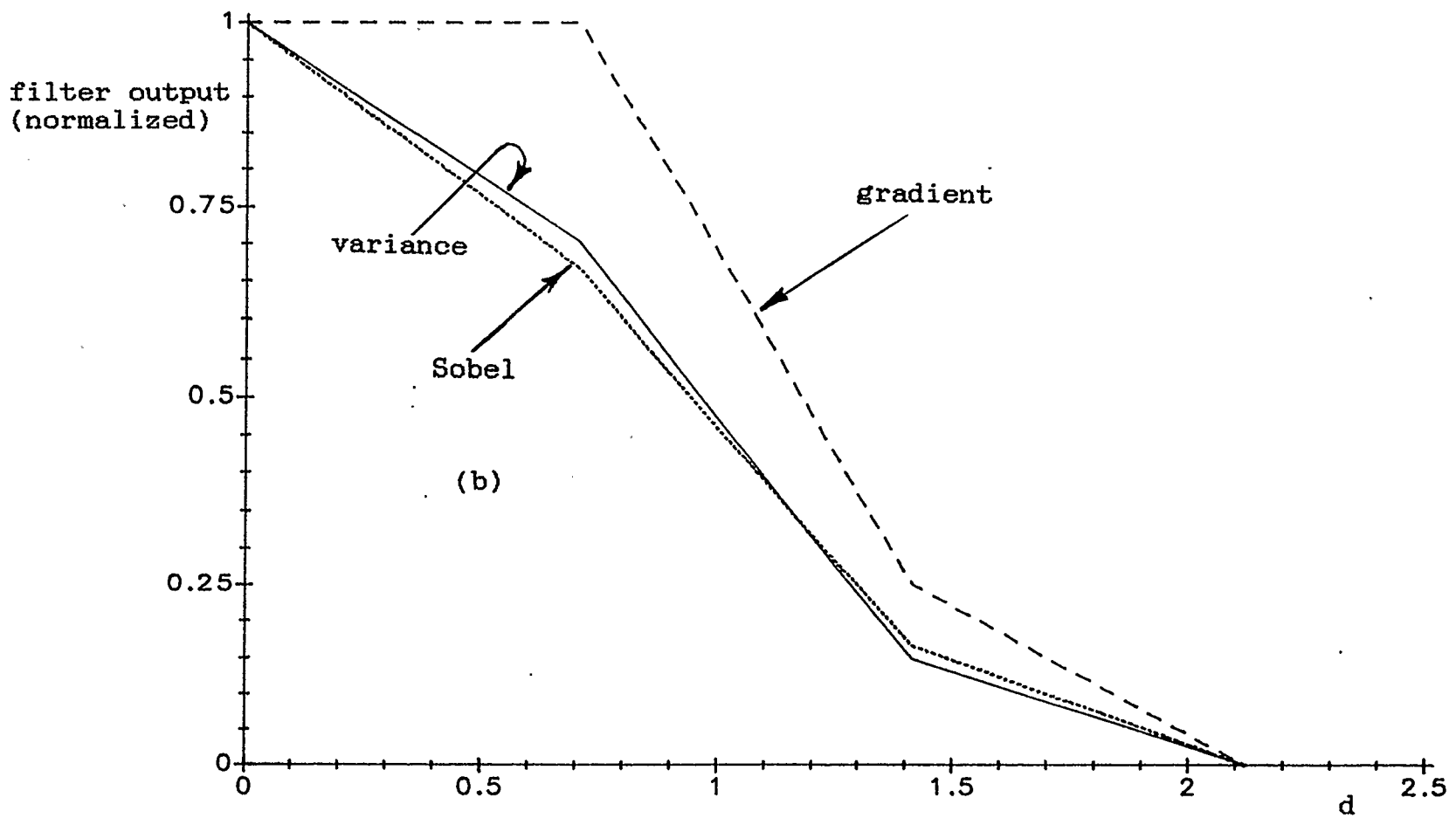


Figure 3.14 (continued)

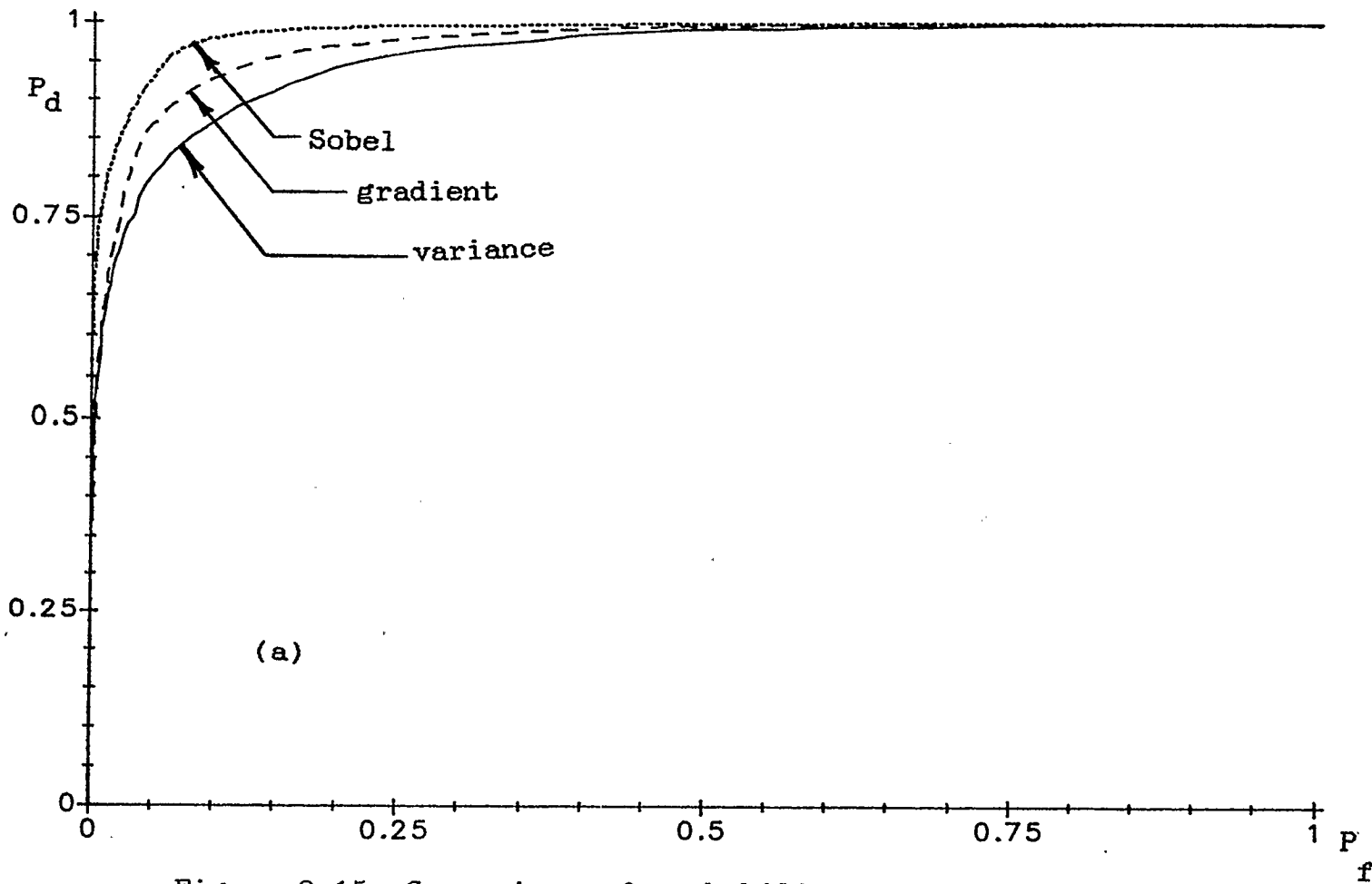


Figure 3.15 Comparison of probability characteristic for variance, gradient, and Sobel edge enhancers  
 (a) vertical edge  
 (b) diagonal edge

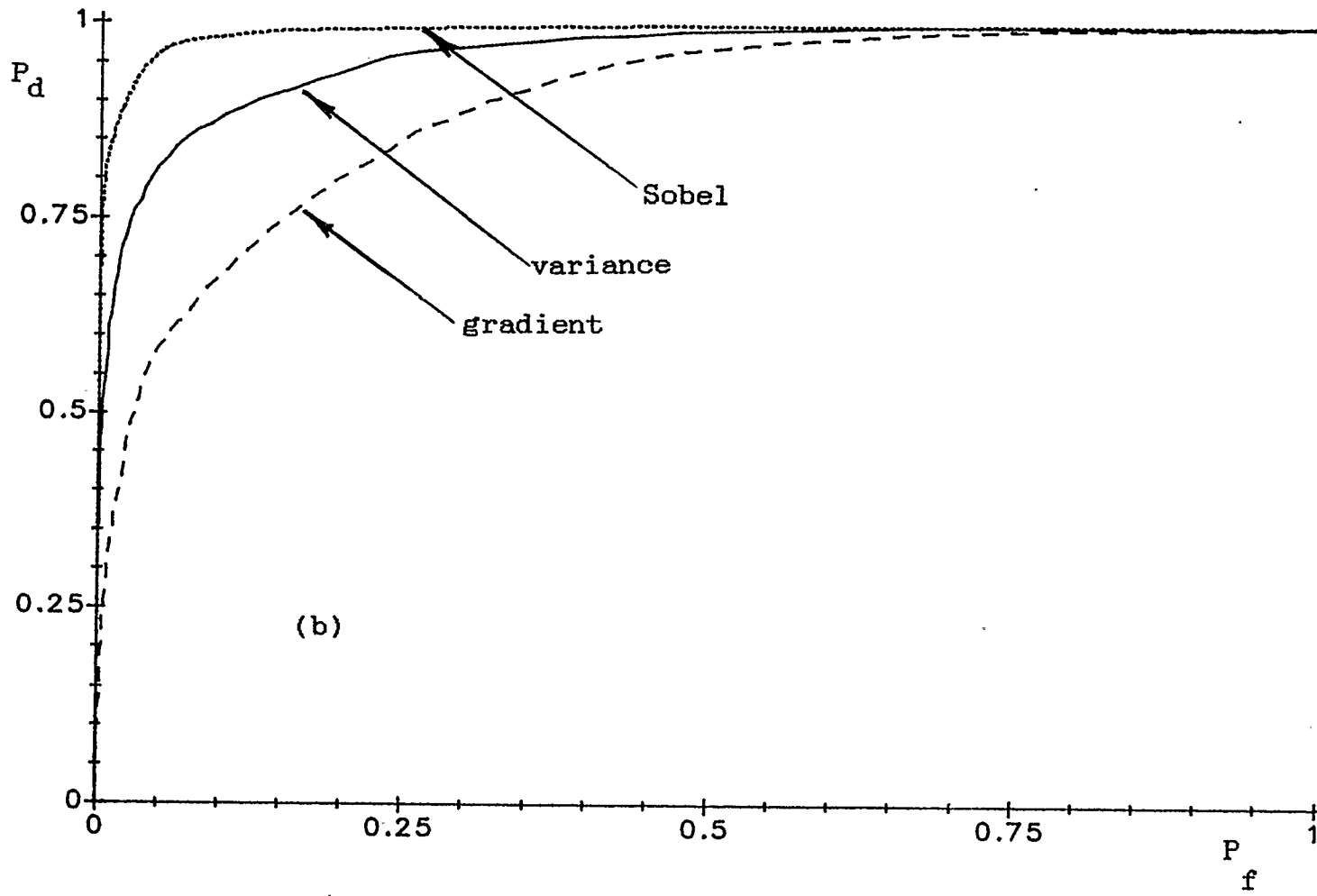


Figure 3.15 (continued)

## Chapter 4

FILTER TESTING4.1 Introduction

A review of noise reduction methods in Chapter 2 shows that a mean filter is the best method for reducing noise where edge detection is important. The review of edge enhancement methods in Chapter 2 also reveals that currently available edge enhancement methods have many shortcomings. The variance filter introduced in Chapter 3 avoids some of these shortcomings. Thus, the combination of the mean filter and the variance filter is deemed to be the most suitable method for edge enhancement and detection in 3D data. Before the variance filter can be applied to clinical data, it is necessary to test the filtering process in a controlled situation. To achieve this aim, the performance of the variance filter is evaluated with a test image. The objectives of this test are to:

1. verify that the variance filter could be used for edge enhancement,
2. verify the theory detailed in Chapter 3, and
3. compare filtering in 2D and 3D.

The listed objectives are achieved by first, applying the filters to a test image with a low noise level. This is sufficient to verify that the variance does indeed behave as an edge enhancer. Second, Equations (3.10) and (3.11) are used to calculate the theoretical limits for the noise level input to the filters. These noise limits are calculated for all possible combinations of 2D and 3D, width 3 and width 5, and with and without prefiltering. Thirdly, the filters are applied to the test image with noise levels at the calculated limit. The results of the application may then be used to verify the theory of Chapter 3 and to compare 2D and 3D filtering.

In this chapter the artificially generated test image is presented. The combination of the mean and variance filters is then demonstrated on the test image with low noise. Results of tests with both 2D and 3D filters, with and without prefiltering are presented. From these results, the theory of Chapter 3 is verified and a comparison of 2D and 3D filtering is done.

## 4.2 The Test Image

Methods developed in this study are to be eventually applied to the accurate location of the left ventricle in human cardiac scintigrams (a full description of the human heart and cardiac scintigrams is found in Chapter 5). Cardiac scintigrams consist of a set of 16 2D images synchronized with the beat of the heart. Thus, a set of cardiac scintigrams is a 3D data set with two spatial axes and one temporal axis. In the images, the left ventricle appears as a roughly oval shaped object that varies in size during the heart beat. At the end diastole phase (when the ventricle is largest) the left ventricle measures approximately 15 pixels on its longest axis and 10 pixels on its shortest axis. Depending on the patient, at the end systole phase (when the ventricle is smallest), the left ventricle may measure anywhere from 3 to 8 pixels on any axis.

The test image is designed to simulate roughly the time-varying left ventricle spatial dimensions. Figure 4.1 shows pictorially how the test image is generated. The left ventricle is represented by a disc of constant intensity in the spatial domain. Sample values of the disc and the background are unity and zero respectively. In the temporal domain, the radius of the disc varied between 3

pixels and 13 pixels in a sinusoidal fashion.

As with any simulation, there are variables which confound the interpretation. For example, in scintigrams the edges are not sharp and the left ventricle can be as small as 3 pixels in diameter. However, the model is sufficient to meet the test requirements.

#### 4.3 The Processing Sequence

The testing of the filter sequence is done as follows:

1. Generate the left ventricle model (ie. discs)
2. Add noise of a known variance to the image
3. Use a mean filter to reduce the noise in the image
4. Use a variance filter to enhance the edges
5. Use a simple edge tracking algorithm to follow the enhanced edge

Step 3 is omitted when it is desired to examine the variance filter independently of prefiltering. The above sequence is illustrated by the four images shown in Figure 4.2. Because of the difficulties in displaying a 3D data set in its entirety, 2D slices in the spatial domain are shown. The noise level in Figure 4.2(a) is 0.5. The

filters which produced the images in Figure 4.2 are 3D and of width 3. As expected, the variance filter enhances the edge of the disc.

A radial search algorithm is used to track the enhanced edge. This algorithm is shown pictorially in Figure 4.3. In the radial search algorithm, samples along a radial path are searched for a maximum. The centre which defines the radial path is at the centre of the image, and therefore, the algorithm must assume that the object is centred in the image. Once a maximum is found along a search path, it is assumed to be at an edge. The two samples radially adjacent to the maximum are used to determine whether the maximum is just inside the edge, or just outside the edge. If the sample is just outside the edge, then the adjacent sample on the inside of the edge is taken to mark the edge, otherwise, the maximum is used. The algorithm searches a series of radial paths and outputs a set of points which all lie just inside the edge. An example of the points detected by this algorithm is shown in Figure 4.2(d). This method of edge tracking is simple. Sophisticated edge tracking algorithms are considered to be beyond the scope of the present study.

#### 4.4 Theoretical Versus Test Results

Equations (3.10) and (3.11) are used to predict the maximum allowable noise to be added to the test image. The predictions used here are based on a 90 percent confidence interval. Tables 4.1 and 4.2 show the predicted limits as calculated from Equations (3.10) and (3.11). Table 4.1 shows the noise limits for the filter sequence without prefiltering. Similarly, Table 4.2 shows the noise limits for the filter sequence with prefiltering. With one exception, these calculated limits are used as the noise levels for testing. The exception occurs when prefiltering is used with the 3D width 5 case. In this case, a lower noise level,  $\sigma_n=3.0$ , is used. The reason for this exception is discussed later in this section.

Test results are presented in Figures 4.4 through 4.11. Figures 4.4 through 4.7 show the results of the test without prefiltering and Figures 4.8 through 4.11 show the results of the test with prefiltering.

In Figures 4.4 through 4.7 it can be seen that, within the limits of the specified confidence interval, edge detection is successful. The theory presented in Chapter 3 predicts that with a 90 percent confidence interval, edge detection should be possible with a 9.75 percent chance of

a background sample being mistaken for an edge sample and/or vice versa. More specifically, the theory predicts that, of 25 points on the detected edge, 2.5 points (2 or 3) will be in error. Note that these errors do not include those points which are displaced from the edge because of blurring. The results presented in the figures support this prediction. It should also be observed from Figures 4.4 through 4.7 that wider variance filters produce broader peaks. The significance of this observation is shown in Figures 4.8 through 4.11.

As expected, prefiltering allows edge detection with lower SNR. However, the improvement realized by prefiltering is tempered by the effects of blurring as shown in Figures 4.8 to 4.11. These effects are evident in two ways. First, blurring reduces the effectiveness of the edge enhancer. This reduction leads to improvements less than those initially expected from Equation (3.11). Second, blurring distorts the shape of the edge. Thus, the predicted noise limit for the prefiltered, 3D width 5 case was not attainable. Although edge detection was possible with the 2D width 5 case, severe distortion due to edge blurring was observed. Blurring at edges reduces the noise limit and causes errors in the shape of the detected edge.

The failure of the theory to predict the noise limits

in the cases where blurring is severe exposes a flaw in the modelling of errors in Chapter 3. Only peak and background samples are considered in Chapter 3. Because of blurring, intermediate-value samples occur near edges. These samples are not explicitly peak or background samples. The intermediate values are greater than the values of the background samples. Therefore, it is not unlikely that a sample near an edge may vary higher than the sample at the edge. The effect is, that although the edge has been correctly detected, its position is shifted from where it should be. Figure 4.12 illustrates, in a 1D analogy, why these errors are possible. The amount of shifting of the detected edge is restricted by the amount of blurring, and is, therefore, controllable by the window width.

Furthermore, 3D processing may allow edge detection in cases where it is not possible with 2D processing. The numbers in Table 4.2 illustrate this. The maximum noise level with a 2D width 5 filter was calculated to have a standard deviation of 1.11. Although the 3D width 5 filter did not meet its expectations, edge detection was possible with a noise level 3.0 times that of the step size. Therefore, if one is dealing with a case where the standard deviation of the noise is twice the step size, edge detection would not be possible without 3D processing.

#### 4.5 Filtering in 2D Versus 3D

As was stated in Chapter 3, whenever possible, it is advantageous to filter data in 3D rather than 2D. The predicted limits of the filters calculated in Section 4.4 were borne out in practice with the exception of window width effects. The theory indicates that the 2D width 5 filter should be similar in performance to the 3D width 3 filter. However, the comparison of figure 4.5(c) to figure 4.6(c) shows the effects of window width. The extra blurring in the 2D width 5 case results in a poorly-detected edge.

Therefore, an increase in the number of dimensions used for processing results in either 1) a larger number of samples in a window of the same width, or 2) a comparable number of samples in a window of smaller width. The combination of these two effects means that reliable edge detection in data with a lower SNR can be achieved by increasing the number of dimensions in processing.

TABLE 4.1

| Number of dimensions | width | N   | df  | U    | L     | $\sigma_{\text{edge}}^2$ | $\sigma_n^2$ | $\sigma_n$ |
|----------------------|-------|-----|-----|------|-------|--------------------------|--------------|------------|
| 2                    | 3     | 9   | 8   | 2.92 | 0.515 | 0.222                    | 0.047        | 0.216      |
| 2                    | 5     | 25  | 24  | 1.73 | 0.657 | 0.222                    | 0.136        | 0.368      |
| 3                    | 3     | 27  | 26  | 1.69 | 0.666 | 0.222                    | 0.142        | 0.376      |
| 3                    | 5     | 125 | 124 | 1.25 | 0.819 | 0.222                    | 0.419        | 0.648      |

TABLE 4.2

| Number of dimensions | width | N   | df  | U    | L     | $\sigma_{\text{edge}}^2$ | $\sigma_n^2$ | $\sigma_n$ before prefiltering |
|----------------------|-------|-----|-----|------|-------|--------------------------|--------------|--------------------------------|
| 2                    | 3     | 9   | 8   | 2.92 | 0.515 | 0.1                      | 0.017        | 0.38                           |
| 2                    | 5     | 25  | 24  | 1.73 | 0.657 | 0.08                     | 0.049        | 1.11                           |
| 3                    | 3     | 27  | 26  | 1.69 | 0.666 | 0.08                     | 0.052        | 1.18                           |
| 3                    | 5     | 125 | 124 | 1.25 | 0.819 | 0.08                     | 0.151        | 4.34                           |

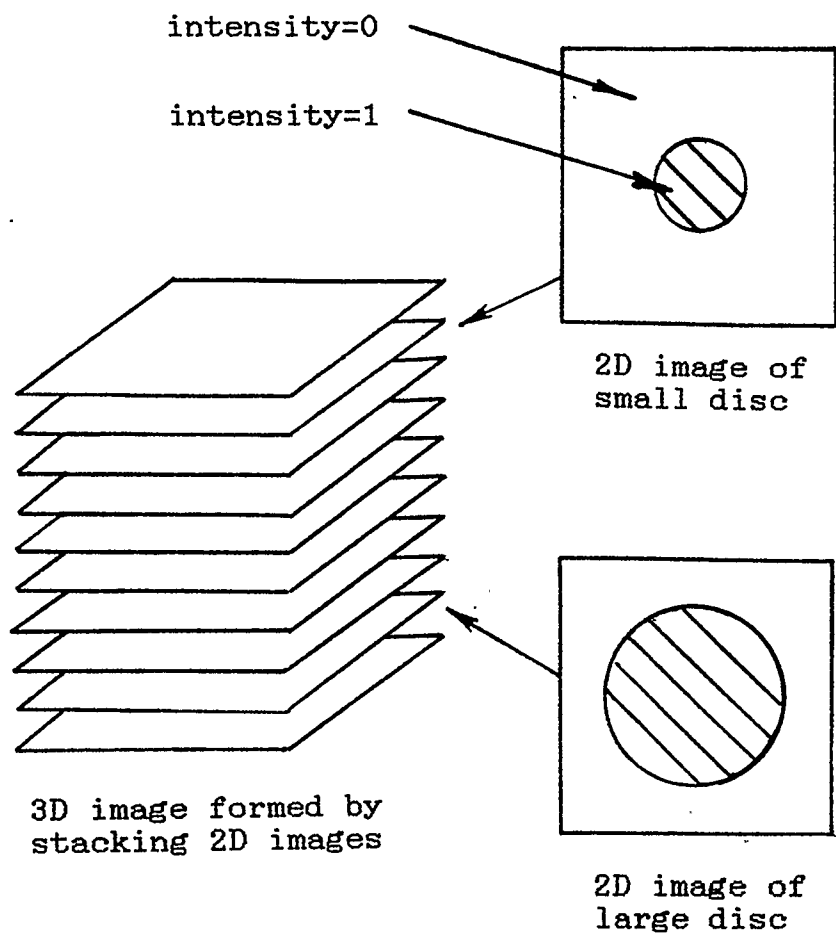
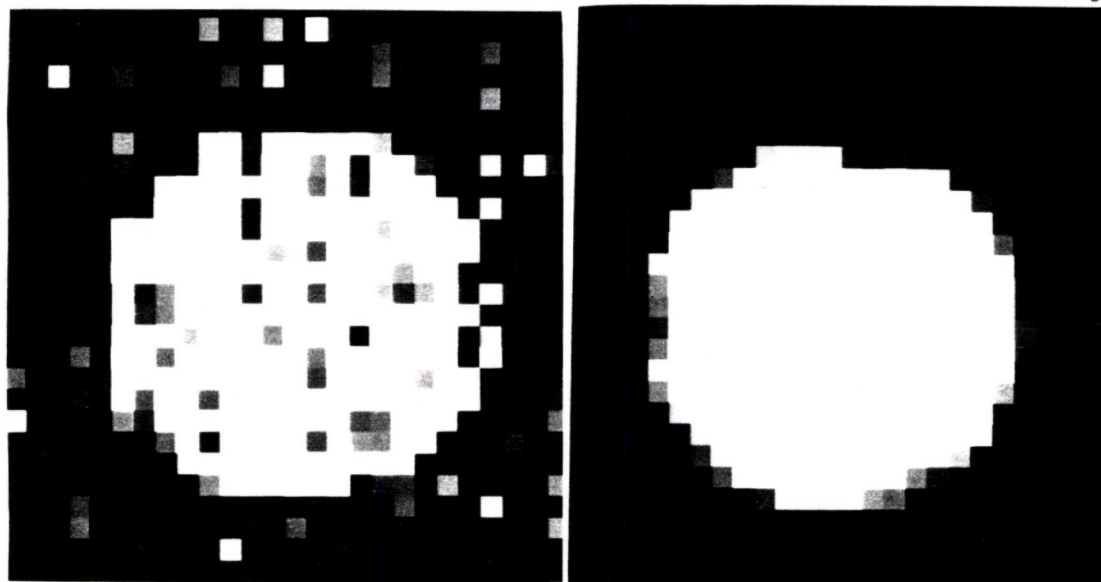
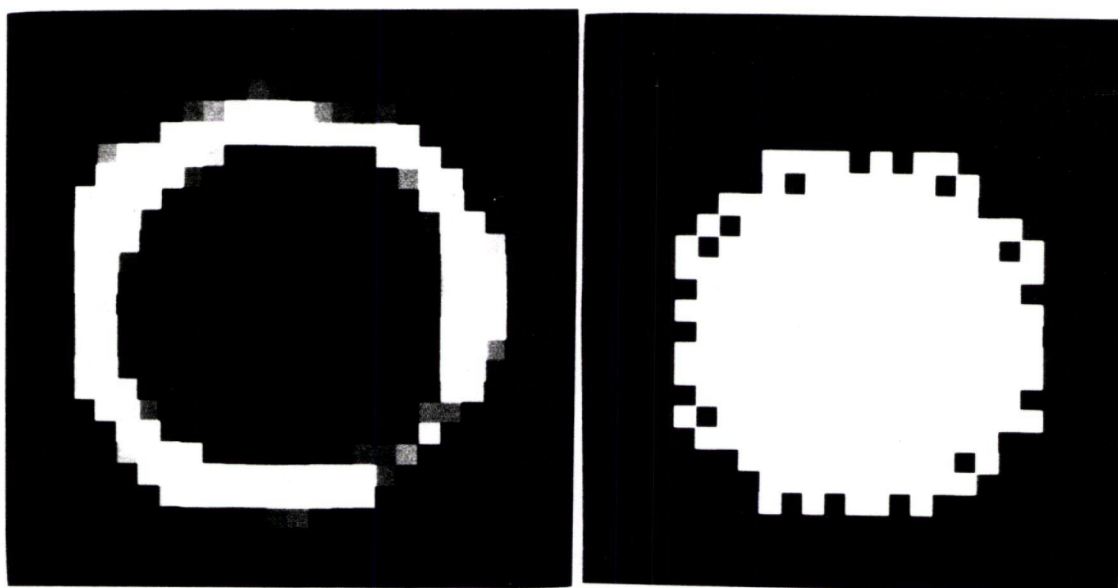


Figure 4.1 Generation of the 3D test image



(a)

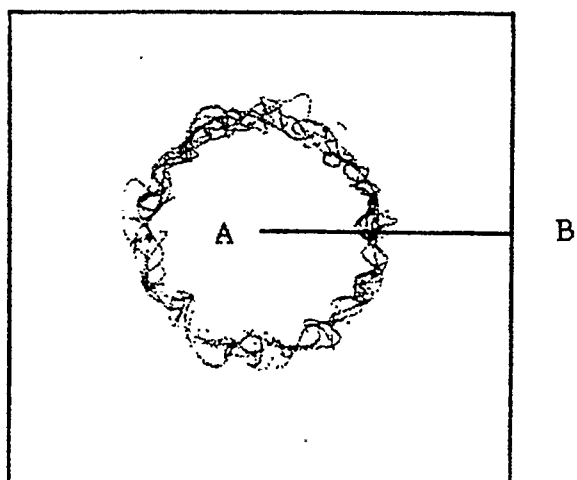
(b)



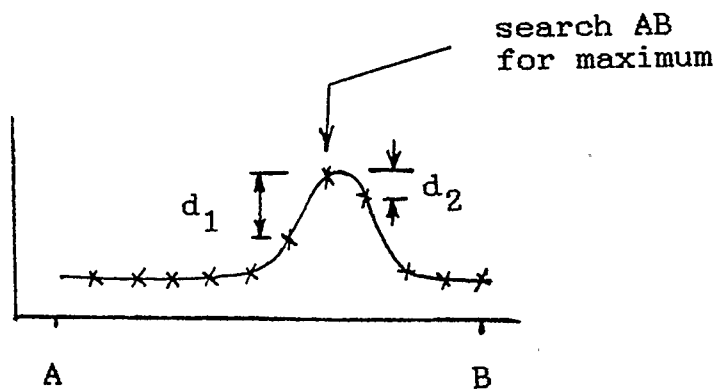
(c)

(d)

Figure 4.2 Example of data in the filtering sequence (standard deviation of noise = 0.5)  
(a) original image (radius = 8)  
(b) after 3D width 3 mean filter  
(c) after 3D width 3 variance filter  
(d) points on the detected edge



(a)



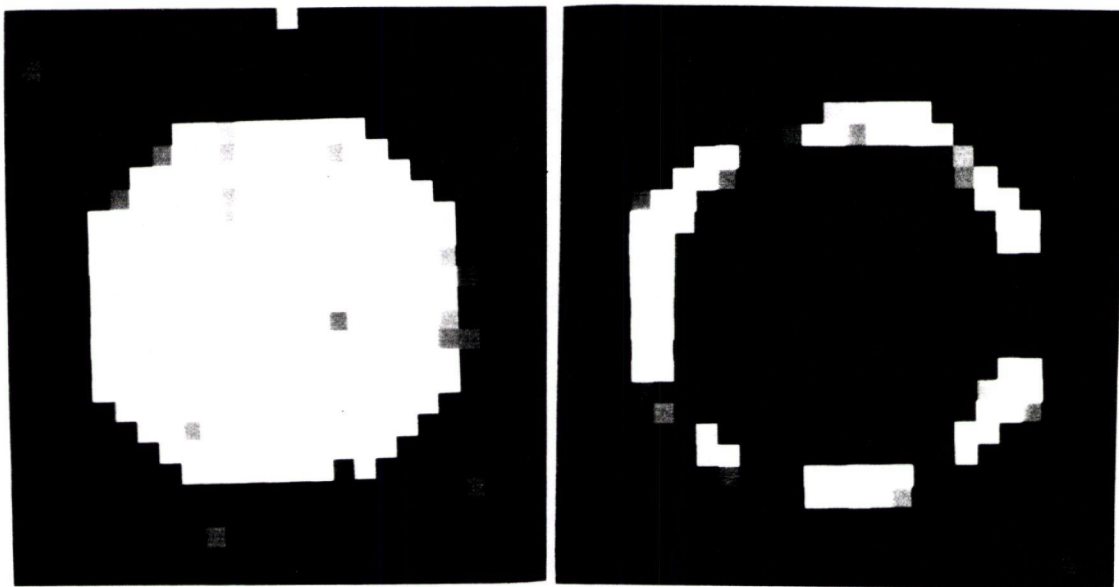
(b)

```

if  $d_1 < d_2$  then
  maximum is just outside
  the edge
else
  maximum is just inside
  the edge

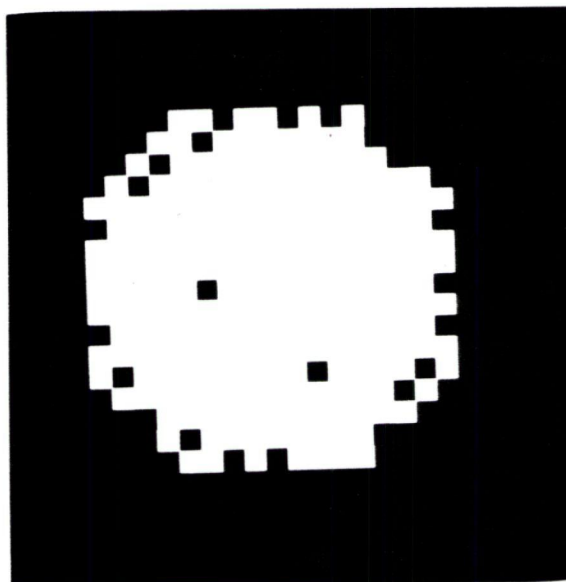
```

Figure 4.3 Pictorial description of the radial search algorithm  
 (a) 2D slice of variance filter output  
 (b) profile of the slice along AB



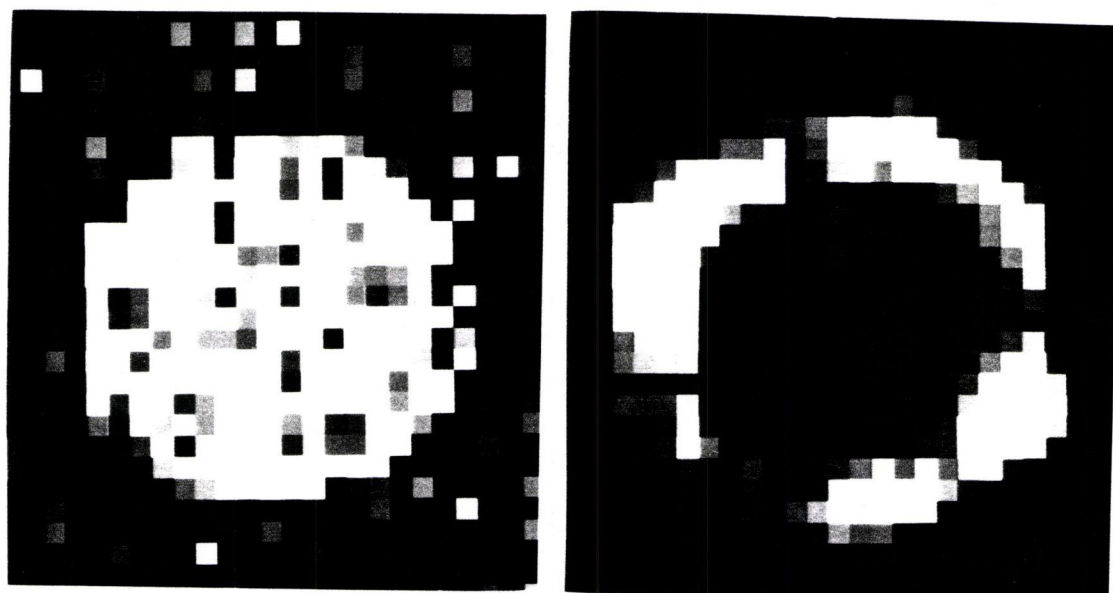
(a)

(b)



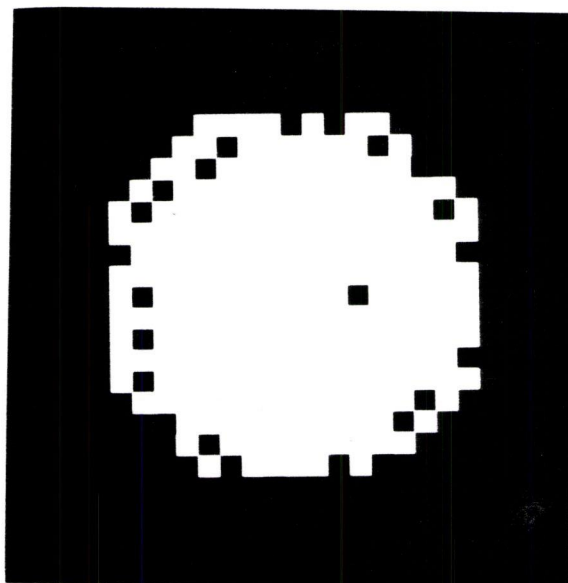
(c)

Figure 4.4 Output of the filter sequence (no prefiltering) with 2D width 3 filters  
(a) original ( $\sigma = 0.216$ )  
(b) variance filter<sup>n</sup> output  
(c) points on the detected edge



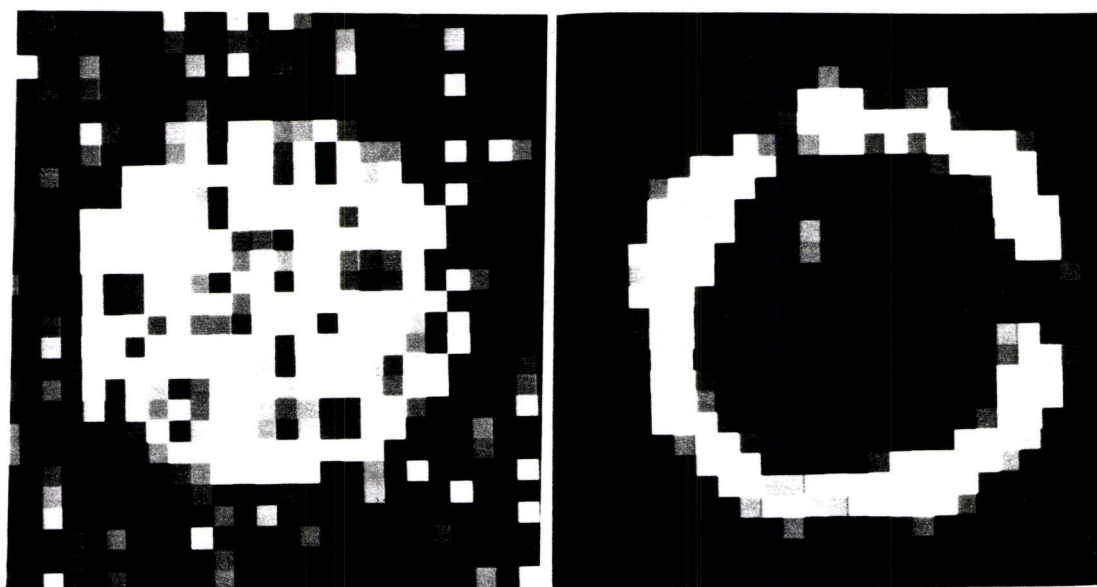
(a)

(b)



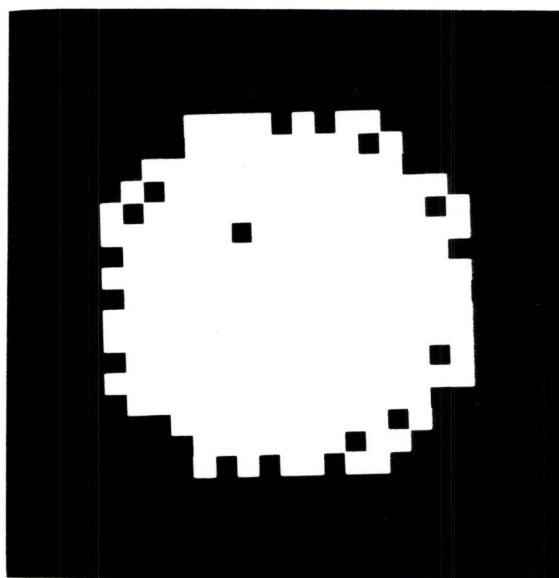
(c)

Figure 4.5 Output of the filter sequence (no prefiltering) with 2D width 5 filters  
(a) original ( $\sigma_n=0.368$ )  
(b) variance filter<sup>n</sup> output  
(c) points on the detected edge



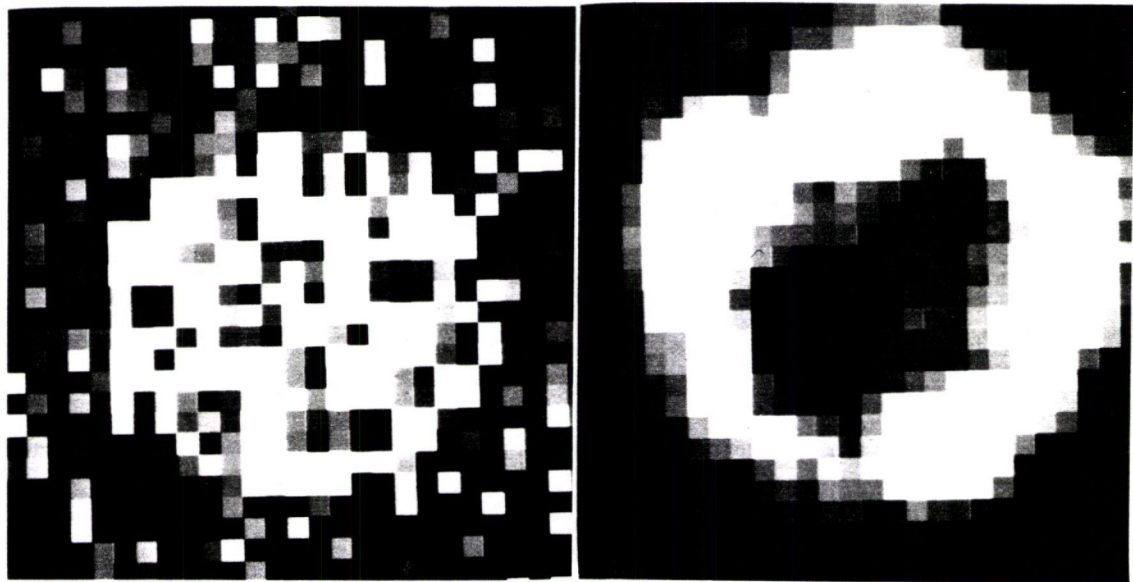
(a)

(b)



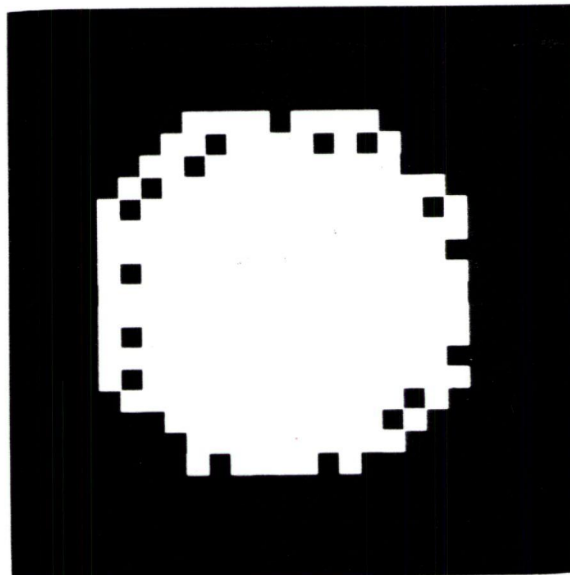
(c)

Figure 4.6 Output of the filter sequence (no prefiltering) with 3D width 3 filters  
(a) original ( $\sigma_n = 0.376$ )  
(b) variance filter<sup>n</sup> output  
(c) points on the detected edge



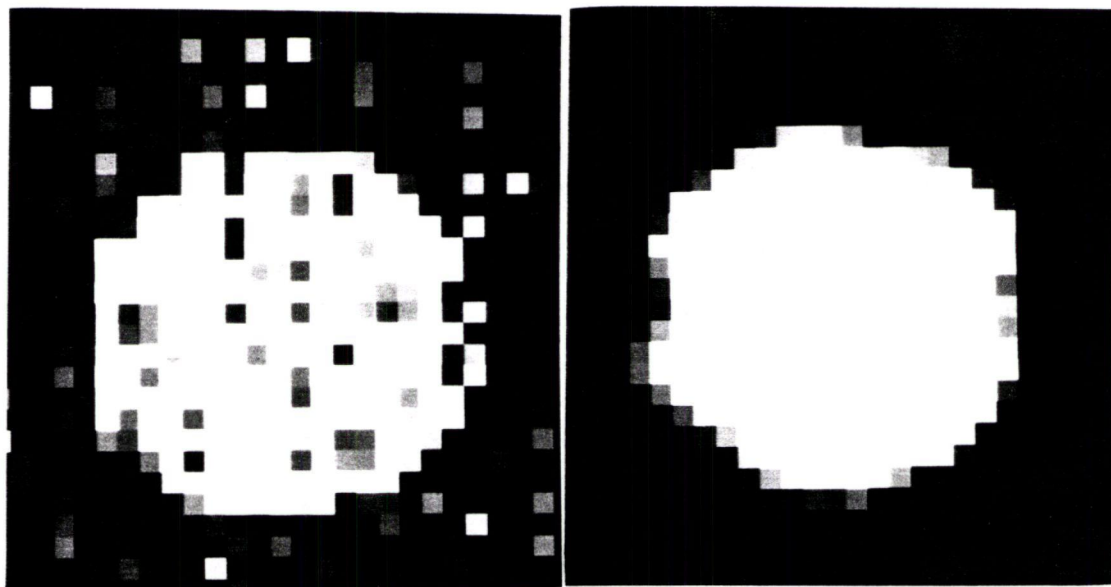
(a)

(b)



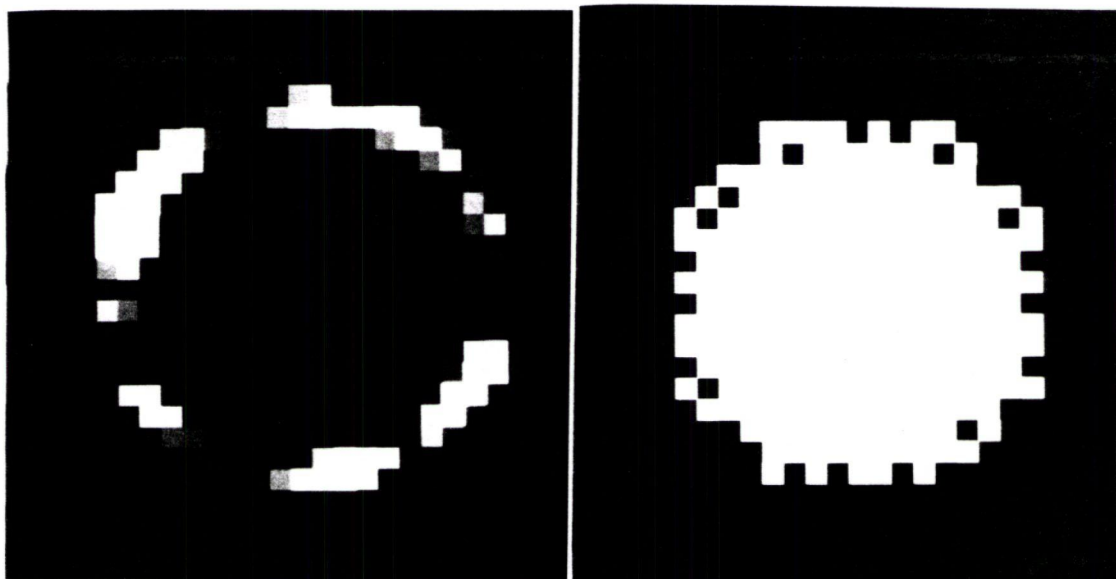
(c)

Figure 4.7 Output of the filter sequence (no prefiltering) with 3D width 5 filters  
(a) original ( $\sigma = 0.648$ )  
(b) variance filter<sup>n</sup> output  
(c) points on the detected edge



(a)

(b)



(c)

(d)

Figure 4.8 Output of the filter sequence (with prefiltering) with 2D width 3 filters  
(a) original ( $\sigma_n=0.39$ )  
(b) mean filter<sup>n</sup> output  
(c) variance filter output  
(d) points on the detected edge

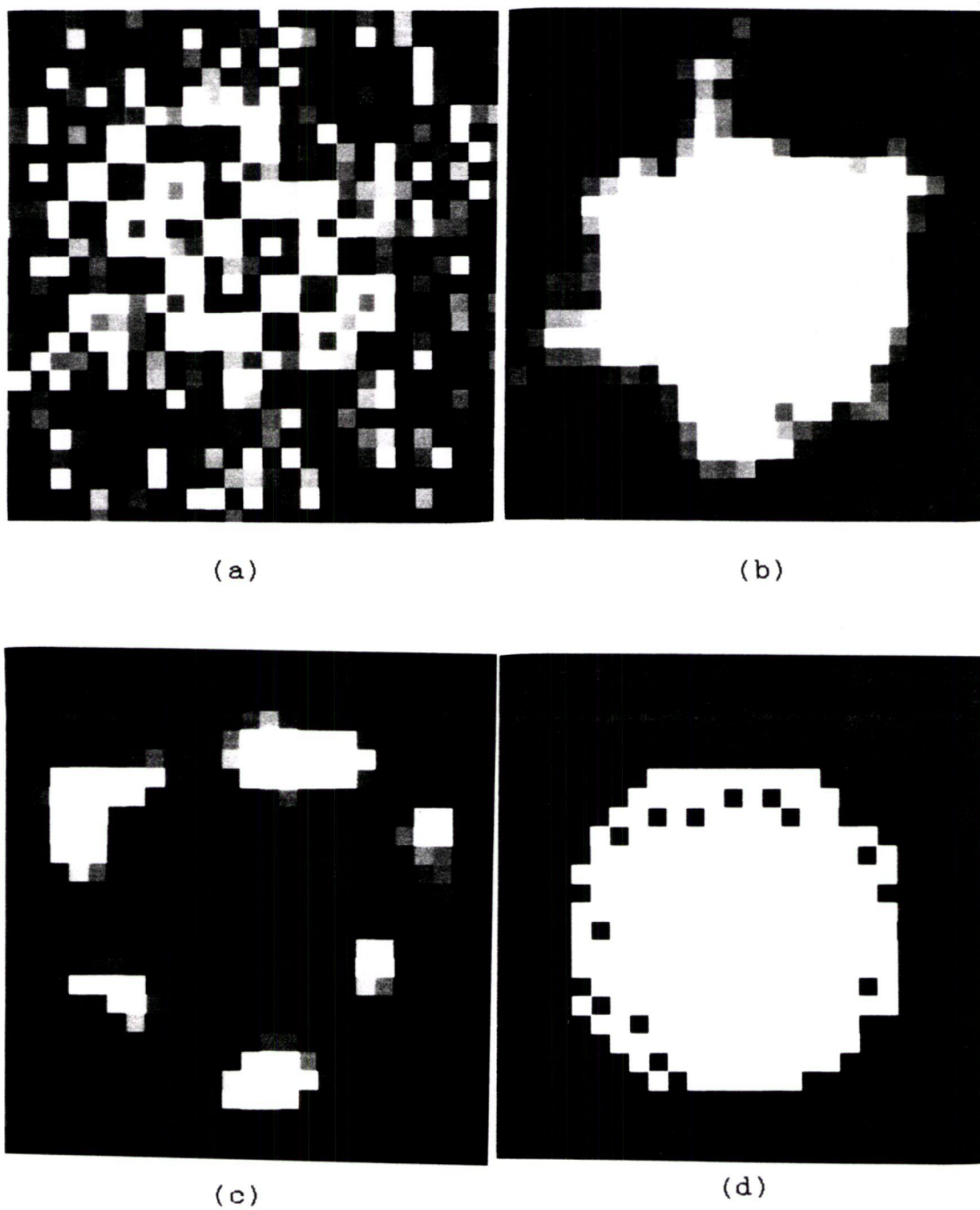
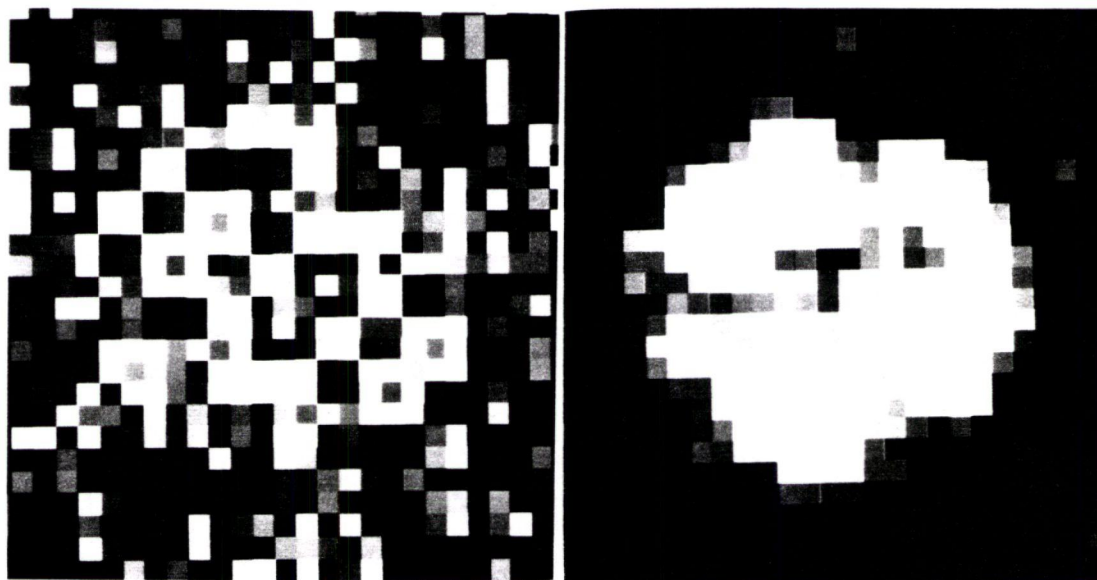
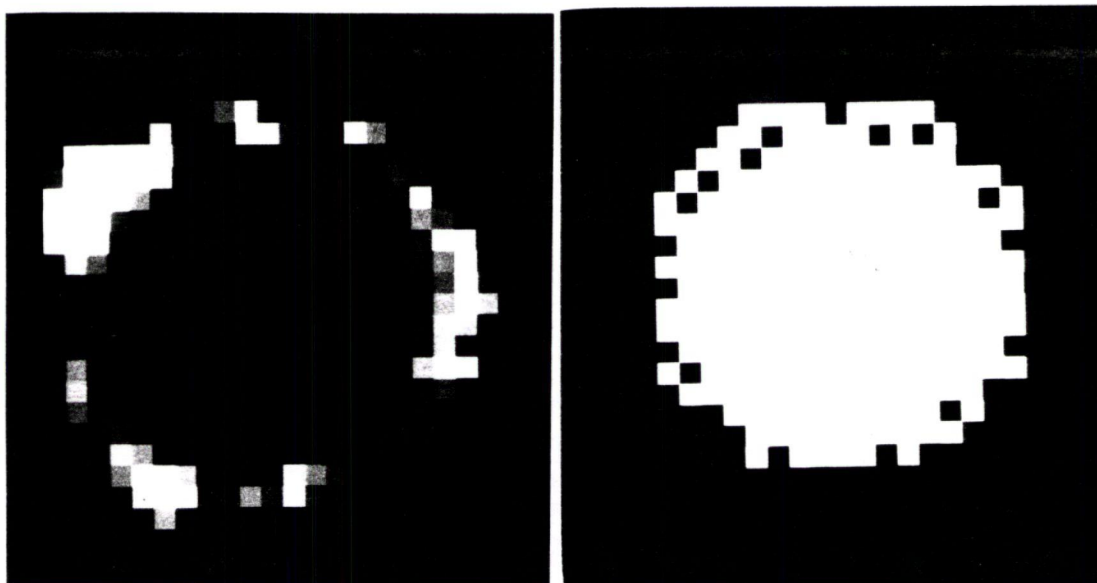


Figure 4.9 Output of the filter sequence (with prefiltering) with 2D width 5 filters  
(a) original ( $\sigma_n=0.1.11$ )  
(b) mean filter<sup>n</sup>output  
(c) variance filter output  
(d) points on the detected edge



(a)

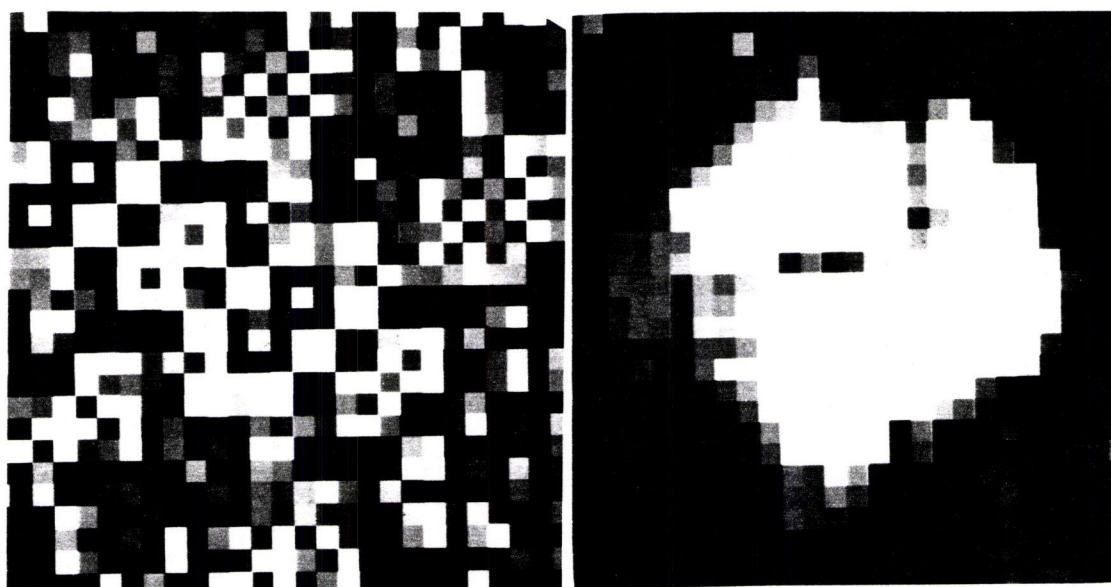
(b)



(c)

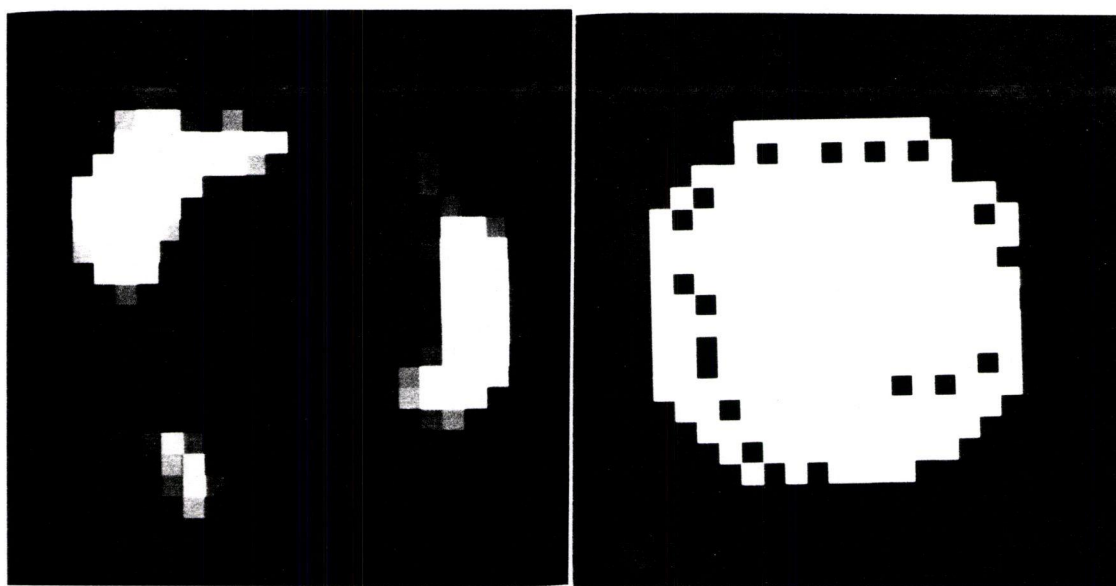
(d)

Figure 4.10 Output of the filter sequence (with prefiltering) with 3D width 3 filters  
(a) original ( $\sigma_n=1.18$ )  
(b) mean filter<sup>n</sup> output  
(c) variance filter output  
(d) points on the detected edge



(a)

(b)



(c)

(d)

Figure 4.11 Output of the filter sequence (with prefiltering) with 3D width 5 filters  
(a) original ( $\sigma = 3.0$ )  
(b) mean filter<sup>n</sup> output  
(c) variance filter output  
(d) points on the detected edge

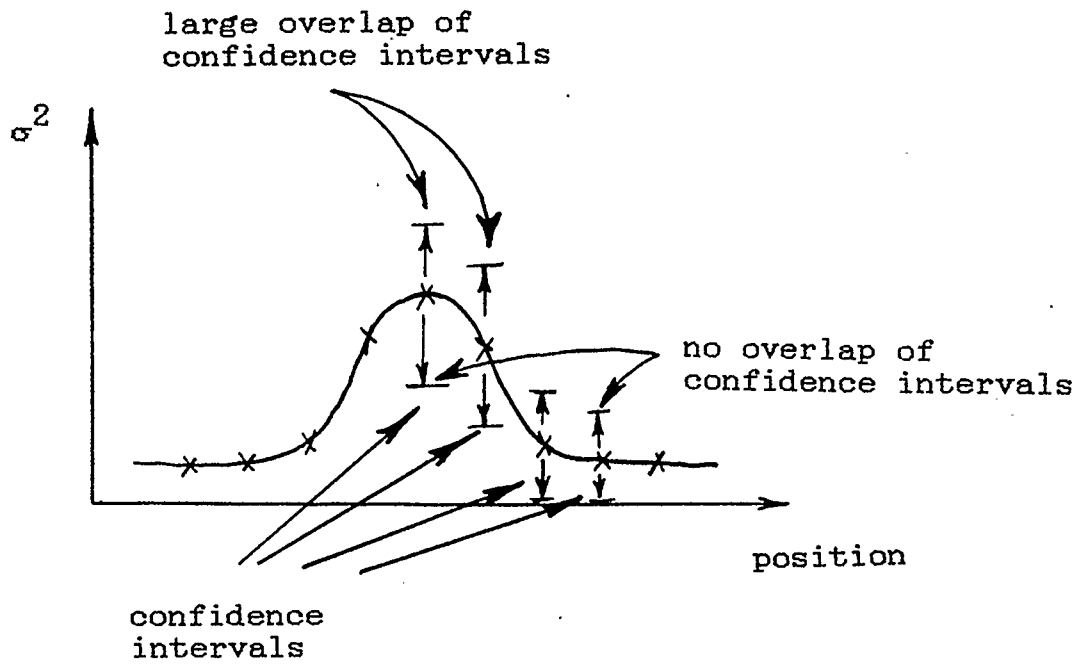


Figure 4.12 1D analogy of errors caused by blurring

## Chapter 5

APPLICATION TO  
NUCLEAR CARDIAC SCINTIGRAMS

5.1 Introduction

Although the methods presented in this thesis are applicable to any multidimensional signal processing application, the motivation for the study was a problem in nuclear medical image processing. This problem is detection of the left ventricle in nuclear cardiac scintigrams. While it is recognized that the properties of nuclear cardiac scintigrams differ somewhat from those of the test image considered in Chapter 4, the methods developed in this thesis may, never the less, be applied to both cases.

An understanding of the functioning of the human heart is beneficial to understanding the application to cardiac scintigrams. Therefore, a brief description of blood circulation through the heart is presented. The concept of the "ejection fraction" is also presented. The process of producing nuclear cardiac scintigrams is described in Section 5.2.3. Finally, in this chapter, the results of

application of 3D noise reduction and variance filtering to nuclear cardiac scintigrams are presented.

## 5.2 Description of the Human Heart and Cardiac Scintigrams

### 5.2.1 The Heart

The description given here is illustrated in Figure 5.1[38]. The heart consists of two distinct, vertically separated, halves. Each of the halves contains two chambers, an atrium and a ventricle. The right half of the heart carries unoxygenated blood. The right atrium (C) receives unoxygenated blood from the body via the superior and inferior vena cava (A,B). Blood then passes from the right atrium (C) to the right ventricle (D). The right ventricle pumps the blood, via the pulmonary artery (E), to the lungs to be oxygenated. The left half of the heart carries oxygenated blood. Oxygenated blood from the lungs is passed by the pulmonary vein (F) to the left atrium (G). The left ventricle (H) receives blood from the left atrium (G) via the mitral valve. The left ventricle then pumps the oxygenated blood to the rest of the body through the aorta (I).

The body depends on the left ventricle to supply it with oxygenated blood. Because of the work the left ventricle must do to pump blood to the entire body, it is normally the part of the heart to fail first in the event of heart failure. For these reasons, the left ventricle is important in medical diagnosis.

### 5.2.2 Phases of the Heart Beat and Ejection Fraction

The beat of a heart can be divided into two phases. These phases are called systole and diastole[39]. The systole phase is the compression phase of the heart beat where blood is pumped from the heart to the lungs and to the rest of the body. The diastole phase is the phase where the heart muscle fibres lengthen and the heart fills with blood.

The efficiency with which the heart pumps blood to the rest of the body is of interest in medical diagnosis. A figure of merit called the ejection fraction is used in medicine to evaluate the efficiency of the heart. The ejection fraction is calculated by [40]

$$\text{Ejection fraction} = \frac{V_{ED} - V_{ES}}{V_{ED}} \quad (5.1)$$

where  $V_{ED}$  and  $V_{ES}$  are the volumes of blood in the left ventricle at end-diastole and end-systole, respectively. The ejection fraction is the fraction of blood pumped from the left ventricle during the systole phase.

### 5.2.3 Nuclear Scintillation Camera

The importance of the left ventricle in medical diagnosis raises a need to examine a patient's internal anatomy. Nuclear scintigrams provide physicians with one method of viewing a patient's internal anatomy without surgery. For this reason, nuclear scintigrams are a valuable diagnostic tool. The process of producing a scintigram follows these steps [41]:

1. Radio-active material which emits gamma radiation is injected into a patient's blood stream.
2. Gamma radiation emitted from the patient's blood passes through the first stage of an Anger camera. This first stage is a lead collimator which selects only those gamma rays which have been emitted by specific regions.
3. After the radiation has been collimated it passes through a sodium iodide crystal. Upon striking the crystal the gamma radiation causes photons to be emitted from the crystal, thus producing

scintillations.

4. An array of photo-multiplier tubes is used to detect the scintillations. The array of photomultipliers has coarse resolution. The resolution is increased by using electronic weighting circuitry to calculate the position of a scintillation by comparing the relative intensities of the scintillation as determined by each photo-multiplier tube.
5. The intensity of each pixel in the resulting image is the number of gamma rays calculated to have been emitted from that location. Consequently the brightness of a pixel in a scintigram indicates how much blood is in the patient's body along the path determined by the collimator.

The apparatus for producing scintigrams is illustrated pictorially in Figure 5.2.

The scintigrams used in the present study were of the human heart. Regions containing more blood appear bright in a scintigram whereas those containing little blood appear dark. Since the heart contains a relatively large amount of blood compared to the surrounding tissue, it is shown clearly in a scintigram.

In order to minimize the patient's risk, a small

dosage of radiation is used. Although the small dosage protects the patient, it means that the scintigram must be produced over a period of several minutes. The heart changes its shape during this time. In order to reduce the amount of blurring that would occur because of the heart's own movement, a series of sixteen scintigrams is produced. The scintillation camera is gated by the beat of the patient's heart so that each sixteen images corresponds to only one sixteenth of the heart's beat. A length of time equal to one sixteenth of the heart beat period is short enough for the heart to be considered stationary.

The resolution of the scintigrams is 64 pixels square. The left ventricle of the heart measures approximately 15 pixels across in end-diastole images. In end-systole images the left ventricle may be as small as 3 pixels across and is normally 5 to 10 pixels across.

The test images employed in Chapter 4 contain normally distributed noise, and contain objects and backgrounds with uniform intensities. However, the noise in the scintigrams is a combination of Poisson noise and some unknown background distribution due to radiation sources surrounding the heart[42]. In addition, the left ventricle region of a scintigram has a nonuniform intensity. In spite of these differences, it is shown in the following

sections that the variance filter is effective for enhancement of the edges of the left ventricle.

### 5.3 Modification to the Edge Tracking Algorithm

Unlike the images in Chapter 4, actual scintigrams contain other features in close proximity to the feature of interest. In this case the feature of interest is the left ventricle and other features are the atriums and the right ventricle. The presence of unwanted edges in the heart images motivated a change in the edge tracking algorithm.

In Chapter 4, it was assumed that only one edge could be found along any radial search path. This assumption is not valid with the heart images. Therefore, the edge tracking algorithm is modified for use with cardiac scintigrams. The modified radial search works as follows:

1. Select a point known to be in the centre of the object of interest.
2. Search along one radial path from the selected centre to find an edge which is known to be an edge of the left ventricle.
3. Track the rest of the edge by searching along successive radii as in step 2, but searching only within a specified range centred about the radius of

the edge as detected by the previous search path.

The modified radial search algorithm is illustrated in Figure 5.3. Step 2 is achieved by searching along a radial path away from the rest of the heart. The result is that the detected edge must be an edge of the left ventricle. As has been stated, the objective of this work is not to develop edge tracking algorithms, so the edge tracking method remains simple. However, as is shown, even with this simple edge tracking algorithm, excellent results were obtained for most images.

#### 5.4 Filter Sequence

The heart images were processed using the same sequence described in Chapter 4 for the simulation. The filter sequence as applied to the heart images is as follows:

1. Load heart images into a 32x32x32 array. The heart images are each 64x64 in resolution so only a 32x32 region centred on the left ventricle is taken. The sequence of 16 pictures is repeated twice in the array so that edge effects can be ignored. See figure 5.4 for an illustration of how the image is prepared for processing

2. Use a mean filter to reduce the noise in the image
3. Use a variance filter to enhance the edges
4. Use the simple edge tracking algorithm to follow the enhanced edge
5. Use the tracked edge to define the region of the left ventricle. Integrate the mean filtered image over this area. The integral of this area is equal to the sum of two volumes of blood; one volume being that of the left ventricle, and the other, the volume of blood in front of and behind the left ventricle along the line of sight defined by the collimator.

An example showing steps one through four in the filtering process is given in Figure 5.5. In this example, and all others in this chapter, a 3D window of width 3 was used for processing the data.

### 5.5 Results of Application to Cardiac Scintigrams

Figures 5.6 through 5.10 show the results of application of the filter to a set of 5 test cases. For each of the 5 cases, the detected boundaries for the first and ninth image in the sequence are shown. The set of all sixteen detected boundaries are also presented. The

boundaries are shown overlaying the original-unprocessed scintigrams.

The first four cases demonstrate successful runs. The detected edges correspond to the edge of the left ventricle. In the fifth case, the method has failed. The failure in this case is due to the small size (3 or 4 samples in diameter) of the left ventricle at end-systole. The edge detected is a combination of the left ventricle edge and the boundary of the remainder of the heart. In order to be able to deal with objects of a small size which have been distorted, as is the case here, different methods would have to be developed.

The detected edges shown in Figures 5.6 through 5.10 were used to calculate the integral of the left ventricle region of each scintigram. Figures 5.11 through 5.15 show the resulting plot of the integral versus position in the heart beat cycle. As was stated in Section 5.4, the integral of the left ventricle region equals the volume of blood in the left ventricle plus the volume of blood in the foreground and background. If the foreground and background quantities can be estimated, the ejection fraction can be calculated from the data in the integration curves. Errors in the integral at end-systole are obvious in Figure 5.15. Again, these errors are due to the small

size of the left ventricle in the image.

### 5.6 Summary of Cardiac Scintigram Application

The simple edge tracking algorithm employed in Chapter 4 was modified to tackle the problem of additional irrelevant edge information contained in the scintigrams. This simple edge tracking method falls short of what may be accomplished with careful study of the edge tracking problem, but for the purposes of this thesis the method was adequate.

The filter sequence was demonstrated and worked well on the trial cases used. With the exception of the end systole scintigrams of one case, the filter sequence successfully enhanced and tracked the edge, and was able to produce a plot of the integral of left ventricle region.

Problems encountered in the applications suggest areas for future study. Further work should be directed towards better edge tracking which can tackle the problem of missing edge information. Also, automatic detection may fail if the left ventricle is too small for enhancement. Algorithms may be modified to allow for human intervention in the case of failure in automatic detection.

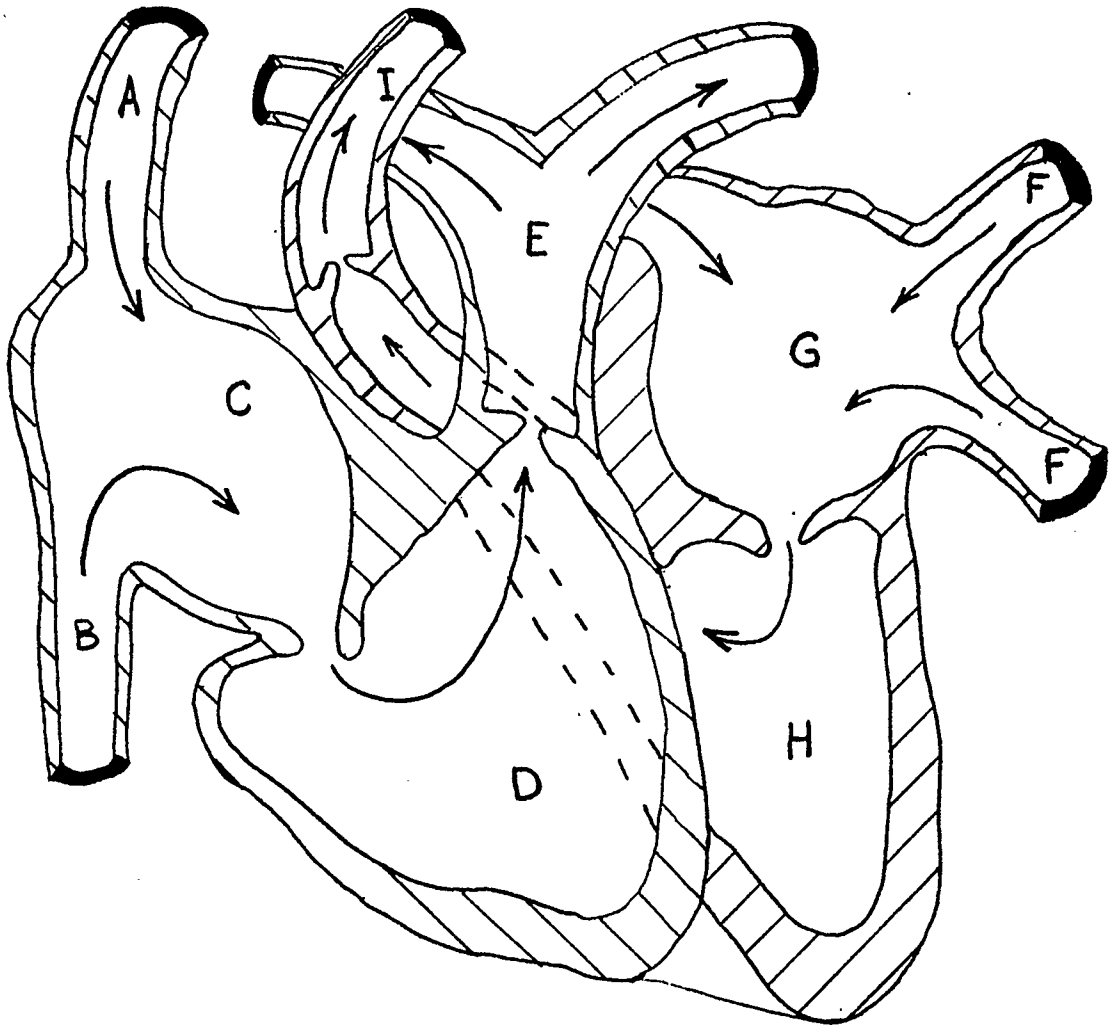


Figure 5.1 Cut-away view of the human heart showing blood circulation

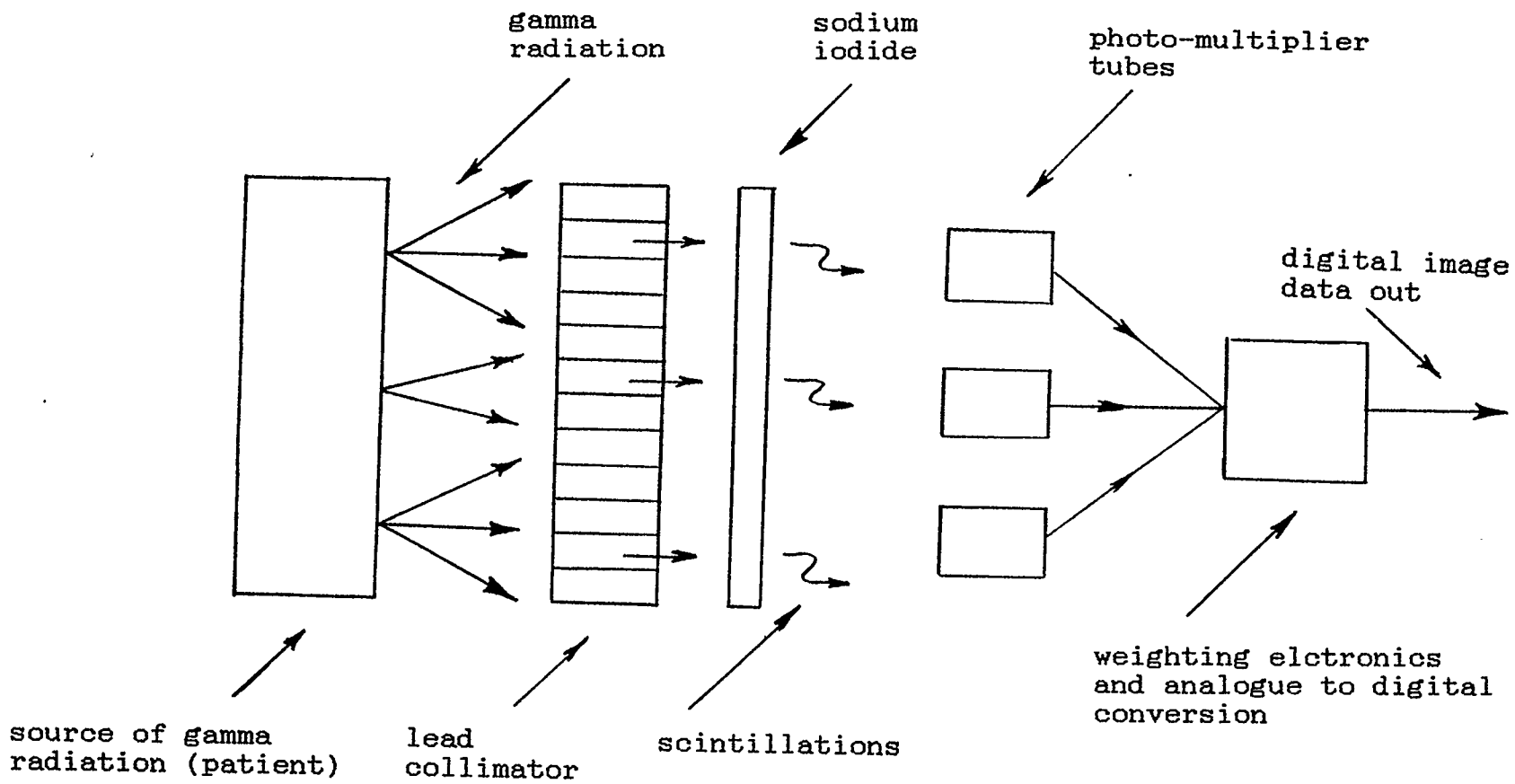
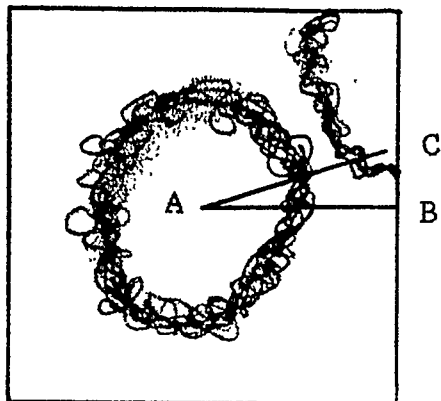


Figure 5.2 Apparatus for producing nuclear cardiac scintigrams



2D slice of the  
variance output

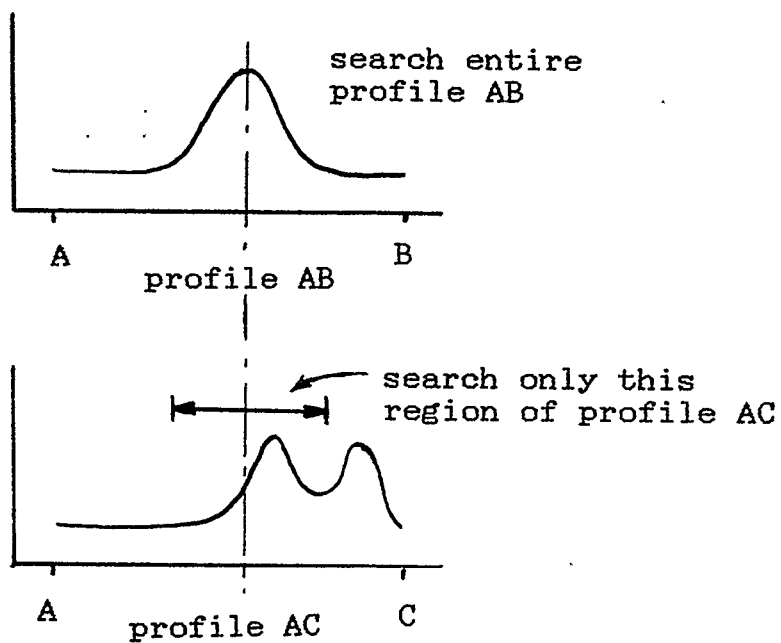


Figure 5.3 Pictorial description of the modified  
radial search algorithm

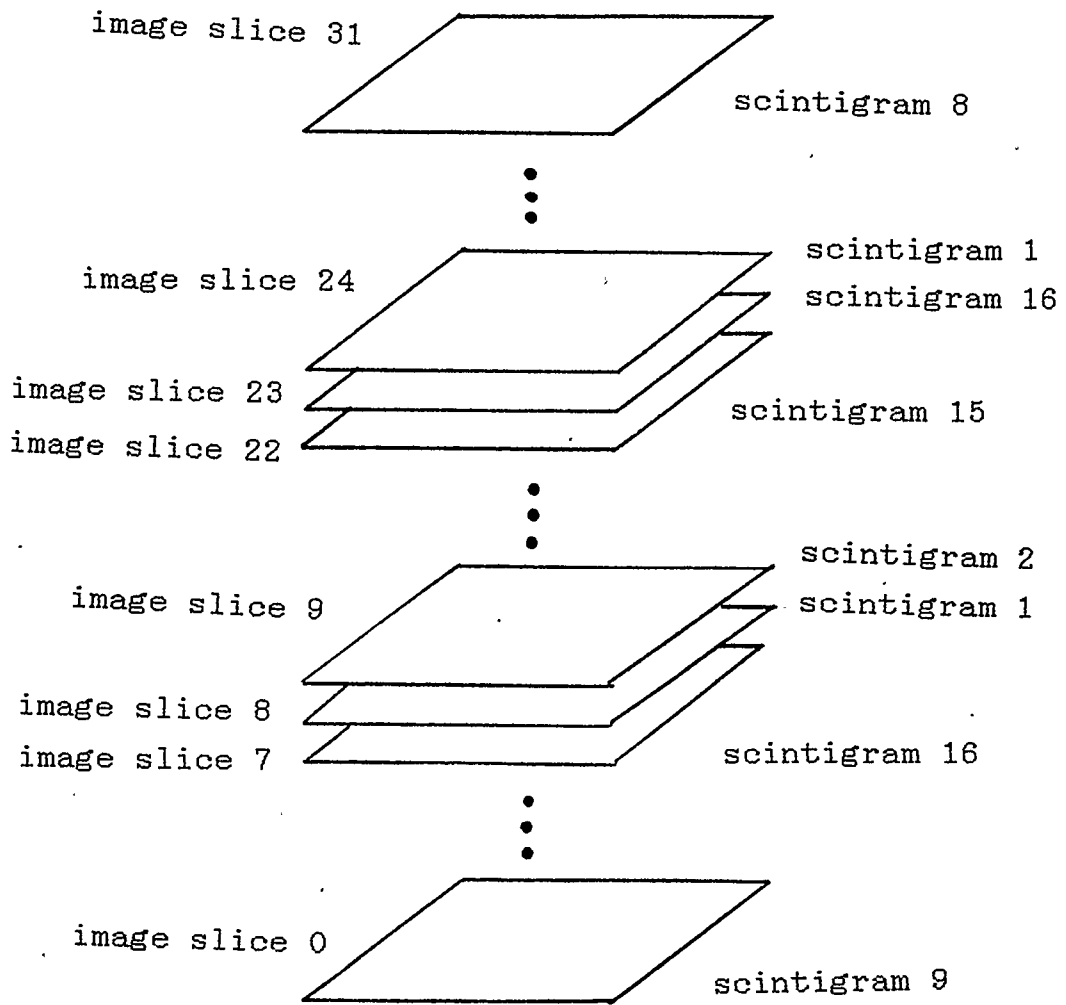
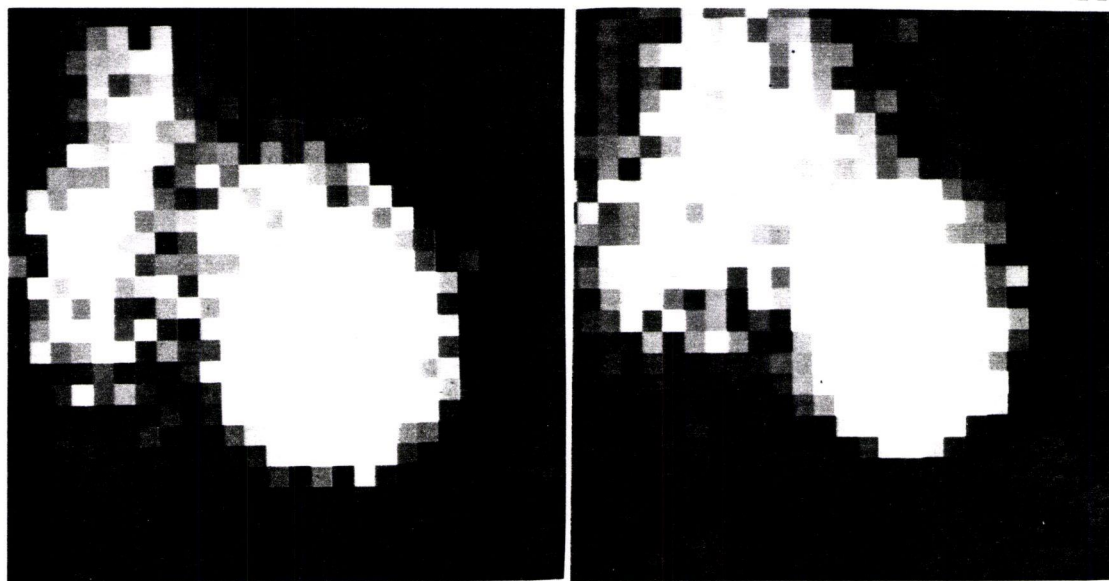
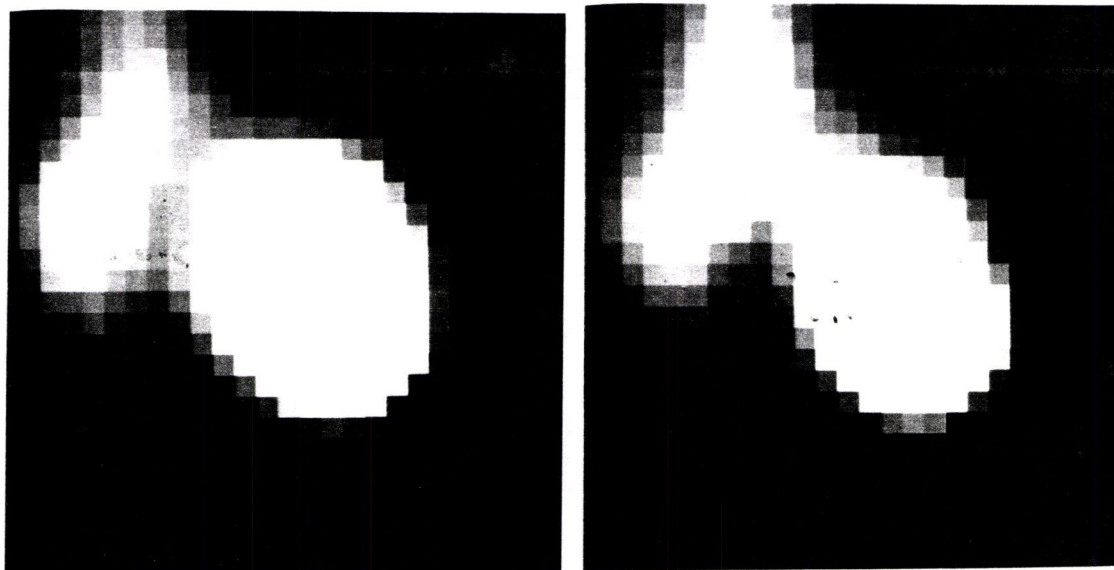


Figure 5.4 Generation of a 3D image from a set of nuclear cardiac scintigrams



(a)

(b)

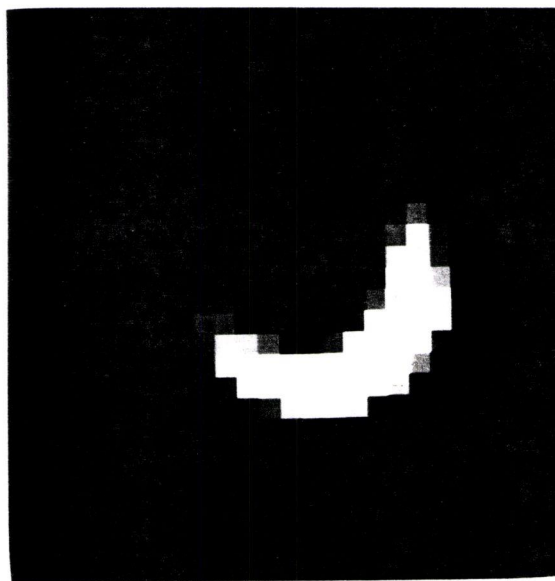


(c)

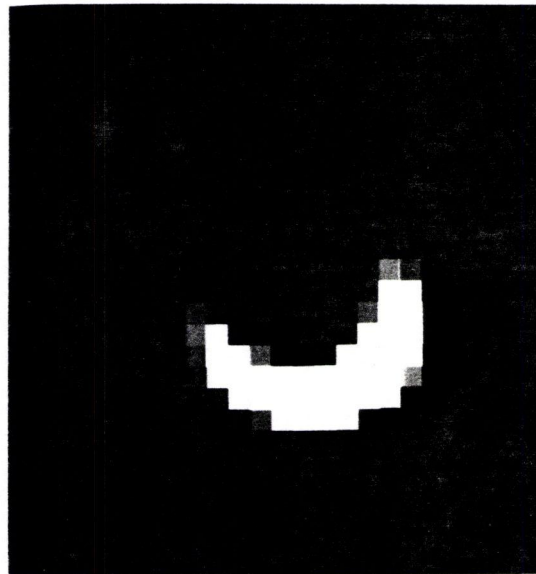
(d)

Figure 5.5 Example of the 3D filter sequence applied to cardiac scintigram data showing the end diastole and end systole images at each step

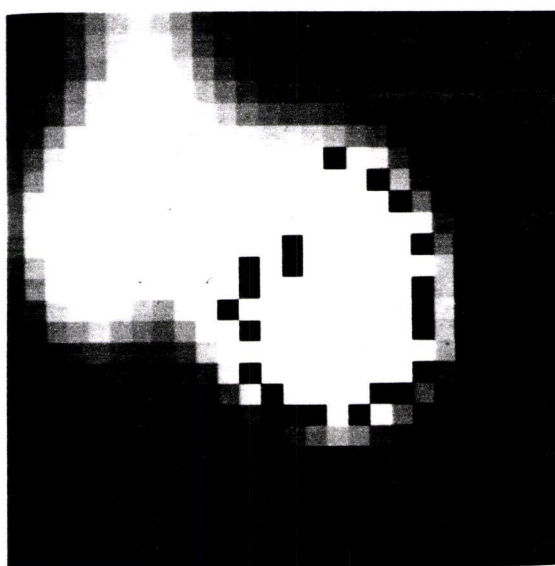
- (a) (b) original image
- (c) (d) mean filter output
- (e) (f) variance filter output
- (g) (h) points on the detected edge



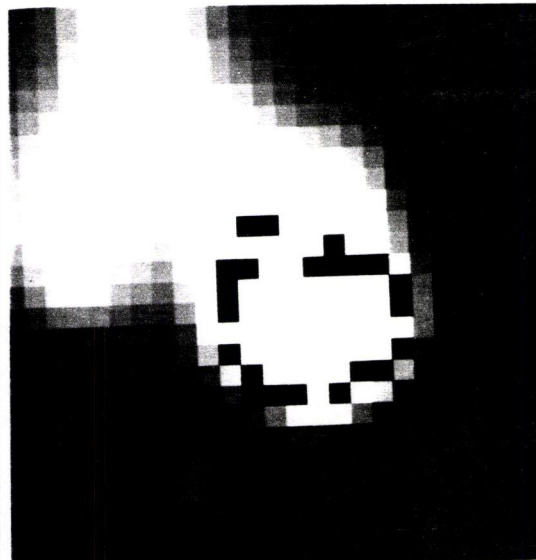
(e)



(f)



(g)



(h)

Figure 5.5 (continued)

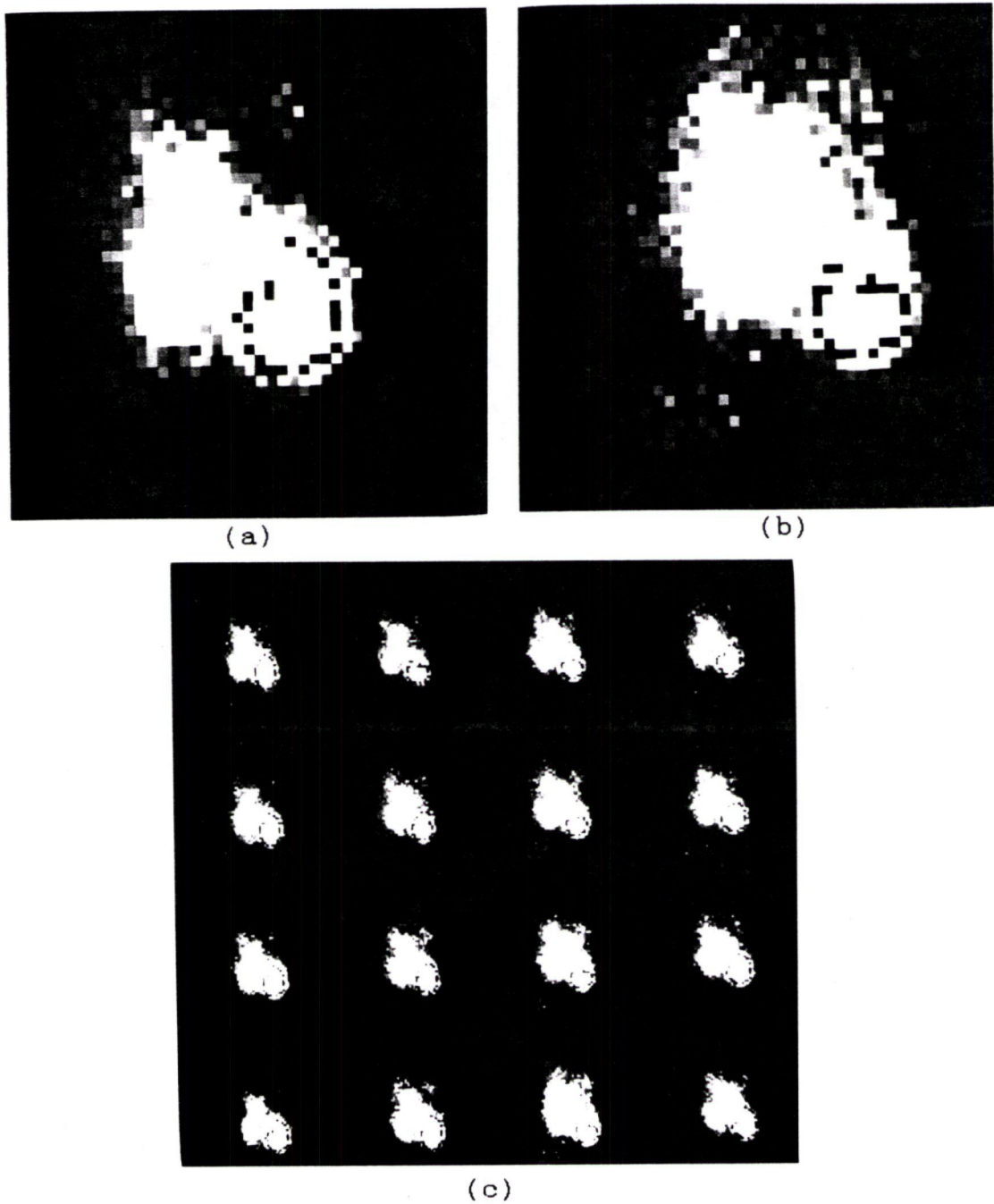
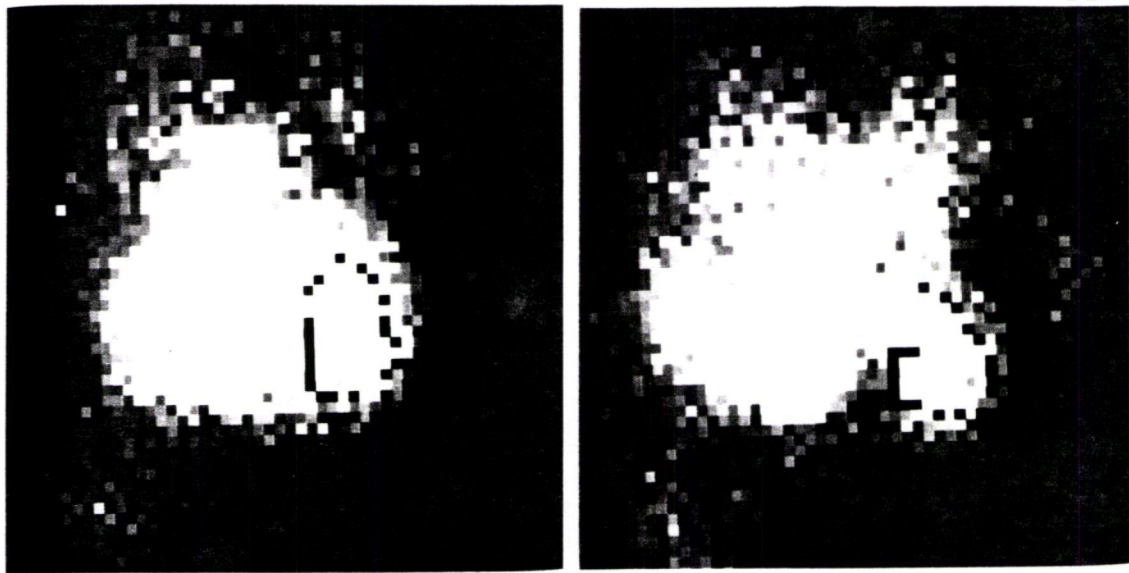
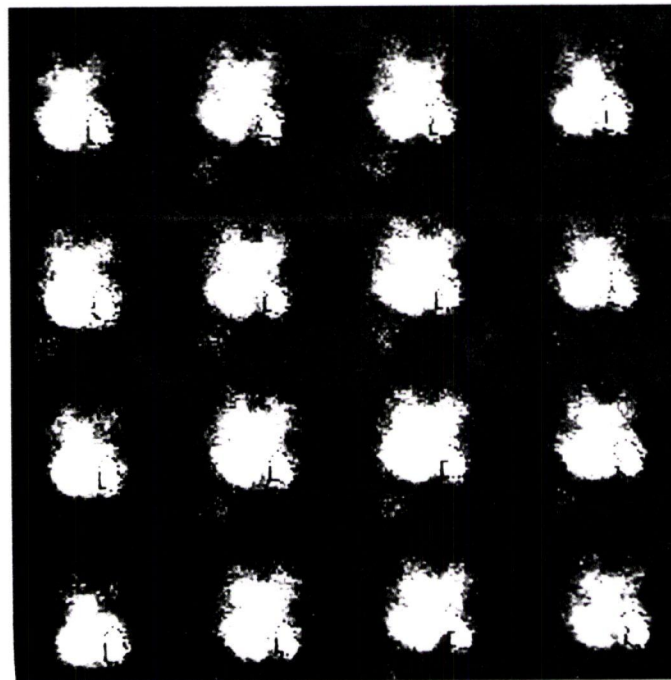


Figure 5.6 Results of application to cardiac scintigrams  
(case 1)  
(a) points on the detected edge for the end  
diastole  
(b) points on the detected edge for the end  
systole  
(c) points on the detected edges for all 16  
scintigrams



(a)

(b)



(c)

Figure 5.7 Results of application to cardiac scintigrams  
(case 2)  
(a) points on the detected edge for the end  
diastole  
(b) points on the detected edge for the end  
systole  
(c) points on the detected edges for all 16  
scintigrams

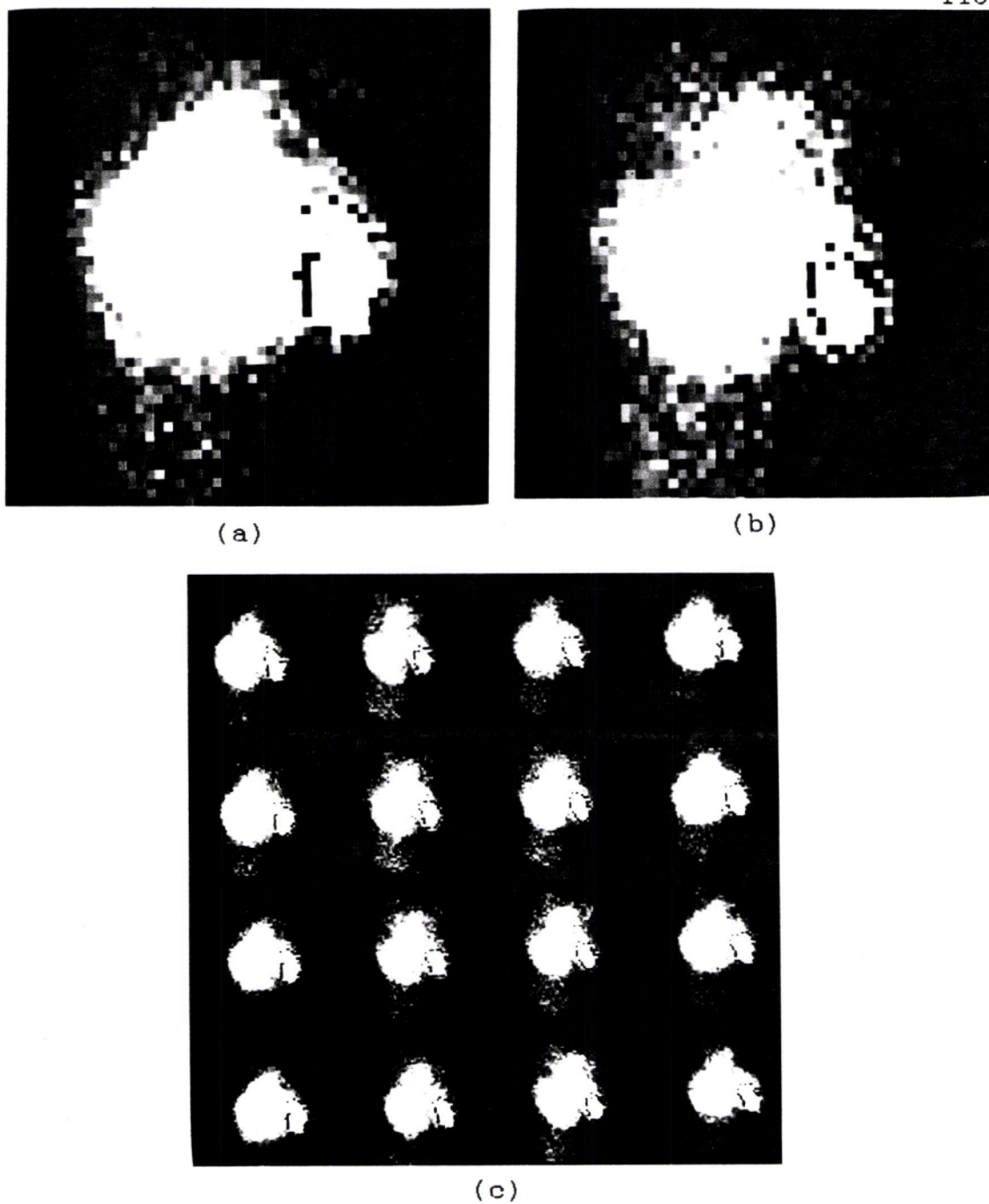


Figure 5.8 Results of application to cardiac scintigrams  
(case 3)  
(a) points on the detected edge for the end  
diastole  
(b) points on the detected edge for the end  
systole  
(c) points on the detected edges for all 16  
scintigrams

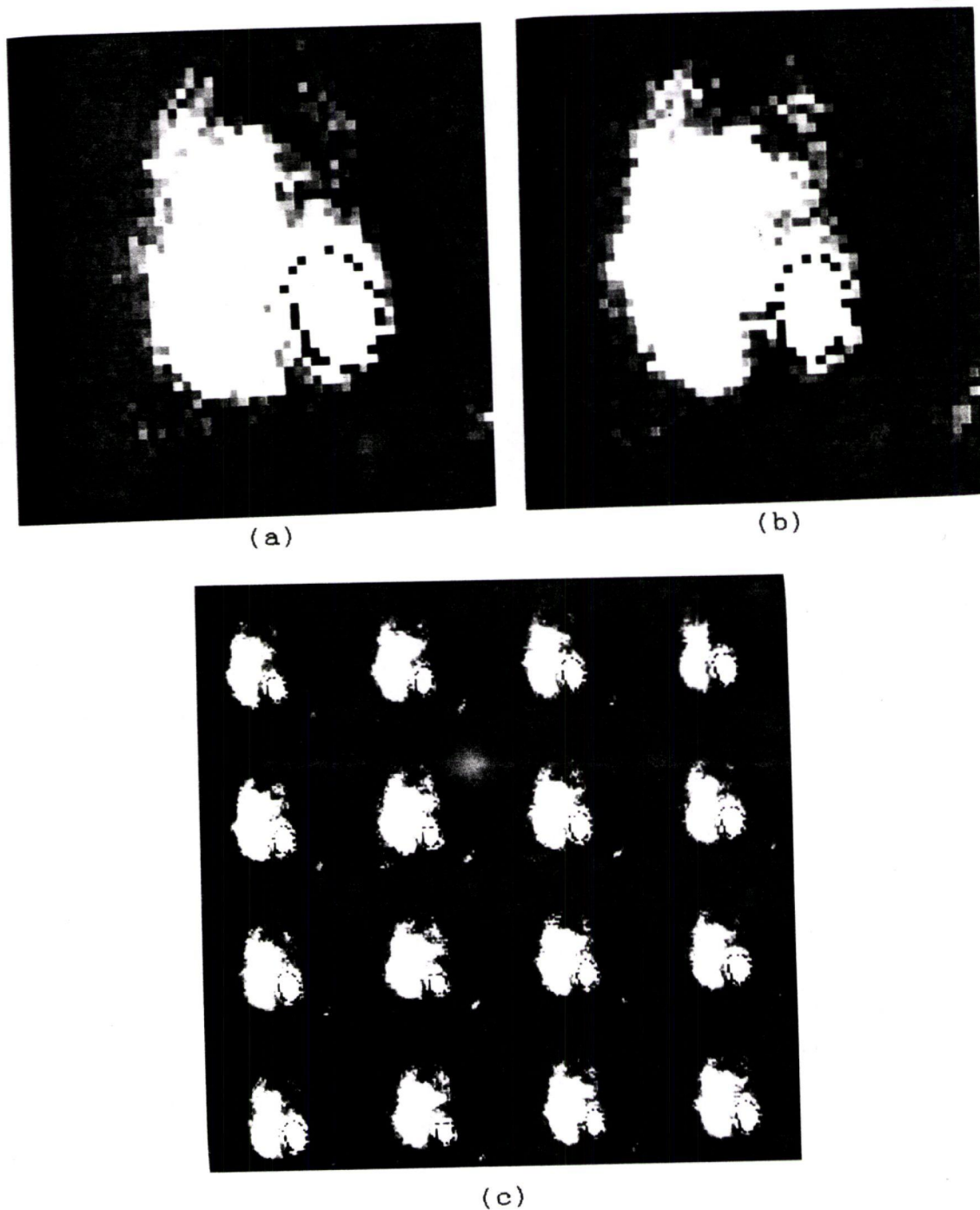


Figure 5.9 Results of application to cardiac scintigrams  
(case 4)  
(a) points on the detected edge for the end  
diastole  
(b) points on the detected edge for the end  
systole  
(c) points on the detected edges for all 16  
scintigrams

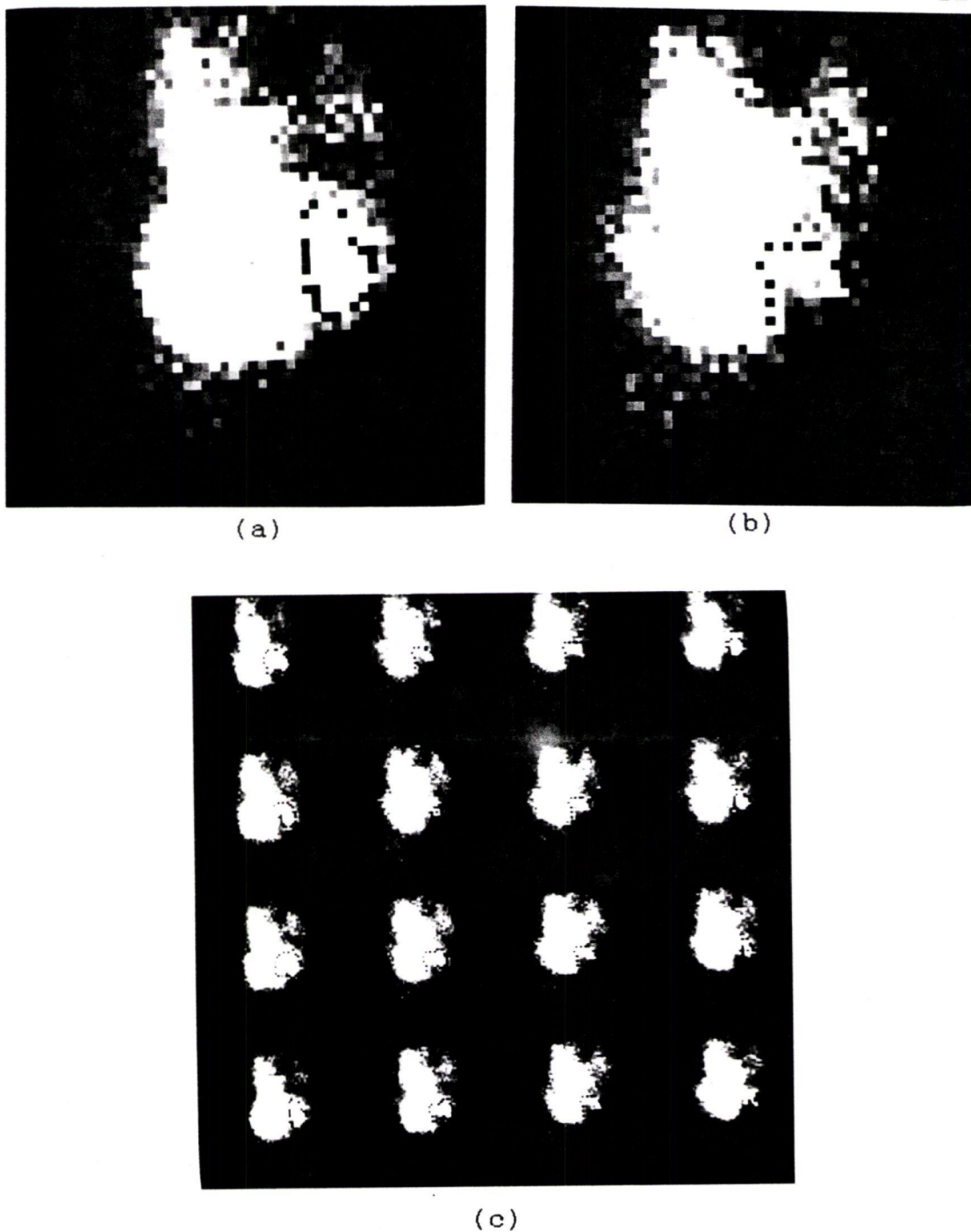


Figure 5.10 Results of application to cardiac scintigrams (case 5)  
(a) points on the detected edge for the end diastole  
(b) points on the detected edge for the end systole  
(c) points on the detected edges for all 16 scintigrams

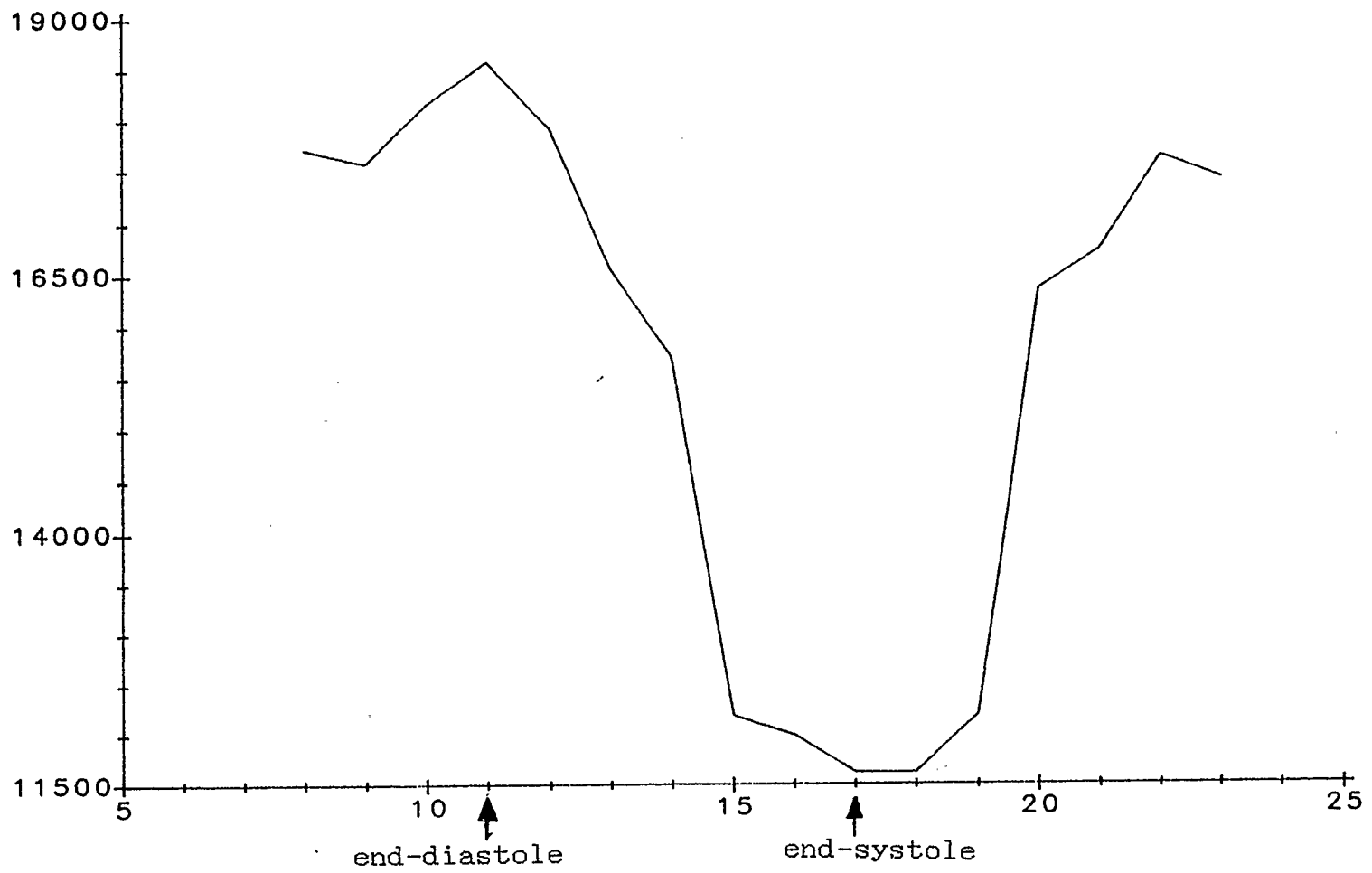


Figure 5.11 Integral of the left ventricle region versus time in the heart beat (case 1)

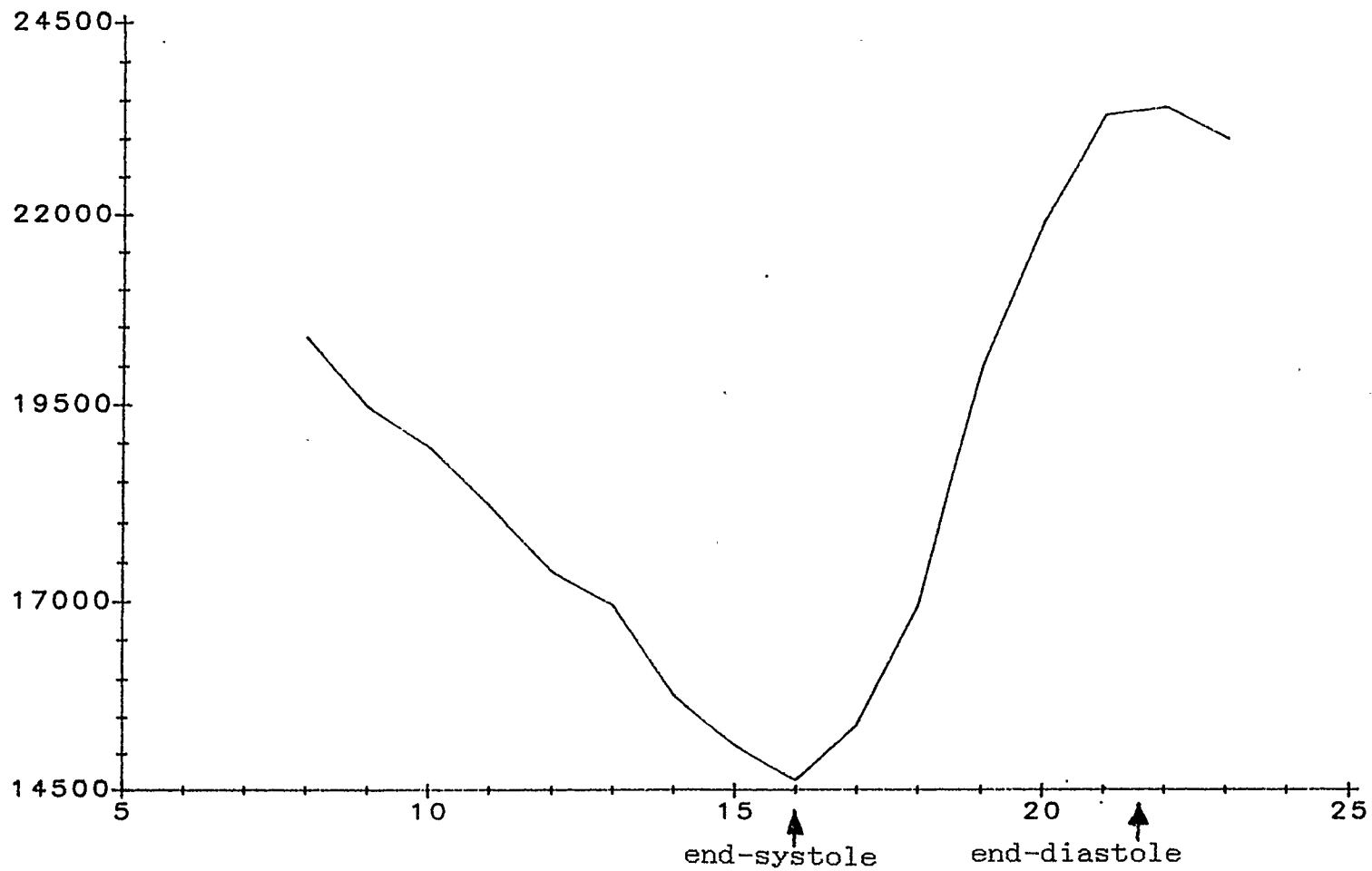


Figure 5.12 Integral of the left ventricle region versus time in the heart beat (case 2)

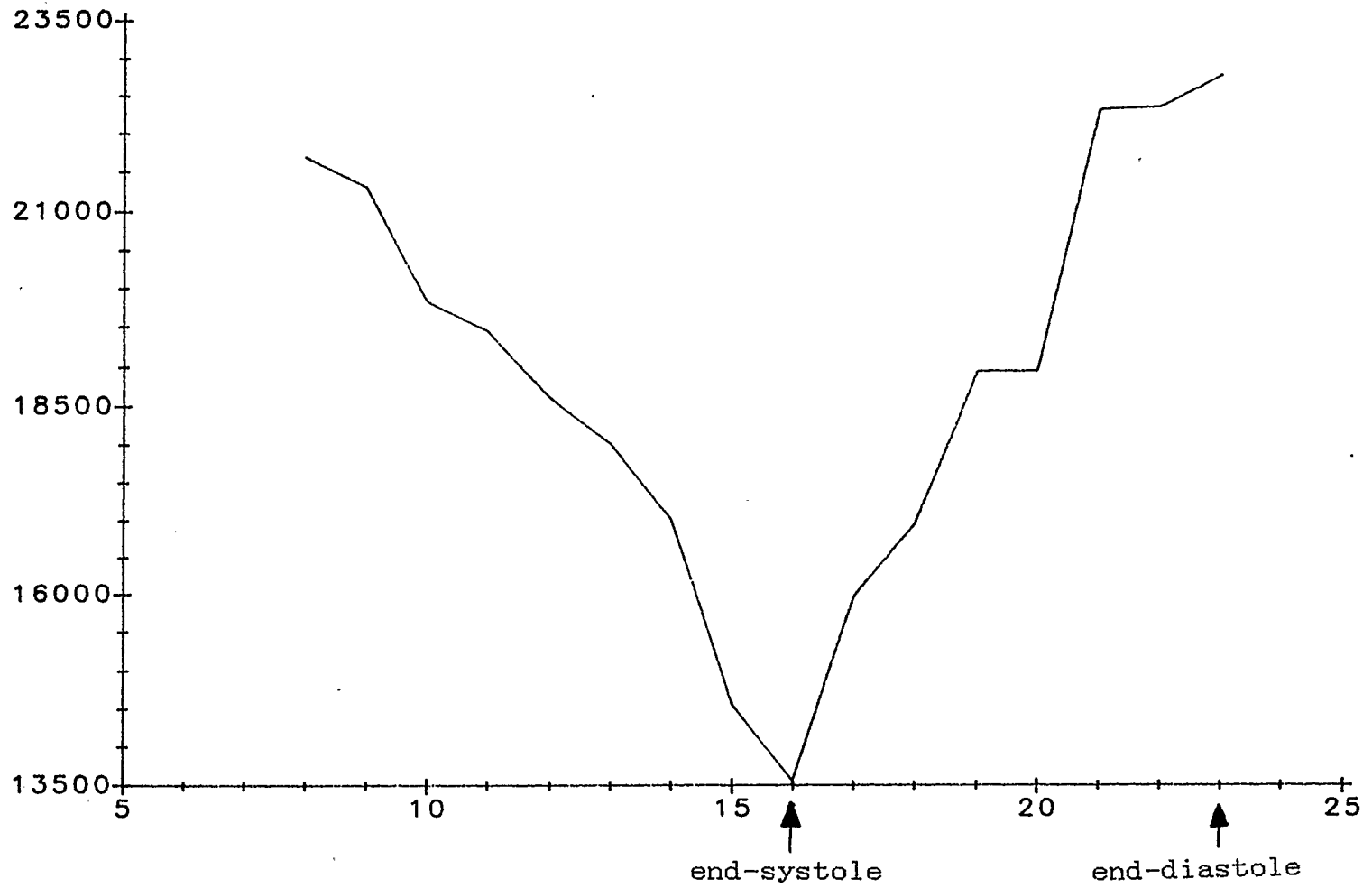


Figure 5.13 Integral of the left ventricle region versus time in the heart beat (case 3)

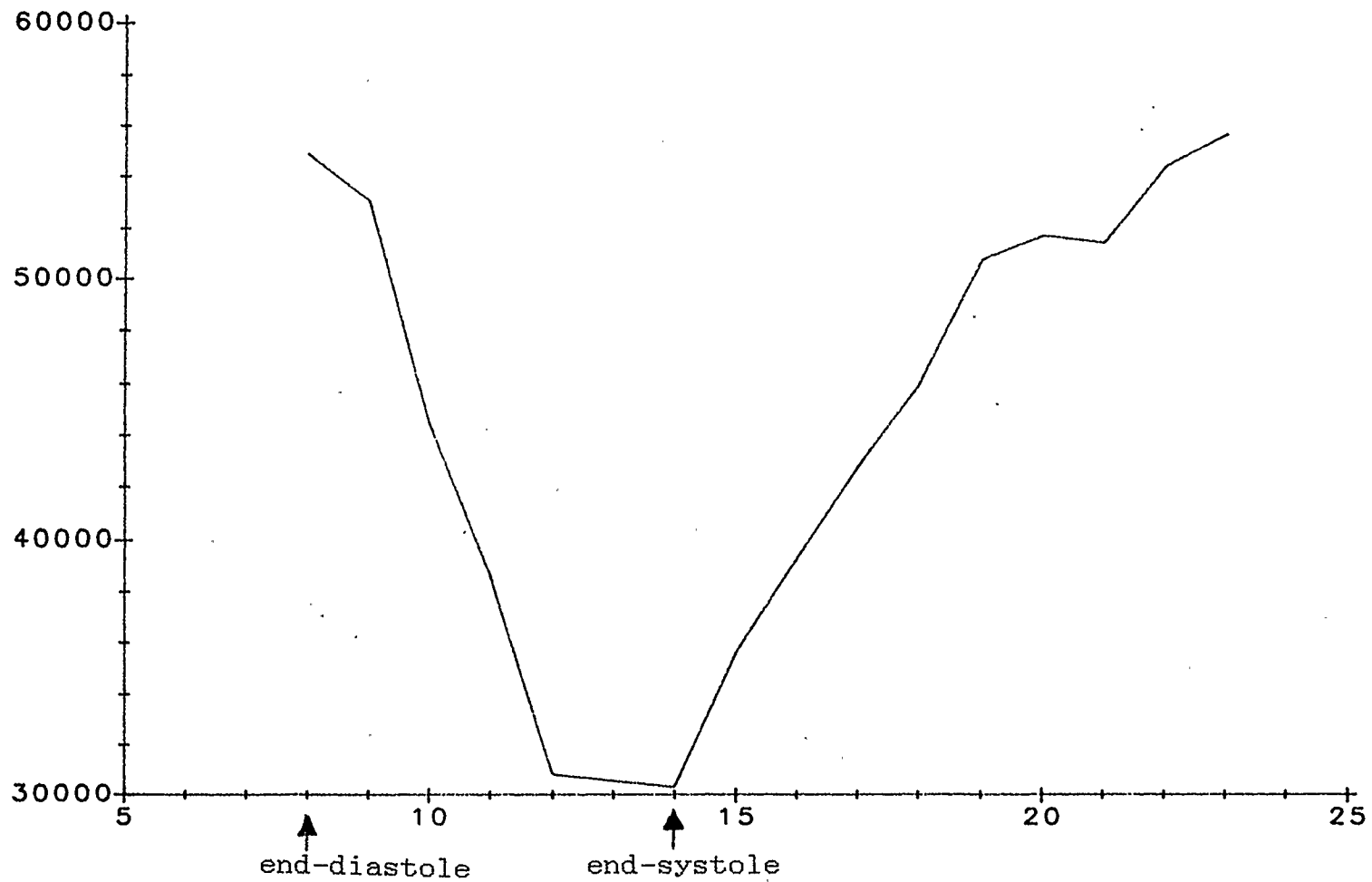


Figure 5.14 Integral of the left ventricle region versus time in the heart beat (case 4)

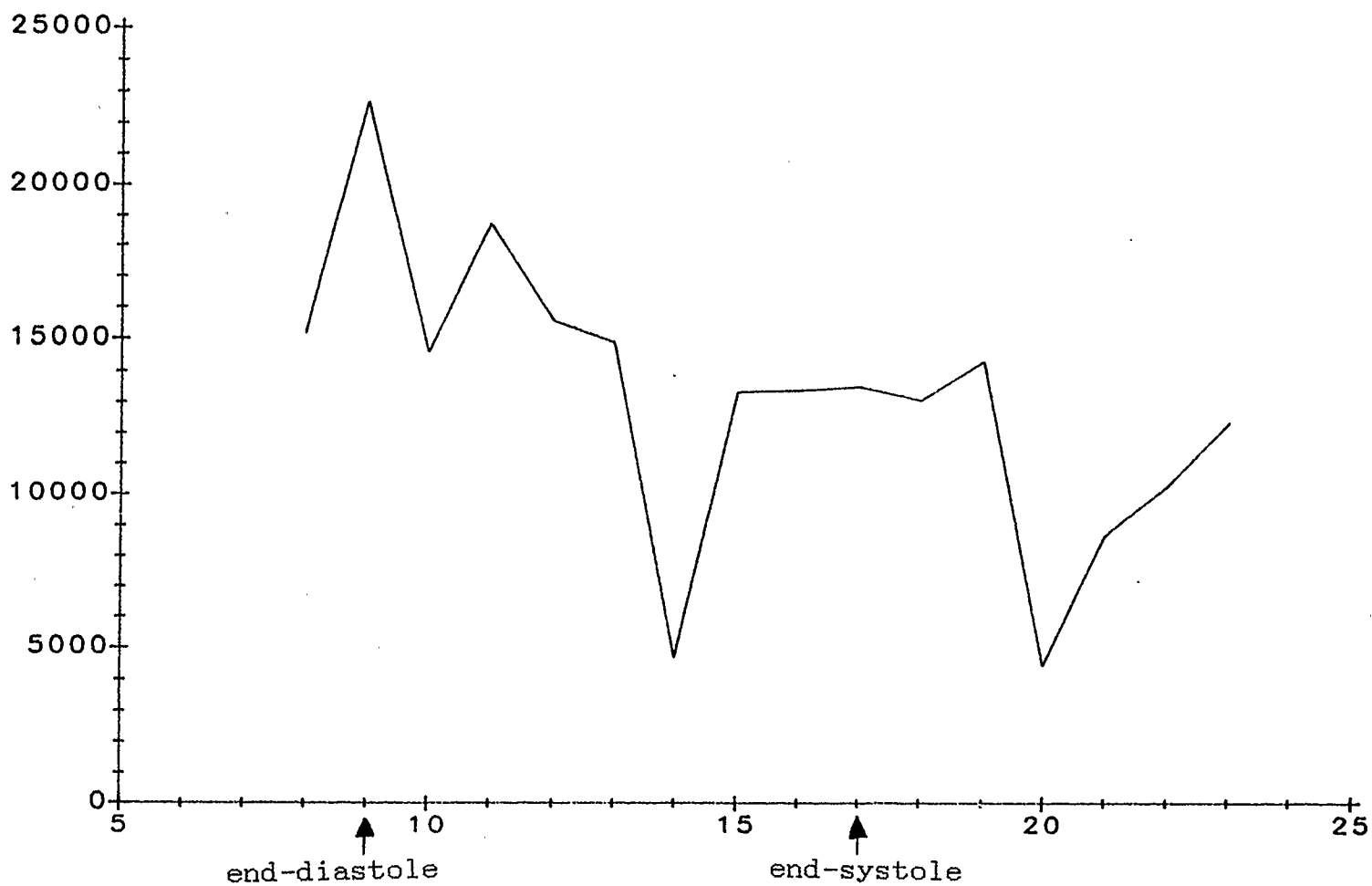


Figure 5.15 Integral of the left ventricle region versus time in the heart beat (case 5)

## Chapter 6

DISCUSSION6.1 Introduction

Results presented throughout this thesis are summarized in this chapter. Conclusions about noise reduction and edge enhancement are restated. It is reiterated that 3D processing is advantageous in image processing. Results of filter testing and application to nuclear cardiac scintigrams are also repeated here. The chapter concludes by presenting recommendations for two areas of further study.

6.2 Summary of Conclusions6.2.1 Summary of Noise Reduction Methods

Noise reduction methods were divided into three categories; 1) linear nonrecursive filters, 2) median filters, and 3) linear recursive filters. Filters in all three categories were shown to be valuable for noise reduction. However, a problem common to these filters is

edge blurring.

The review of noise reduction methods in the three categories led to conclusions about the suitability of each method in edge detection applications. Linear recursive filters require caution when used in edge detection applications because of infinite blurring. The median filter and related methods rely on bimodal distributions and lose their advantages in low SNR applications. The best method for noise reduction in low SNR applications, where edge detection is important, is the linear nonrecursive filter. For images containing constant levels, this filter was shown to be a mean filter.

#### 6.2.2 Summary of Edge Enhancement Methods

Several methods for edge enhancement were examined in Chapter 2. These methods were divided into the categories of 1) thresholding, 2) derivative methods, 3) nonlinear masks, and 4) sliding statistical tests. Each of the edge enhancers examined suffered from some shortcoming which made it unsuitable for 3D processing. It was therefore desirable that some method be found that could blend all edge enhancer properties with extensibility. Such a filter is the variance filter and was described in detail in

Chapter 3. Its desirable properties as an edge enhancer were demonstrated and its limitations were defined. In comparing the variance filter to other edge detectors, the variance filter was demonstrated to be an acceptable edge enhancer with easy extensibility to any multidimensional application.

### 6.2.3 Advantages to Three Dimensional Processing

It was concluded in Chapter 3, from an analysis of the mean and variance filters, that is more advantageous to process image data in 3D rather than 2D. In general, as many dimensions as possible should be used in processing data. The conclusion arose from the observation that an increased number of dimensions in processing increases the number of samples in a window and/or permits a reduced window width. Smaller window widths produce less blurring and lead to more accurate edge detection. Also, it was observed that 3D processing permits edge detection in cases where it is not possible with 2D methods.

#### 6.2.4 Summary of the Filter Testing

The mean and variance filters were tested with artificially generated images. Results of the testing clearly supported the theory in Chapter 3. The simulation also demonstrated the inability of the theory to predict errors caused by blurring at an edge. For example, in cases where the window width was large, the theoretical predictions were not supported. Test results also supported the argument in favor of 3D processing as presented in Chapter 3.

#### 6.2.5 Summary of the Application to Cardiac Scintigrams

The mean and variance filters were applied to nuclear cardiac scintigrams. Results of the application were presented in Chapter 5. Excellent results were obtained from the application of the mean and variance filters in conjunction with a rudimentary edge tracking algorithm. In the majority of test cases the left ventricle of the heart was successfully detected. Exceptions arose from one of two reasons. Either the left ventricle in the image was too small for detection by these methods, or, not all the edge information was contained in the original image.

### 6.2.6 Main Conclusions

The main conclusions of this thesis are repeated here:

1. Linear nonrecursive filters should be used for noise reduction in applications where edge detection is important. More specifically, when constant levels are in an image are obscured by noise, a mean filter should be used.
2. The variance filter is a good edge enhancer and its versatility makes it valuable for any multidimensional application.
3. Image data should be processed in 3D rather than 2D, whenever possible. In general, as many dimensions as are available should be used.

### 6.3 Recommendations for Further Study

Two important problem areas were identified in this thesis. These problems suggest directions for further study.

The first major problem was in the theoretical analysis. Errors that occurred because an edge was blurred were not modelled. Rather, only those errors where

background samples are mistaken for variance peaks were accounted for. Since the probability distribution of the variance, the chi-square distribution, is well known, an excellent opportunity exists to model the edge detection errors which occur at broad edges. Such a model would enable the evaluation of edge enhancers based on the accuracy of the edge detected for an object. This would provide a significant improvement over the evaluation of edge enhancers using probability curves like those presented in Chapter 3. Although the probability curves are useful in comparing methods, conceptually, they are removed from the real problem of defining the boundary around an object.

The second major problem encountered in the study was the tracking of an edge, after an edge enhancer had been used. A question continually arises in image processing literature; after using image processing techniques, how does one convert the image data into some convenient mathematical model usable by a computer? The human vision system performs the human equivalent to this task continually, but the problem is almost hopelessly complicated for computers. As was indicated earlier, the method used in this study was simple and rudimentary, but it was not reliable. Some people have advocated "artificial intelligence" as the solution to this problem.

The recommendation here is that the task be divided between the computer and its human operator. This symbiotic process allows the computer to do quickly what it does best. A human operator would only intervene in cases where the computer was not able to follow successfully the edge. Only two things need to be developed to allow this process to happen. First, the automated computer algorithm must be able to determine when it has failed, and second, an interactive process facilitating easy operator intervention is needed. These developments would allow the computer to do quickly what it can do best, but take advantage of "real intelligence" when needed.

## REFERENCES

- [1] P. DeSouza, "Edge detection using sliding statistical tests", **Computer Vision, Graphics, and Image Processing**, Vol 23, 1983, pp. 1-14.
- [2] N. D. A. Mascarenhas, L. O. C. Prado, "A Bayesian approach to edge detection in images", **IEEE Transactions on Automatic Control**, Vol AC-25, No 1, February 1980, pp. 36-43.
- [3] I Kadar, "A class of robust edge detectors based on latin squares", **Pattern Recognition**, Vol 11, May 1979, pp. 329-339.
- [4] P. T. Cahill, E. Ornstein, S. L. Ho, "Edge detection algorithms in nuclear medicine", **IEEE Transactions on Nuclear Science**, Vol NS-23, No 1, February 1976, pp. 555-559.
- [5] S. M. Kay, G. J. Lemay, "Edge detection using the linear model", **Proceedings of the IEEE International Conference on Acoustics, Speech, and Signal Processing**, March 19-21, 1984, San Diego, Vol 3, pp. 48.11.1-48.11.4.

- [6] N. Otsu, T. Kasvand, "A new family of nonlinear edge detectors for noisy images", *Proceedings of the SPIE International Society of Optical Engineers*, Vol 435, 1983, pp. 10-17.
- [7] W. K. Pratt, *Digital Image Processing*, John Wiley and Sons, NewYork, 1978, pp. 478-503.
- [8] I. E. Abdou, W. K. Pratt, "Quantitative design and evaluation of enhancement/thresholding edge detectors", *Proceedings of the IEEE*, Vol 67, No 5, May 1979, pp. 753-763.
- [9] L. R. Rabiner, B Gold, *Theory and Application of Digital Signal Processing*, Prentice-Hall, 1975, pp. 75-81.
- [10] S. Haykin, *Communication Systems*, John Wiley and Sons, 1978, pp. 531-533.
- [11] *ibid.*
- [12] Pratt, *op. cit.*, pp. 291-299
- [13] R. C. Gonzalez, P. Wintz, *Digital Image Processing*, Addison-Wesely, London, 1977, pp. 58-64.

- [14] J. S. Lee, "Digital image enhancement and noise filtering by use of local statistics", **IEEE Transactions on Pattern Analysis and Machine Intelligence**, Vol PAMI-2, No 2, March 1980, pp. 165-168.
- [15] Pratt, op. cit., p. 427
- [16] M. P. Ekstrom, "Realizable Weiner filtering in two dimensions", **IEEE Transactions on Acoustics, Speech, and Signal Processing**, Vol ASSP-30, No 1, February 1982, pp. 31-40.
- [17] J. F. Abramatic, L. M. Silverman, "Nonlinear restoration of noisy images", **IEEE Transactions on Pattern Analysis and Machine Intelligence**, Vol PAMI-4, No 2, March 1982, pp. 141-149.
- [18] P. M. Narendra, "A separable median filter for image noise smoothing", **IEEE Transactions on Pattern Analysis and Machine Intelligence**, Vol PAMI-3, No 1, January 1981, pp. 20-29.
- [19] R. A. Stein, T. J. Fowlow, "The use of median filters for edge detection in noisy signals", **Proceedings of ISCAS 85**, Kyoto, Japan, 1985, pp. 1331-1334.

- [20] Y. H. Lee, S. A. Kassam, "Generalized median filtering and related non linear techniques", *IEEE Transactions on Acoustics, Speech, and Signal Processing*, Vol ASSP-33, No 3, June 1985, pp. 672-683.
- [21] N. A. Narayan, A. Rosenfeld, "Image smoothing by local use of global information", *IEEE Transactions on Systems, Man, and Cybernetics*, Vol SMC-11, No 12, December 1981, pp. 826-831.
- [22] A. Antoniou, *Digital Filters: Analysis and Design*, McGraw-Hill Inc., 1979, pp. 196-215.
- [23] L. T. Bruton, N. R. Bartley, "Three dimensional image processing using the concept of network resonance", *IEEE Transactions on Circuits and Systems*, Vol CS-32, No 7, July 1985, pp. 664-672.
- [24] Antoniou, op. cit., pp. 248-249
- [25] Rabiner, et. al., op. cit., pp. 205-209
- [26] *ibid.*
- [27] Pratt, op. cit., pp. 478-503

- [28] *ibid.*
- [29] Abdou, et. al., *op. cit.*
- [30] DeSouza, *op. cit.*
- [31] A. C. Bovik, T. S. Huang, D. C. Munson Jr.,  
"Nonparametric edge detection with an assumption on  
minimum edge height", **Proceedings of the IEEE Computer  
Society Conference on Computer Vision and Pattern  
Recognition**, Jun 19-23, 1983, Washington D.C., pp.  
142-143.
- [32] DeSouza, *op. cit.*
- [33] W. J. Dixon, F. J. Massey Jr., **Introduction to  
Statistical Analysis**, McGraw-Hill Inc., 1969, p. 102.
- [34] *ibid* pp. 466-467
- [35] Abdou, et. al., *op. cit.*
- [36] *ibid.*
- [37] *ibid.*

- [38] C. W. Taber, *Taber's Cyclopedic Medical Dictionary*, F. A. Davis Company, Philadelphia, 1956, pp. 146-149.
- [39] *ibid.*
- [40] D. E. Grove, *Boundary Detection in Cardiac Scintigrams for Ejection Fraction Determination*, MSc Thesis, University of Calgary, January 1985, pp. 5-10.
- [41] *ibid.*
- [42] *ibid.*